# Voltage Stability of the Power Grid with Integrated Wind Turbines

by

## Michael Manarovici

B.Sc., The University of British Columbia, 2001

A THESIS SUBMITTED IN PARTIAL FULFILMENT OF
THE REQUIREMENTS FOR THE DEGREE OF

MASTER OF APPLIED SCIENCE
IN
THE FACULTY OF GRADUATE STUDIES
(ELECTRICAL AND COMPUTER ENGINEERING)

THE UNIVERSITY OF BRITISH COLUMBIA
April 2005

# Abstract

There has been a transition from non-renewable fossil fuels to renewable and clean energy sources. A result of this transition is the installation of a significant amount of wind turbines. The increasing presence of wind power requires additional voltage stability analysis of the power system. This is due to the considerable voltage fluctuations produced by changes in the wind speed which may affect some commercial and industrial loads. This problem is substantially more important as grid capacity is pushed to its limit. As a result, there is an interest in steady state and transient voltage stability analysis of the power grid with integrated wind turbines. This thesis studies the effect of wind speed variation on motor-type industrial loads, fed from the grid via a weak connection – long distribution line, in combination with a partial supply from locally installed distributed energy source – wind turbine. Two types of studies were conducted: 1) studies that involve a three phase fault on the strong line, and 2) studies that involve the continuous steady state operation of the wind turbine with typical wind variations. Type one studies examine the transient voltage stability of the system. They compare the static load model to a dynamic load model. In addition, the accuracy of constant power factor PV curves is compared to the equivalent circuit of induction machine PV curves at predicting a voltage collapse. It will be demonstrated that the dynamic load model and the equivalent circuit of induction machine PV curves is the only combination considered that accurately predicts the transient voltage stability of the system. The effect of a weak line (WL), between the grid and the load, is compared to a medium strength line (ML). Other factors which will be varied are: the post fault re-closing times and the load composition. Type two studies focus on the continuous operation of wind turbines. These cases explore the steady state voltage stability of fixed speed wind turbines (FSWT) compared to doubly fed induction generator (DFIG) wind turbines. The dependence on wind power is increased to determine their penetration limit. It will be shown that the use of the DFIG wind turbine produces less voltage fluctuations and has the potential for larger penetration in the power system.

# Table of Contents

# List of Tables

# List of Figures

# Acknowledgments

A project similar to this one is rarely completed by a single person. It is usually a collaboration of ideas and insights from a number of different people. Indeed, this thesis is no different. Recognition needs to be acknowledged to those who have participated, in some way, to the realization and completion of this thesis.

I would like to send my deepest appreciation to Dr. José Martí. The opportunity that he provided me will never be forgotten. His ability to select a timely and practical research topic was astonishing. His unconditional support and vast knowledge of power systems proved indispensable throughout this thesis. The trust and the friendship that we have developed over the past year will continue for many more years to come. Once again, thank you Dr. Martí.

I would also like to thank Dr. Juri Jatskevich for his participation in this thesis. His clear direction and goal oriented approach was useful to keep me on track. His belief in my work and my ability to produce meaningful results was invaluable. He played a key role during the course of this thesis and I would like to acknowledge his contribution.

In addition, Dr. Hermann Dommel openly shared his wisdom of power engineering. His willingness to answer questions in a clear and understandable manner is a characteristic that sets Dr. Dommel apart from other professors. Thank you for your participation in this thesis.

I need to recognize two of Dr. Martí's students with whom I collaborated: Tarek Aboul-Seoud and Thibaut Sanchez. It was a pleasure to work with each of them and to have someone to bounce ideas off of when research needed a fresh direction.

I would like to thank all the members of the Real-Time Power Simulation Lab at UBC for their candid conversations over lunch. A special thank you goes to Tom De Rybel.

Last but not least, I would like to extend a warm thank you to my parents who encouraged and supported me throughout.

# 1. Introduction

The availability of electricity is important for the functioning of modern society. It is used to provide the energy needed to operate information technology, lighting, food storage, appliances and industrial processes. The demand for electrical energy in North America is increasing at a rate of 2-3% per year [1]. The primary energy sources to meet this demand are fossil fuels, nuclear fission and hydroelectricity [1]. A drawback of generating electricity from these sources is their harmful environmental impact. The use of fossil fuels produces pollutants, such as carbon dioxide ($CO_2$), sulphur oxides ($SO_x$) and nitrogen oxides ($NO_x$) [2]. Nuclear power generates radioactive isotopes known as nuclear waste. The construction of hydroelectric dams and basins causes the flooding of large areas and destroys local ecosystems. Furthermore, fossil fuel and uranium reserves are limited. As a result, many countries are encouraging the use of renewable and clean energy sources. There are several forms of distributed power generation: solar cells, tidal power, biomass combustion and wind power. Of these, wind power has emerged as one of the most viable forms of renewable and clean energy.

## 1.1 Historical Background

Wind energy has been utilized for many centuries to sail ships, to grind grain and to pump water. The conversion of wind energy to mechanical energy was frequently performed. At the end of the XIXth century, the potential to use electricity to perform work was demonstrated. In 1891, Poul La Cour developed the world's first wind turbine which generated electricity in Denmark [2]. In 1941, a twin-bladed wind turbine rated at 1250 kW was installed in Vermont, USA [2]. It was one of the largest wind power installations of its time. Subsequent interest in wind systems declined as the grid became more reliable and electricity prices declined. The oil shock of the 1970's, which heightened awareness of North America's energy problems, coupled with substantial financial and regulatory incentives for alternative energy systems, stimulated a renewal of interest in wind power. The wind boom was short lived. By the mid 1980's, installation of new wind turbines almost came to a complete halt for a decade. Meanwhile, in Europe, wind turbine technology continued to advance especially in Germany, Spain and

1

Denmark. These countries were prepared for the revived growth in wind turbine installations which began in the late 1990's. Wind power capacity has been increasing by 25% per year from 1995 to 2003 [2]. The world leader in installed capacity is Germany followed by USA, Spain Denmark and India (see Table 1) [3].

| Country | Total Wind Power Installed at the End of 2003 |
|---------|----------------------------------------------|
| Germany | 14 609 MW |
| USA | 6 370 MW |
| Spain | 6 202 MW |
| Denmark | 3 110 MW |
| India | 2 110 MW |
| Others | 6 750 MW |
| World Total | 39 151 MW |

**Table 1: Total wind power installed at the end of 2003.**

## 1.2 Wind Turbines Generators and Integration to the Grid

With this large increase of wind turbines being connected to the grid, system operators and manufacturers need to ensure that they are integrating grid compatible generators. Similar to other current generating power plants, wind turbine must meet requirements concerning automatic operation, monitoring and safety. There are several specifications that need to be considered during operation. The dynamic behaviour of operation in parallel with the grid is critical. This is of particular concern in weak grid systems. The direct coupling of the wind turbine to the grid forces the generator to operate in synchronism with the grid. On the other hand, variations in wind speed, which is used as the prime mover for wind turbine generators, cause variations in the applied torque. The result is fluctuations in electrical power output. These fluctuations may be large enough to cause a loss of synchronism. Smaller gusts of wind generate over currents in the system. This may cause the current protection breakers of the load to trip, preventing over heating of the load. This would be an unacceptable consequence of the integration of wind turbines to the grid. Therefore, the quality of the energy fed into the utility grid is largely determined by the technical concepts of the electrical system.

Typically, wind turbines are connected to the grid at distribution voltage levels (approximately 10 kV to 40 kV). The distribution voltage levels are appropriate because of the typical power outputs of wind turbines of a few MW. In addition, the typical distances that this power needs to travel to arrive at the load, tens of kilometres, makes distribution voltage levels desirable. In comparison, high costs have restricted the connection of a single wind turbine to transmission level voltages [4]. Integrating wind turbines to local low voltage levels is appropriate for supplying small consumers for example, households, buildings and farms. Thus, wind turbines are commonly integrated to the power grid at distribution voltages.

Grid compatible wind turbine systems are possible with either induction generators or synchronous generators. With modern power electronic devices, achieving grid compatibility is made simpler. Attention will be placed on the two most common types of wind turbine generators: fixed speed wind turbines (FSWT) and doubly fed induction generator (DFIG) wind turbines. FSWT consist of an induction generator with a squirrel cage rotor. They have been the most successfully used wind turbine generators for decades [4]. Their low cost and minimal maintenance are the characteristics that are most attractive. On the other hand, DFIG have gained recognition because they are more efficient. For a given wind speed, the DFIG will produce more electrical power than the FSWT. This is possible because DFIG operate as variable speed wind turbines. This is one of the many advantages of DFIG which justify the increased cost.

A number of research papers have recently been published studying various wind turbine generators. Descriptions of the generator significantly vary in the literature. In [5], no dynamic model is used whereas in [6] a first-order generator model was implemented. In 1996, Jenkins and Saad-Saoud [7] utilized a third-order model and at the proceedings of the European wind energy conference, in 1999 [8], a fifth-order model was presented. Kazachkov et. al. investigated second-order and fourth-order wind turbine models [9]. Petru et. al. and Thiringer concluded that a fifth-order generator model was necessary to accurately represent the transient response of the wind turbine [10] and [11]. Verifications of models with practical measurements on installed wind turbine systems are rarely published [10]. The operation of a wind turbine with a broad range of wind speeds was subsequently presented in [12]. They focused on the wind turbine,

implemented as a full-order (fifth-order) generator model, in isolation of the power system. [13] and [14] illustrated a comparison of FSWT and DFIG. [13] reports that the voltage fluctuations, caused by variations in the wind speed, are significant when FSWT are installed. [14] reports that, when DFIG are installed to the grid, then the voltage fluctuations are negligible. The response of the wind turbine to large disturbances in the power grid is rarely investigated in the literature [10]. In 2004, [15] presented one of the more in depth considerations of the integration of wind turbines to the power grid. In [15], Sun concluded that the DFIG wind turbine model successfully returned to normal operating condition after the clearing of a single phase to ground fault. There remains significant amount of research to be completed on the full effects of the integration of wind turbines to the power grid.

## 1.3 Voltage Stability Analysis

Another area of research that is gaining increased attention is steady state and transient voltage stability analysis. This is a result of a recent initiative to operate the power system closer to its voltage stability limit. From 1996 to 2001, electrical energy consumption increased by 2.1% per year [1]. However, electrical generation installation expanded by 1.0% and transmission capacity increased by only 0.8% [1]. As a consequence, grid reliability is becoming an electric utility problem. For example, large scale voltage collapses have recently occurred in Sweden (December 27, 1983), France (January 12, 1987), Japan (July 23, 1987) [16] and most recently in Canada and the United States of America (August 14, 2003) [17]. Between 1984 and 2000, there have been 11 outages affecting more than 4000 MW in North America [17]. General principles of voltage collapse can be formulated which were common to all examples. A system enters an unstable state when the operating conditions change, due to a disturbance or increased load demand, which results in an uncontrollable decline of the voltage. Heavily stressed systems are more susceptible to voltage stability problems. Their lack of capacity to deliver reactive power is the main factor of voltage instability. The operating conditions may change for a variety of reasons; however, the cause of the voltage

collapse is inherent in the weakness of the grid. Therefore, voltage stability issues have generated significant consideration.

Voltage stability analysis is becoming essential for power system planning and operation. The purpose of voltage stability analysis is to determine the maximum power that can be transmitted to the load while the system is in transient conditions. Power-voltage (PV) curves (or alternatively reactive power-voltage, QV curves) are calculated for each relevant contingency. Much of the recent literature discusses the methods to compute the PV curves. Direct computation of PV curves by solving the equations of the load flow, known as continuous load flow solution, is considered to be the most accurate and reliable method to determine the post contingency margins [18]. However, the method is complicated, time consuming and computationally demanding [19]. Faster solution techniques are necessary for practical applications. The full coupled Newton's iterative procedure was studied by [20]. They found that the Jacobian matrix became ill conditioned near the loading limit. This produced numerical instability in Newton's method and its variant the fast decoupled Newton's method. Chang et. al. [21] proposed a curve fitting technique that required the calculation of three points of the PV curve. Although the lower portion of the PV curve has no practical significance, the method of indices compares the load flow solution of the upper PV curve to the lower PV curve. This provides the relative stability of a particular operating point [22]. In 2004, Sato published a paper discussing the maximum loading limit in power systems [18]. Sato utilized a Lagrange optimization method of iterative Newton-Raphson load flow solutions. This technique has the advantage of rapid convergence. The determination of the critical point of the PV curve requires the solution of a system of non-linear equations. Therefore, it is difficult to establish a high-speed universal method for all contingencies.

There are three more chapters that follow. Chapter 3 describes the mathematical theory of the models in this thesis. Models for wind turbine generators, transmission lines and loads will all be addressed. Chapter 4 presents the case studies that were performed. Both steady state and transient conditions were simulated in a dynamic continuous time simulation program. The voltage stability of the system was determined for each case. The conclusions from this work are outlined in chapter 5.

# 2. Theory

There are three main components of the system: the wind turbine generators, the transmission lines and the load. Each of these components is described below. The equations that govern the models are demonstrated. This provides a mathematical foundation for the results that will be presented.

## 2.1 Wind Turbine Generators

### 2.1.a FSWT Model

FSWT consist of an induction generator with a squirrel cage rotor. Their robust nature has been known for decades [4]. Their low cost and minimal maintenance are the characteristics that are most attractive.
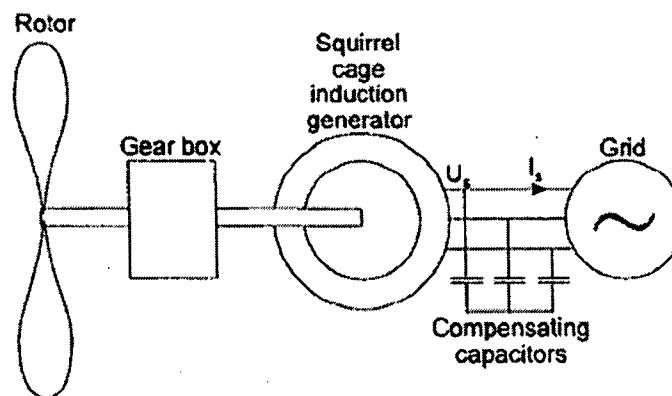


**Figure 1: Fixed speed wind turbine with direct grid coupling [23].**

The rotor is connected to a gearbox which changes the low rotational speed of the turbine blades to a high rotational speed on the generator side. One of the major disadvantages of the integration of FSWT is the reactive power consumption required. This is especially important during start up and under weak grid conditions. Most FSWT are equipped with a thyristor controlled inrush current limiter, known as a soft starter. The thyristor limits the inrush current to typically 1.5 times the nominal operating current. After synchronisation is attained, the thyristor is shorted by the grid's circuit breakers. The soft

starter comes at the expense of a brief but significant 5th harmonic in the power system. Under weak grid conditions, shunt capacitors are installed near the wind turbine to provide reactive power. This is commonly done in wind turbine installations.

The FSWT model is a fourth-order representation of the electrical part and a second-order representation of the mechanical part of an induction machine. It is implemented in a phasor simulation program. Below are the equations for the FSWT [24]:

## Electrical System



$$V_{qs} = R_s i_{qs} + \frac{d}{dt}\varphi_{qs} + \omega\varphi_{ds}$$

$$V_{ds} = R_s i_{ds} + \frac{d}{dt}\varphi_{ds} - \omega\varphi_{qs}$$

$$V'_{qr} = R'_r i'_{qr} + \frac{d}{dt}\varphi'_{qr} + (\omega - \omega_r)\varphi'_{dr}$$

$$V'_{dr} = R'_r i'_{dr} + \frac{d}{dt}\varphi'_{dr} - (\omega - \omega_r)\varphi'_{qr}$$

$$T_e = 1.5 p(\varphi_{ds} i_{qs} - \varphi_{qs} i_{ds})$$

where

$$\varphi_{qs} = L_s i_{qs} + L_m i'_{qr}$$

$$\varphi_{ds} = L_s i_{ds} + L_m i'_{dr}$$

$$\varphi'_{qr} = L'_r i'_{qr} + L_m i_{qs}$$

$$\varphi'_{dr} = L'_r i'_{dr} + L_m i_{ds}$$

$$L_s = L_{ls} + L_m$$

$$L'_r = L'_{lr} + L_m$$

(1)

## Mechanical System

$$\frac{d}{dt}\omega_m = \frac{1}{2H}(T_e - F\omega_m - T_m)$$

$$\frac{d}{dt}\theta_m = \omega_m$$

where the subscripts are defined as follows,

| Subscript | Definition |
|-----------|------------|
| d | d axis quantity |
| q | q axis quantity |
| r | Rotor quantity |
| s | Stator quantity |
| l | Leakage inductance |
| m | Magnetizing inductance |

**Table 2: Definition of subscripts for equation 1.**

All electrical variables and parameters are referred to the stator. This is indicated by the prime superscript in Equation (1). In addition, the stator and rotor quantities are modelled in the direct-quadrature (dq) axis. The dq reference frame is rotating at synchronous speed with the q-axis 90 degrees ahead of the d-axis. The d-axis coincides with the maximum of the stator flux. This implies that $V_{qs}$ equals the terminal voltage and $V_{ds}$ equals zero. The prime mover for the FSWT is a variable wind speed obtained from [12]. There are four main assumptions. First, all rotating masses are represented by one element, known as a lumped-mass representation. A rigid shaft is considered and thus the resulting torsional forces are neglected. Thirdly, a quasi-static approach is used for the description of aerodynamic part of the wind turbine. Finally, magnetic saturation in the FSWT is neglected. The FSWT model is suitable for the studies of interest.

### *2.1.b DIFG Model*

The DFIG wind turbine design provides distinct advantages over the FSWT generators. The DFIG is a wound rotor induction generator with the stator connected to the grid. It is characterised by an AC-DC-AC link between the rotor and the grid. This provides the system with important control features. Firstly, the converter link enables the DFIG to operate at variable speeds. The use of a control scheme on forced commutated insulated gate bipolar transistor (IGBT) converters allows for the frequency of the converter to be superimposed on the frequency of the rotating field of the rotor. This enables for more efficient conversion of the wind power. Therefore, for a given wind speed, the DFIG will produce more electrical power than the FSWT. Furthermore,
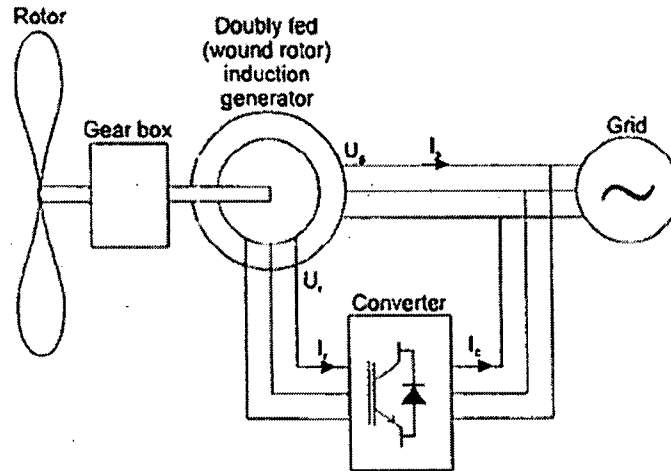
**Figure 2: Doubly fed induction generator wind turbine design [23].**

variable speed wind turbines are much less likely to loose synchronism with the grid. The converter link also permits the control of reactive power. The reactive power consumed by the generator is compared to a reference value. A proportional integral (PI) controller is used to reduce any difference. This imposes less capacity demand from the power grid. These advantages result in an increased cost of the DFIG system. Also, there are more components to be maintained which means that the DFIG is less robust. However, these drawbacks are deemed to be justifiable for the increase in power quality produced by the DIFG.

Equation (1) applies to the DFIG model as well. In addition, there are two important control schemes. The first is the maximum power tracking for a selected wind speeds. In Figure 3, the tracking characteristic is defined by four points: A, B,C, and D. From zero turbine speed to the turbine speed at point A, the output power is zero. Point A and point B are connected by a straight line. Between point B and point C, the characteristic is the locus of the maximum power output for a given turbine speed. This ensures that the maximum amount of power is extracted from the wind. Point C and point D are linked by a straight line. From point D onward, the power output is fixed at 1 p.u. This is achieved by pitch angle control system. The pitch angle is kept at zero degrees until the speed at point D is reached. Beyond point D, the pitch angle is proportional to the speed deviation from point D. See Figure 4.
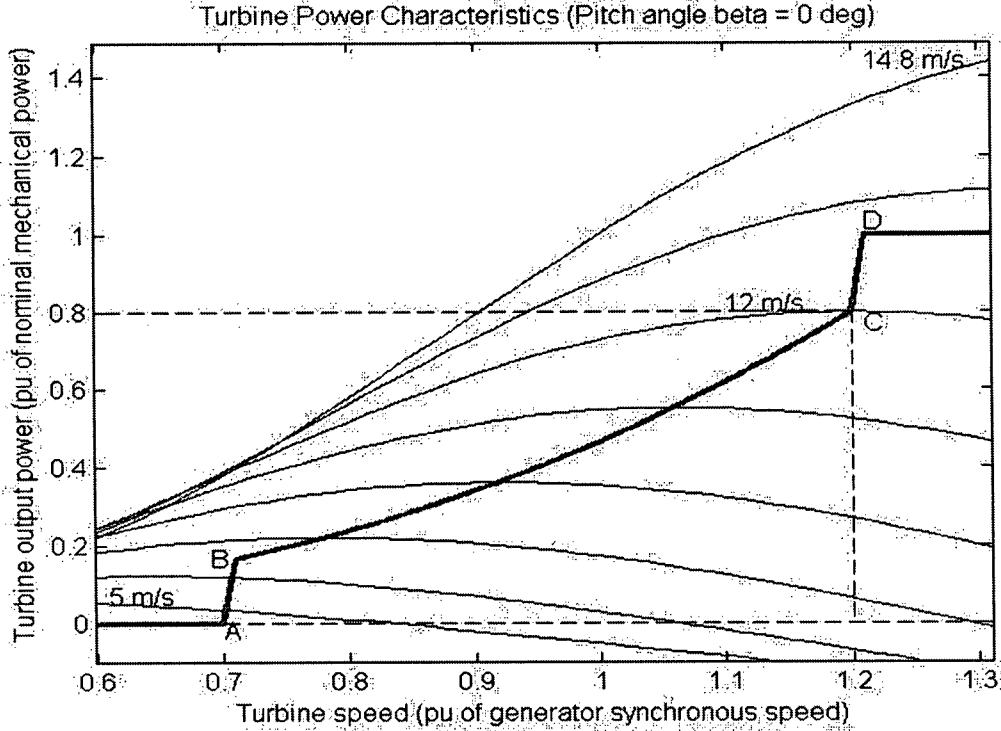
**Figure 3: DFIG power characteristics for selected wind speeds [24].**
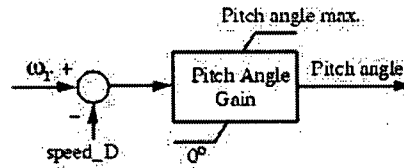


**Figure 4: Pitch control scheme for DFIG [24].**

The second control system is used for the rotor side converter. The purpose of this controller is to regulate the voltage and reactive power transferred to the grid. The reactive power is exchanged between the rotor side converter and the grid through the generator. The power error, defined by the difference between electrical output power measured at the wind turbine terminals and the reference power obtained from the tracking characteristic, is brought to zero by a proportional-integral (PI) regulator. This sets the value for $I_{qr\_ref}$, which is the current required by the rotor. $I_{qr\_ref}$ is compared to $I_{qr}$ and the error is set to zero by another PI controller. The output of this controller is $V_{qr}$. This voltage is applied across the rotor such that the appropriate current $I_{qr\_ref}$ is induced. See Figure 5

10
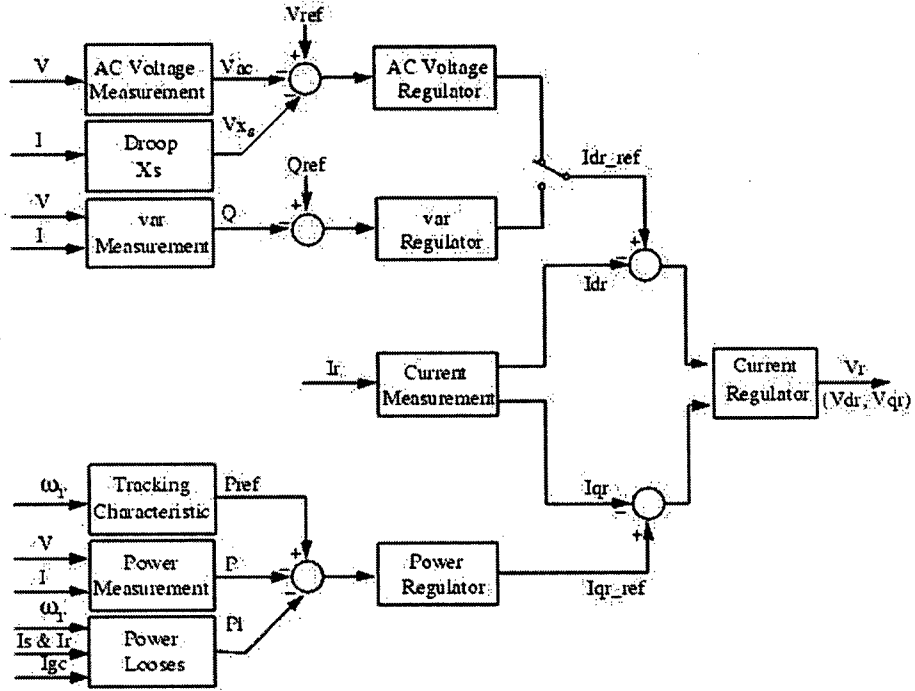
**Figure 5: Rotor side converter control system for the DFIG [24].**

The description above serves to compare FSWT and DFIG. It is clear the DFIG wind turbine is a more complicated system than the FSWT. Some notable features that distinguish them are the AC/DC/AC link between the grid and the rotor, tracking characteristic of the maximum power extractable from the wind and the reactive power control system. The purpose of the case studies is to determine to what extent these additional features of the DFIG improve the power quality and penetration limit.

## 2.2 Transmission Lines

### 2.2.a Basic LR Circuit

Consider the simple LR circuit in Figure 6 where the inductance L and the resistance R are in series with a DC voltage source $V_o$ and a switch. It is assumed that all other resistances in the circuit are negligible compared to R and that all other inductances are negligible compared to L. Initially the switch is open. Immediately after the switch is closed the current is still zero but it is increasing at a rate dI/dt. This creates a voltage LdI/dt on the inductor. Applying Kirchhoff's law gives equation (2):

11
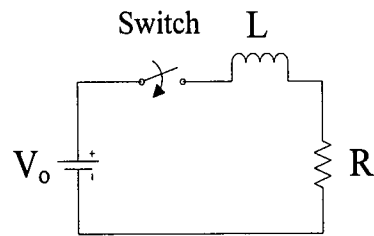
**Figure 6: LR circuit.**

$$Vo - IR - L \frac{dI}{dt} = 0 \qquad (2)$$

The solution to the ordinary differential equation is well known:

$$I(t) = \frac{Vo}{R}(1 - e^{-t/\tau}) \qquad (3)$$

where $\tau$ is the time constant,

$$\tau = \frac{L}{R} \qquad (4)$$

At $t=\tau$, the current is at 63% of its maximum value ($I_{max}=V_o/R$). Below is a graph of the current versus time for the LR circuit with $V_o=10$ volts, $R=10\ \Omega$ and $L=12$ H.
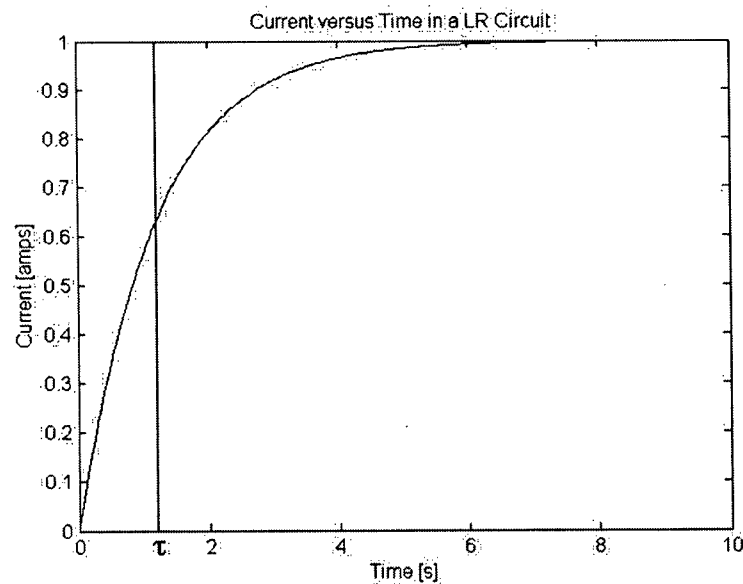


**Figure 7: Current versus time for a LR circuit.**

In the LR circuit above, the inductor represents a basic transmission line model and the resistor represents a basic load. The purpose of this simple example is to demonstrate the importance of transient analysis. Transient analysis allows for the calculation of the time necessary for the system to reach a final steady state value for the current. Notice that for a system with a larger L, the time required to reach steady state would be increased; however, the final steady state value of the current would remain the same. Here the system consists of simple linear components. If the system contained dynamic loads then the increased time to reach steady state may be important for voltage stability. Therefore, steady state analysis provides the initial operating point and the final operating point if the system moves in a slow (quasi-steady state) manner. Transient analysis determines if, and how, the system arrives at the final operating point.

### 2.2.b Constant Power Factor PV Curves

Power-voltage (PV) curves are essential in the voltage stability of the power system. Constant power factor PV cures represent static steady state curves for voltage stability. Their accuracy at predicting transient voltage stability will be examined. To obtain these curves, the system is represented by Figure 8. The derivation of the constant power factor PV curves follows.
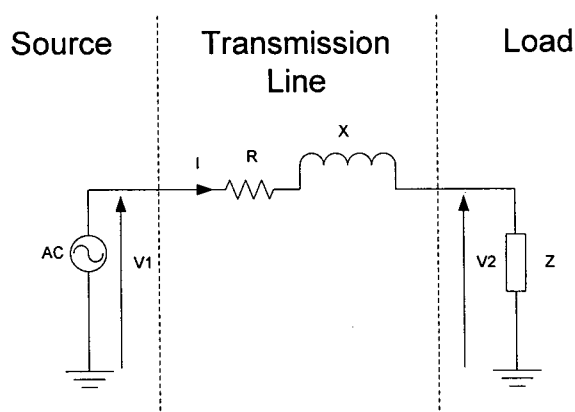


**Figure 8: Simplified circuit diagram for constant power factor PV curves.**

Notice that the transmission line is represented by an inductor and a resistor in series. This is acceptable because the power lines that are modeled are less than 80 km long. As transmission lines increase in length, the shunt capacitance needs to be taken in to

account. For transmission lines that are between 80 km and 150 km, then a nominal $\pi$ circuit is necessary to accurately describe the system. When transmission lines are longer than 150 km, then the equivalent $\pi$ circuit is needed. This model includes correction terms to the nominal $\pi$ circuit. A factor of sinh($\gamma$l) is included for the total series impedance and a factor of tanh($\gamma$l) is present for the total shunt admittance, where $\gamma \approx$ j$\omega\sqrt{(LC)}$ and l = the length of the line. These correction factors account for the distributed effects of the parameters [16]. If we plot the phasor diagram of the previous circuit we obtain the following picture.
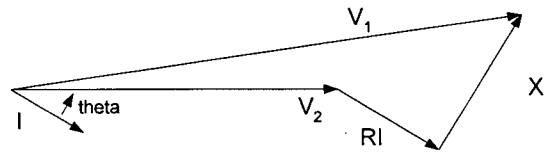


**Figure 9: Phasor diagram of the constant power factor PV curves.**

$$\overline{V}_1 = \overline{V}_2 + \overline{RI} + j\overline{XI} \tag{5}$$

In magnitude,

$$V_1^{\,2} = (V_2 + RI\cos\theta + XI\sin\theta)^2 + (XI\cos\theta - RI\sin\theta)^2 \tag{6}$$

Also,

$$I = \frac{P}{V_2\cos\theta} \tag{7}$$

Putting these equations together, one finally obtains the following equation,

$$V_2^{\,4} + V_2^{\,2}(2RP + 2\tan\theta - V_1^{\,2}) + (RP)^2 + (XP)^2 + (RP\tan\theta)^2 + (XP\tan\theta)^2 = 0 \tag{8}$$

A simplification can be made,

$$
\begin{aligned}
&V_2^{\,4} = V_n^{\,2} \\
&a = 1 \\
&b = 2RP + 2\tan\theta - V_1^{\,2} \\
&c = (RP)^2 + (XP)^2 + (RP\tan\theta)^2 + (XP\tan\theta)^2
\end{aligned}
\tag{9}
$$

Hence,

14

$$aV_n^2 + bV_n + c = 0 \qquad (10)$$

The solution of this equation gives us:

$$V_2 = \sqrt{\frac{-b \pm \sqrt{b^2 - 4ac}}{2a}} \qquad (11)$$

The power factor is kept constant, and the PV curves are plotted by varying the power to the load and calculating the voltage.

### 2.2.c Equivalent Circuit of Induction Machine PV Curves

The equivalent circuit of induction machine PV curves will be compared to the constant power factor PV curves at determining steady state and transient voltage stability. It is anticipated that the additional detail in the equivalent circuit of induction machine PV curves will provide sufficient accuracy to predict transient voltage stability. The system is represented by Figure 8 with one significant change. The load is no longer a constant power factor load. Instead, it is represented by the equivalent circuit of induction machine. The circuit is solved by the following equations.

### Equivalent Circuit of an Induction Machine



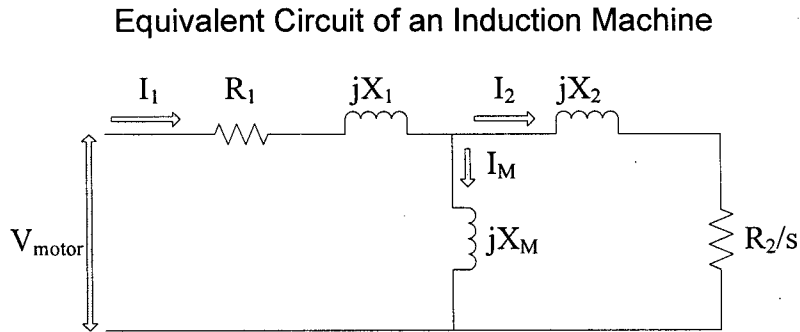Figure 10: Equivalent circuit of an induction machine.

$$Z_2 = \frac{R_2}{s} + jX_2$$

$$Z_{motor} = \frac{jZ_2 X_M}{Z_2 + jX_M} + R_1 + jX_1$$

$$I = \frac{V_{phase}}{(Z_{line} + Z_{motor})} \qquad (12)$$

$$V_{motor} = Z_{motor} I$$

$$Power = real(abs(I)^2 Z_{motor})$$

15

The PV curves are created by varying the slip (s), from 0 to 1. The comparison of the two types of PV curves will be examined in the following chapter.

## 2.3 Load Models

### 2.3.a Exponential Load Model

The exponential load model is described by the following equation [25].

$$P = P_o \left( \frac{V}{V_o} \right)^{\alpha} \tag{13}$$

where $\alpha=0.2$ for a full-load induction machine. This is a steady state model describing an induction machine. It will be used to establish that the system is steady state stable. It will also be compared to the dynamic load model at predicting steady state and transient voltage stability.

### 2.3.b Dynamic Load Model

The dynamic load model is described by a sixth-order induction machine model displayed in Equation (1). This is sufficient to capture the transients of the system. The induction motor is operated with a constant load torque of approximately 1 p.u. The dynamic load model will be used to determine the transient voltage stability of the system. It will be compared to the exponential load model for steady state and transient voltage stability.

# 3. Case Studies

In this section, several cases are examined which demonstrate the potential problems of integrating wind turbines to the power grid. These potential problems are avoidable after careful consideration of the system. Therefore, proper analysis of the system will ensure reliable integration of wind power. Two types of studies were conducted: 1) studies a three phase fault on the strong line, and 2) studies that involve the continuous steady state operation of the wind turbine with typical wind variations. Type one studies (Cases 1 and 2) will monitor the voltage stability in an extreme situation. They will compare the static load model to a dynamic load model. As well, the accuracy of constant power factor PV curves will be compared to the equivalent circuit of induction machine PV curves at predicting voltage collapse. The effect of a weak line (WL), between the grid and the load, will be compared to a medium strength line (ML). Other factors which will be varied are: the post fault re-closing times and the load composition. Type two studies (Cases 3 and 4) will focus on the continuous operation of wind turbines. These cases explore the voltage stability of FSWT compared to DFIG wind turbines. The dependence on the wind turbines will be increased to determine their penetration limit.

## 3.1 Case 1

In case 1, the wind turbine is represented by a constant voltage source. It will supply 20% of the total power. It is connected to the load by a strong line (SL). The grid is also represented by a constant voltage source but it is connected to the load by a WL. For concreteness, a distribution voltage level was chosen for the power lines. This is a typical voltage level at the point of common connection between the grid and the wind power. The distribution lines are compensated by shunt capacitors. The load is an induction machine, with a squirrel cage rotor, rated at 10MVA and 6.9kV. This represents an aggregate of many smaller loads. Breakers have been installed at each end of the distribution lines. When opened, they represent a sudden reduction in the wind speed effectively creating a three phase fault on the SL. The effects of a three phase fault

on the SL after two seconds are examined (Case 1A). Several quantities were monitored: the power through each line, the load bus voltage, the stator current and the percent voltage drop across the WL. The effects of re-closing the breakers after the fault has been cleared (Case 1B) and varying the percentage of resistive load (Case 1C) are demonstrated. Below is a diagram of the system.
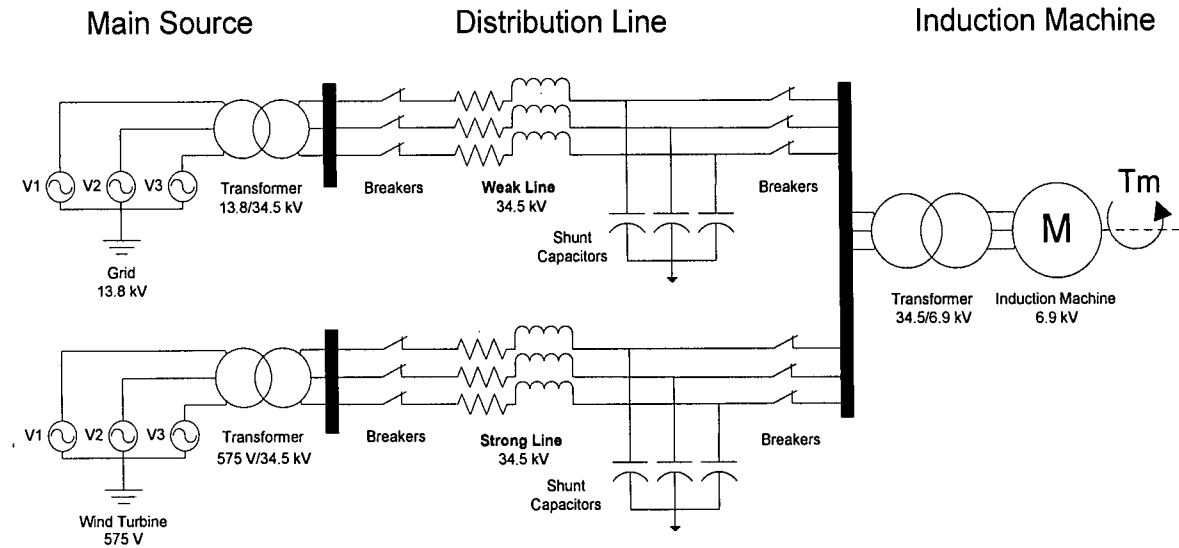


Figure 11: Diagram of case 1.

|  | Medium Line | Strong Line | Transformer 13.8/34.5kV | Transformer 575V/34.5kV | Transformer 34.5/6.9kV |
|---|---|---|---|---|---|
| Line Length L | 66 km | 25 km | N/A | N/A | N/A |
| Reactance X | 32.75 Ω | 12.50 Ω | 1.73 Ω | 8.11 Ω | 1.54 Ω |
| Resistance R | 3.28 Ω | 1.25 Ω | 0.10 Ω | 0.45 Ω | 0.09 Ω |
| Shunt Capacitor Q | 3.8 MVAR | 2.0 MVAR | N/A | N/A | N/A |
| Power Base S | N/A | N/A | 12 MVA | 2.2 MVA | 12 MVA |

Table 3: System parameters for case 1. X/R ratio obtained from [1] and [16].

### 3.1.a Case 1A

To assess the voltage stability of the system, constant power factor PV curves are produced. This is the most commonly used type of PV curve. The more stable PV curve represents both lines are operational and the less stable PV curve represents only the WL is operational. Superimposed on the PV curves is the exponential load model for the
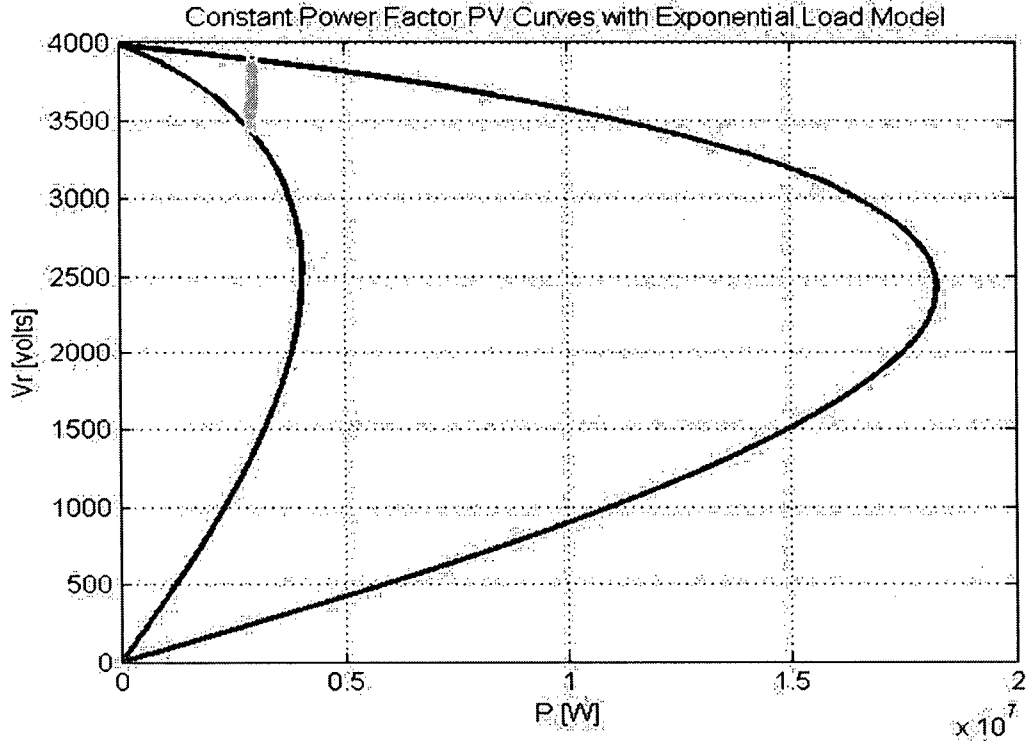
18

**Figure 12: Constant power factor PV curves with exponential load model for case 1A.**

induction motor of the system. The exponential load model is frequently used. It is a static steady state representation of an induction machine. By examining Figure 12, one can determine if the system will be stable or unstable in steady state. In this case, the load model crosses the stable region of each PV curve. This means that, given appropriate initial conditions, the system is steady state stable. In addition, the system is steady state stable regardless if both lines were initially operational or if only the WL was initially operational. Furthermore, if the operating conditions of the system were to vary slowly, in a quasi steady state manner, from one PV curve to the other then the system would follow the exponential load model depicted in Figure 12. Again the system would be deemed stable. Based on Figure 12, it is assessed that the system is steady state stable and quasi steady state stable. In the following results, it will be examined if this static steady state analysis correctly predicts the transient behaviour of the system.

The system is implemented in a software program that is capable of performing continuous time transient simulations. In addition, the software program models the induction motor dynamics. After two seconds, the SL is disturbed by a three phase fault. Three phase faults are rare but they represent the worst situation for voltage stability.
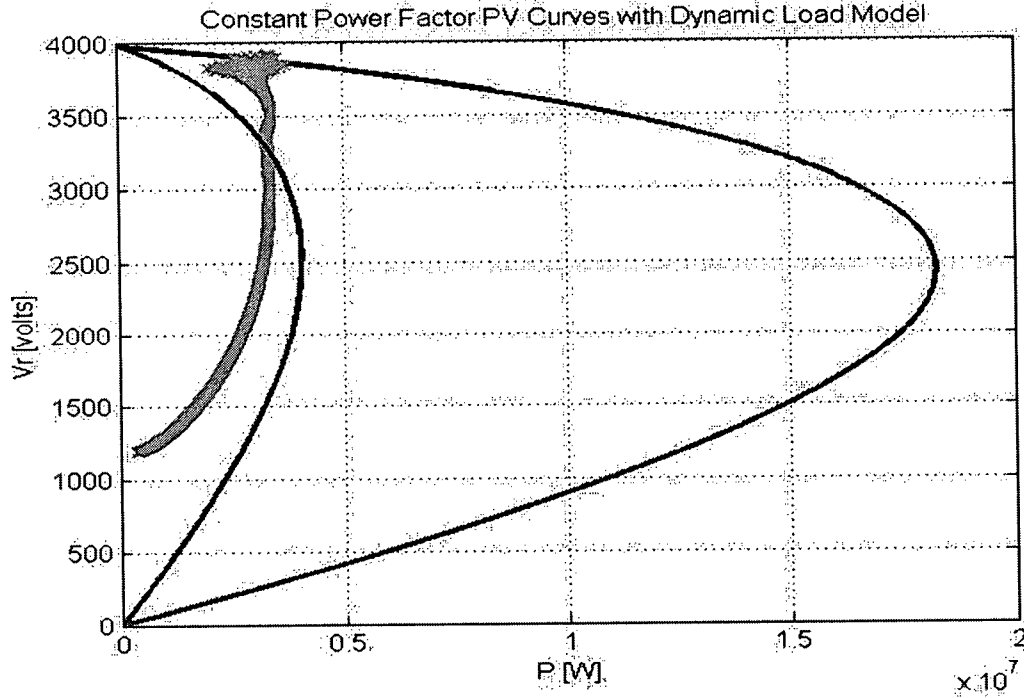
19

**Figure 13: Constant power factor PV curves with dynamic load model for case 1A.**

In this case, it is assumed that attempts at re-closing the breakers were unsuccessful. The operating point in the PV plane is plotted in Figure 13. It demonstrates that a voltage collapse occurs in the system as a result of the three phase fault with unsuccessful re-closing. Two comments need to be made at this point. First, the results from the dynamical load model (Figure 13) contradict the prediction made by the exponential load model with the constant power factor PV curves (Figure 12). This discrepancy needs to be reconciled. Secondly, it is peculiar that the operation point in the PV plane crosses the stable region of the weaker constant power factor PV curve; however, the system does not reach a stable point. Instead the system experiences a voltage collapse. This indicates that a more accurate PV curve is needed to describe the transient stability of the system when the system operates near the nose of the PV curve.

20

To address the first point, a plot of both load models is presented in

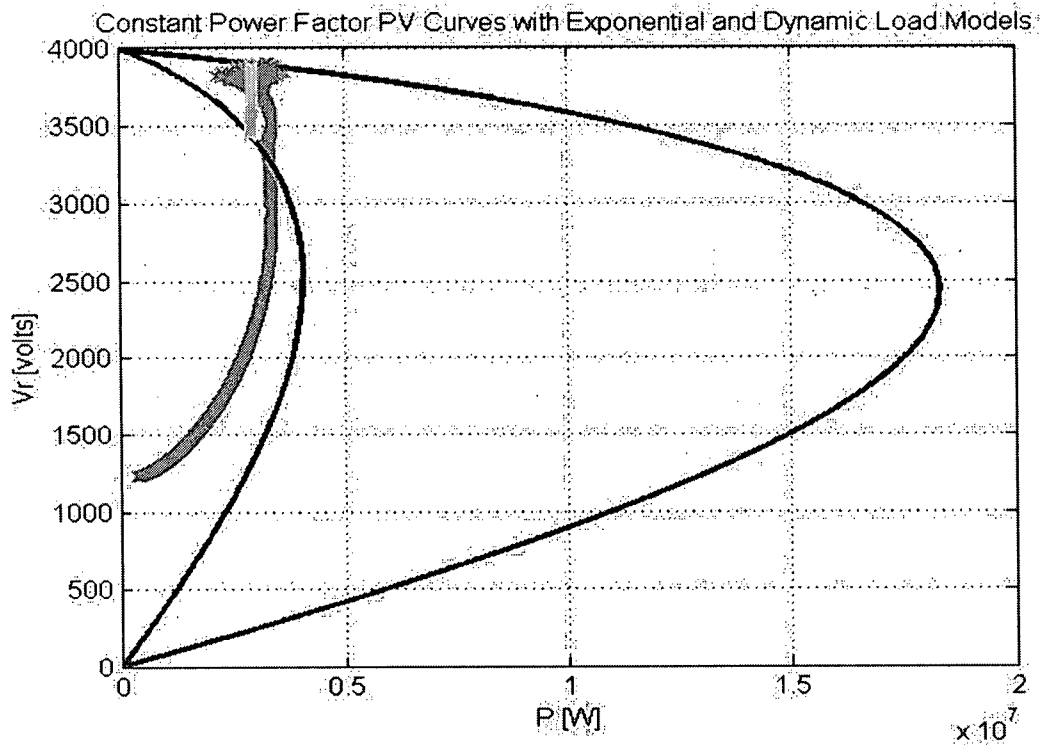Constant Power Factor PV Curves with Exponential and Dynamic Load Models
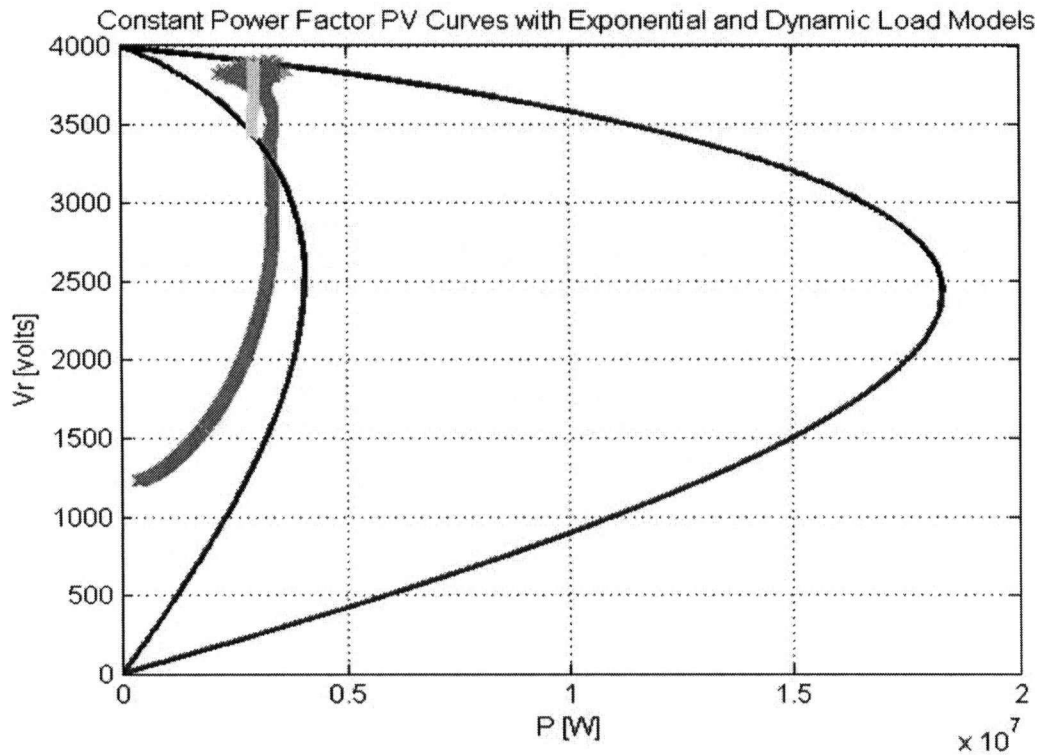


Figure 14. It demonstrates that the exponential load model predicts the system to be more stable than the results from the dynamical load model. Thus, determining that a system is steady state stable does not necessarily imply that the system is transient stable as well. For a particular system, the exponential load model could predict stability but the dynamical load model would reveal a voltage collapse in the system. Therefore, it is important                                                                                                                                                             to

To address the first point, a plot of both load models is presented in



Constant Power Factor PV Curves with Exponential and Dynamic Load Models

Figure 14. It demonstrates that the exponential load model predicts the system to be more stable than the results from the dynamical load model. Thus, determining that a system is steady state stable does not necessarily imply that the system is transient stable as well. For a particular system, the exponential load model could predict stability but the dynamical load model would reveal a voltage collapse in the system. Therefore, it is important                                                                                                    to
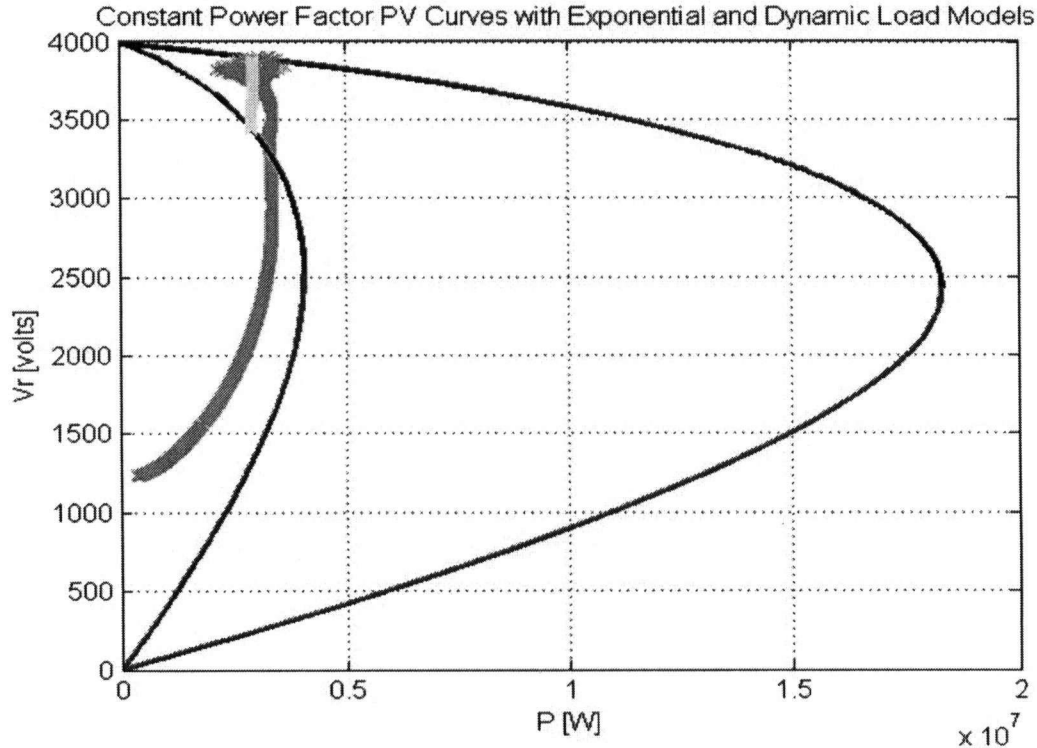
**Figure 14: Constant power factor PV curves with exponential and dynamic load models for case 1A.**

consider the dynamics of the system when examining transient voltage stability. This reconciles the difference between both models.

The second point can be addressed by plotting more detailed PV curves. To reiterate, in Figure 13, the dynamic load model crossed the stable region of the weak constant power factor PV curve. Nevertheless, the dynamic load model predicts a voltage collapse. This implies that the constant power factor PV curves are not accurate when assessing transient stability near the nose of the PV curve. Therefore, a graph of the equivalent circuit of induction machine PV curves and the exponential load model has been produced. In Figure 15, the exponential load model crosses the stable region of both PV curves. One would determine that the system would be steady state stable and quasi steady state stable. This is the same conclusion as before when the constant power factor PV curves were plotted. Hence, the equivalent circuit of induction machine PV curves correctly predict the steady state voltage stability of the system. However, it is known that the dynamic load model predicts a voltage collapse under transient circumstances. It is important to establish if the equivalent circuit of induction machine PV curves correctly predict the transient voltage stability.
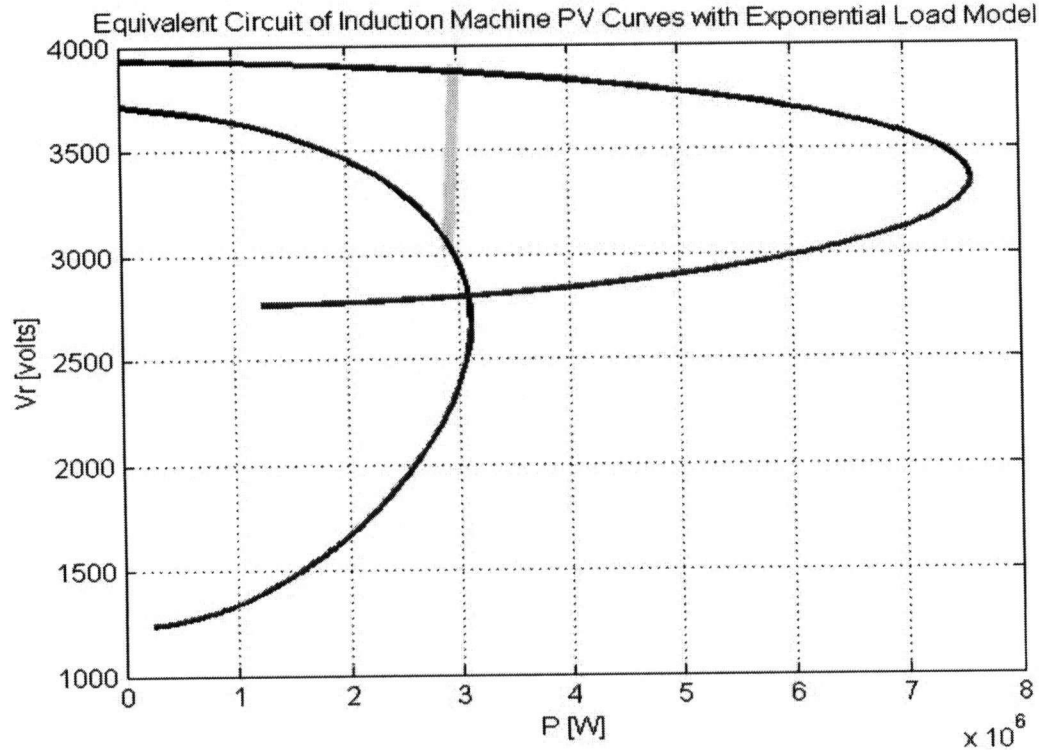
Figure 15: Equivalent circuit of induction machine PV curves with exponential load model for case 1A.

In Figure 16, the dynamic load model is depicted with the equivalent circuit of induction machine PV curves. The dynamic load model does not cross the weak PV curve. A voltage collapse is observed. This is an example of a system where the use of detailed PV curves and of a dynamic load model is the only combination considered that accurately describes the transient voltage stability of the system. It is critical to correctly represent the system in order to avoid unexpected voltage collapses. In addition, as distribution lines are being pushed closer to their limits, the operation point moves closer to the nose of the PV curves. Figure 16 clearly demonstrates the importance of detailed PV curves and load models. Figure 17 displays both the exponential load model and the dynamic load model with the equivalent circuit of induction machine PV curves for comparison. Once again, it is clearly displayed that the exponential load model intersects the stable region of the weak equivalent circuit of an induction machine PV curve whereas the dynamic load model does not intersect the stable region of the weak equivalent circuit of an induction machine PV curve. This emphasises the importance of detailed PV curves and dynamic load models to accurately predict the transient voltage stability of a system.
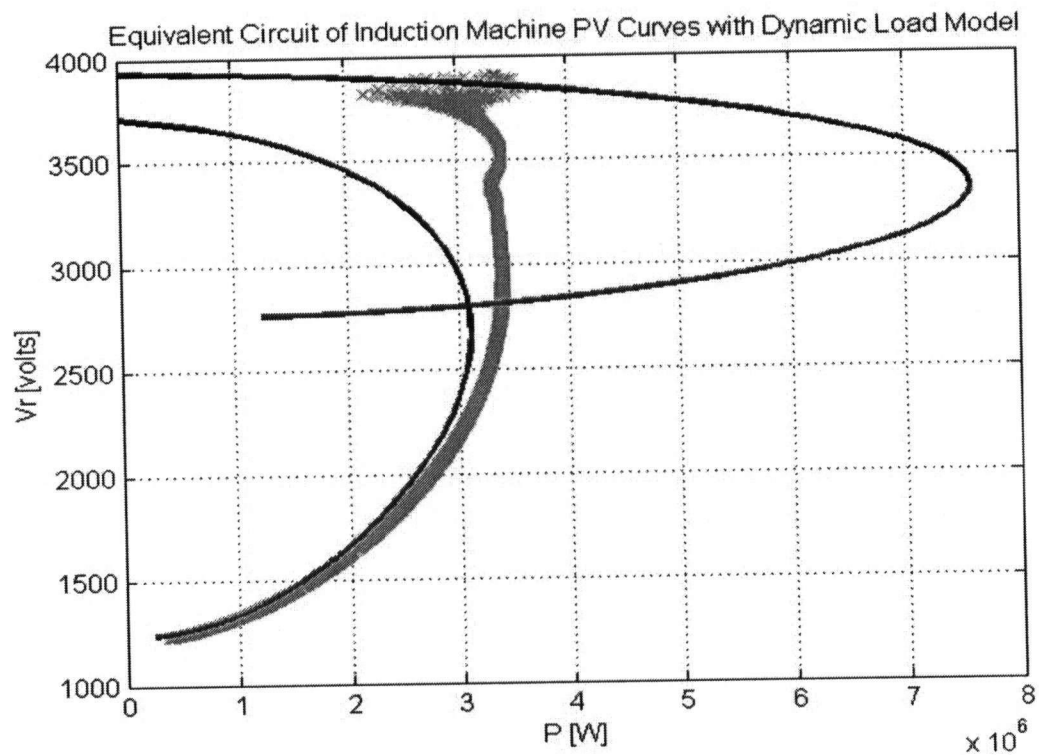
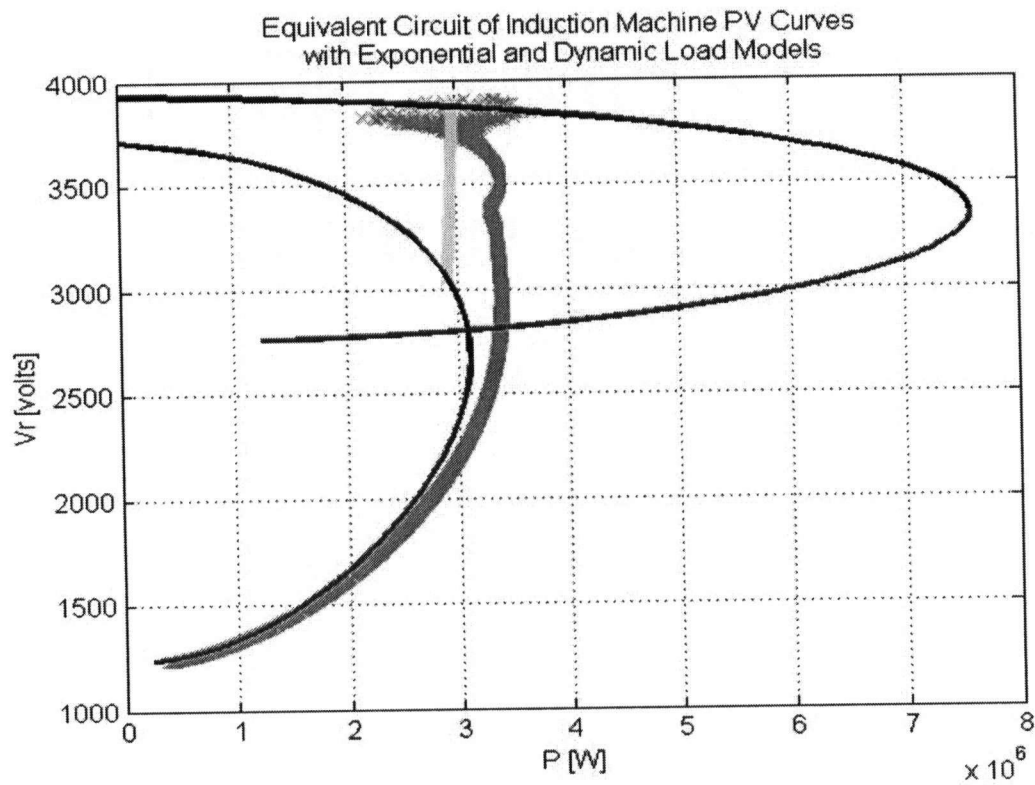**Figure 16: Equivalent circuit of induction machine PV curves with dynamic load model for case 1A.**



**Figure 17: Equivalent circuit of induction machine PV curves with exponential and dynamic load models for case 1A.**

The graph below (Figure 18) allows for a clear comparison between the models that have been discussed to this point. Both, the constant power factor PV curves and the equivalent circuit of induction machine PV curves, are presented; and in addition, the exponential and dynamic load models are plotted together. One can observe the significant difference between the two PV curve system representations. These differences can affect the predicted voltage stability of a given system. This case is an example of such a system where the use of detailed PV curves and of a dynamic load model is the only combination considered that accurately describes the voltage stability of the system. This case represents two types of situations: 1) a sudden reduction in wind speed yielding no power produced by installed wind turbines, and 2) a three phase fault disturbing the strong line with unsuccessful re-closing. As the grid is pushed closer to it limits, the operation point of power systems occurs closer to the nose of the PV curves. Therefore, these differences in the models become increasingly important.
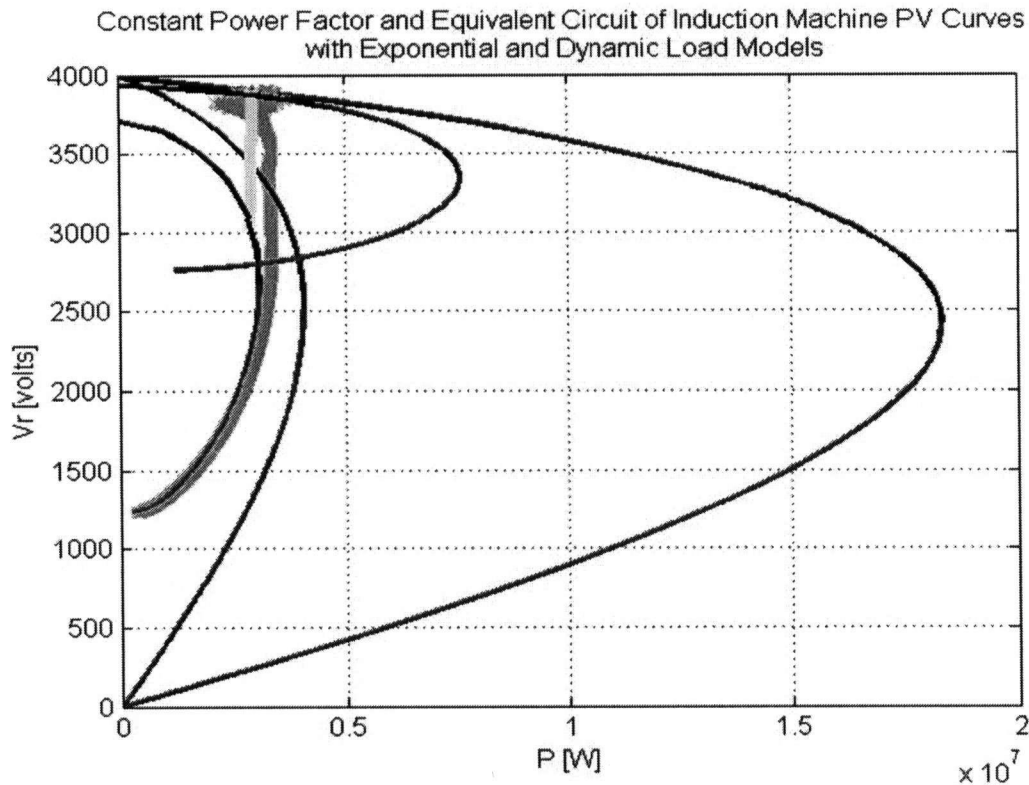


**Figure 18: Constant power factor and equivalent circuit of induction machine PV curves with exponential and dynamic load models for case 1A.**

It is useful to examine the equivalent circuit motor model and determine the exact cause of crash of the motor. The inertia constant of the motor is the first quantity which will be investigated. The inertia constant is a quantity modeled in the dynamic load model. It is one of the distinguishing features between the two load models. For the results presented above, the inertia constant of the motor is H = 3 seconds. The inertia constant is varied to two extreme values: H = 0.1 seconds and H = 10 seconds. Changing the inertia constant of the motor will be monitored by the magnitude of the voltage at the load bus. Below (Figure 19, Figure 20, Figure 21) are the graphs of the results obtained. Based on the results, the inertia constant of the motor is not responsible for the voltage collapse of the system. In other words, regardless of the motor inertia constant a voltage collapse will not occur for this system. It is interesting to note the effect of the inertia constant. From the figures below, one can observe that as the inertia constant of the motor increases, then the time required to experience the voltage collapse increases as well. This is useful because it may determine the time allowed for re-closing after a fault has occurred. Therefore, using a motor with a large inertia constant will provide the most time for re-closing after a fault has occurred.
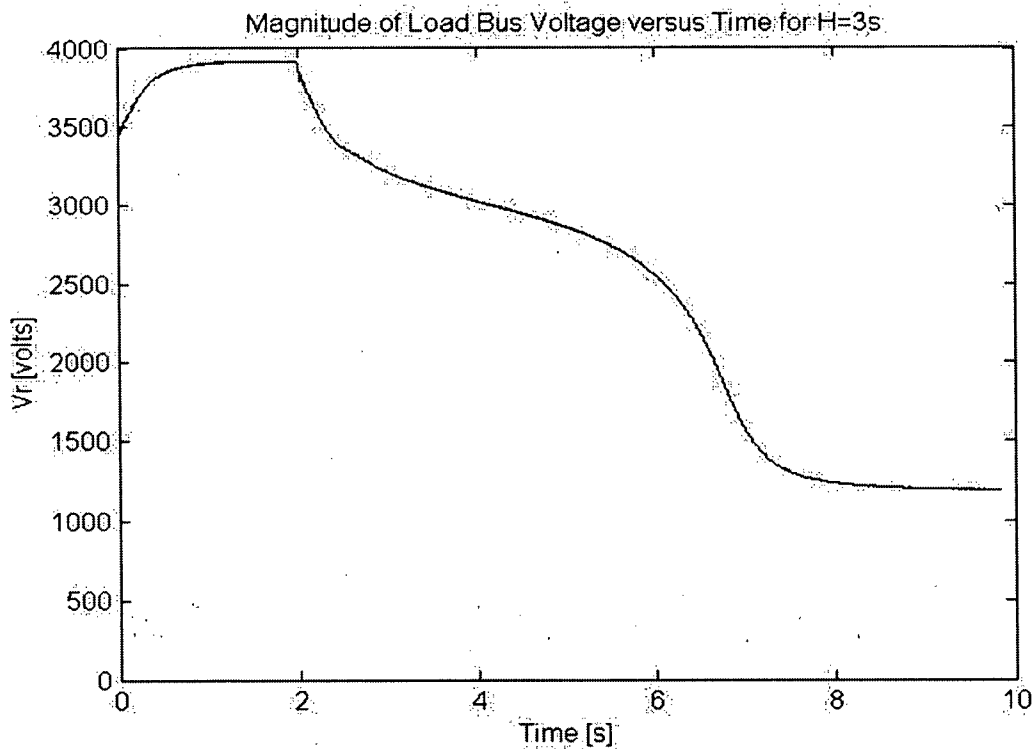


Figure 19: Magnitude of the load bus voltage versus time with H=3s for case 1A.
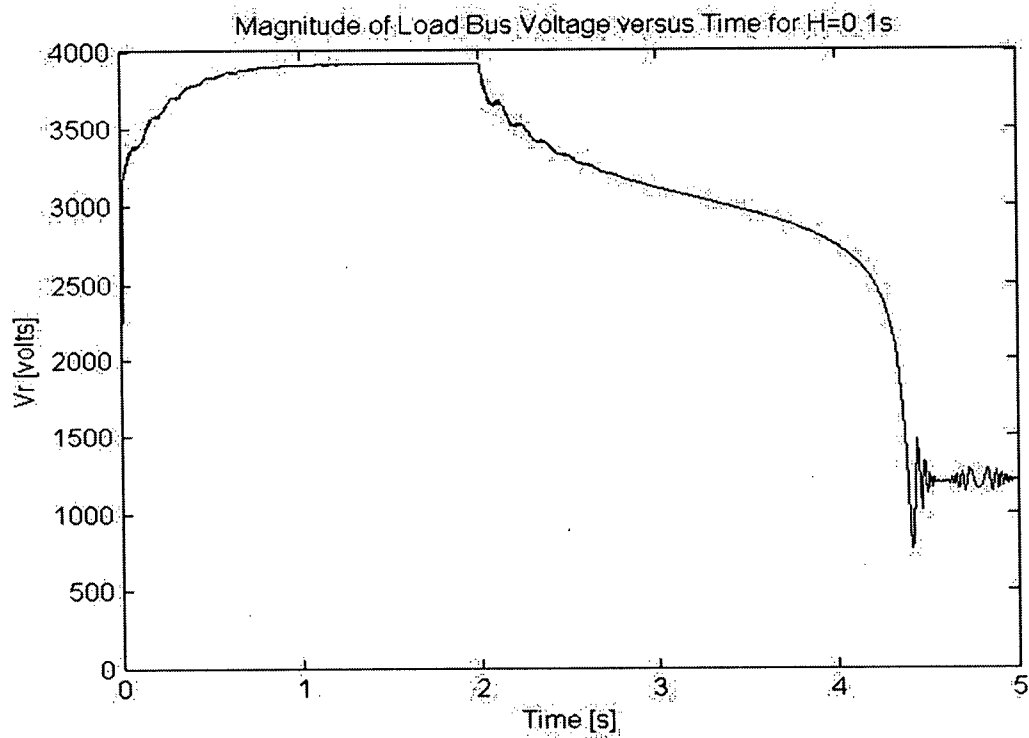
**Figure 20: Magnitude of the load bus voltage versus time with H=0.1s for case 1A.**
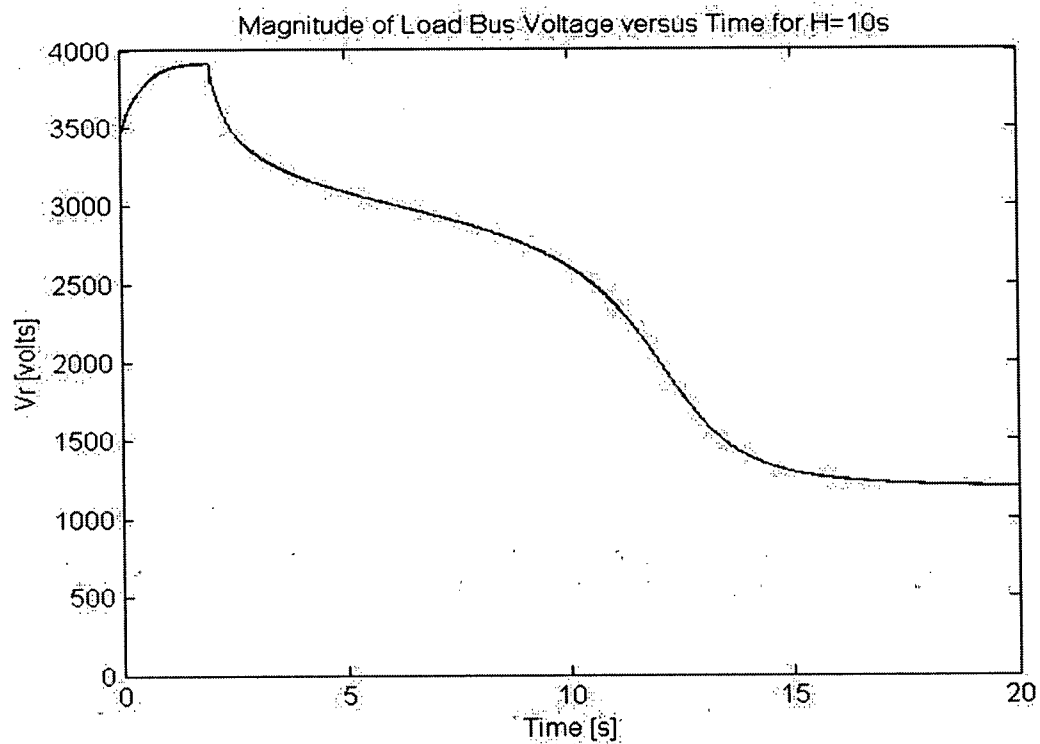


**Figure 21: Magnitude of the load bus voltage versus time with H=10s for case 1A.**

The results above did not completely address the reason for the voltage collapse. Another logical quantity to vary is the magnetising inductance ($X_M$). By considering the equivalent circuit of an induction machine, increasing the magnetising inductance results in more current travelling to the rotor branch. This creates an equivalent circuit which is more resistive and hence more stable. Once again, the magnitude of the load bus voltage will be monitored for a voltage collapse. The inertia constant is set to its original value of H = 3 seconds. The magnetising inductor is increased from 4.1375 p.u. to 5.1719 p.u. (or 125% its original value). Below (Figure 22, Figure 23, Figure 24) are the results obtained by changing $X_M$. The results show that as the magnetising inductance is increased, then the time necessary for the voltage collapse to occur increases as well. This is true until the magnetising branch inductance is set to a value of 5.1719 p.u. At this value for $X_M$, no voltage crash is seen in a 50 second simulation. The system appears to be stable and the motor demonstrates no signs of collapse. Thus, the magnetising inductance is partly responsible for the voltage stability of this system.
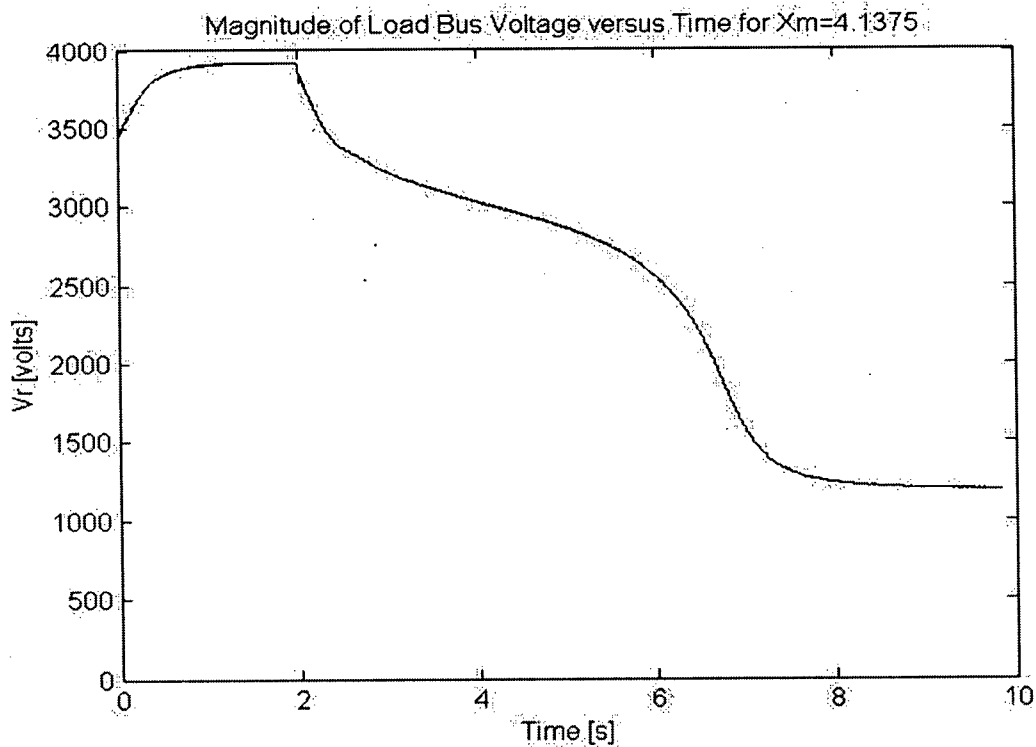


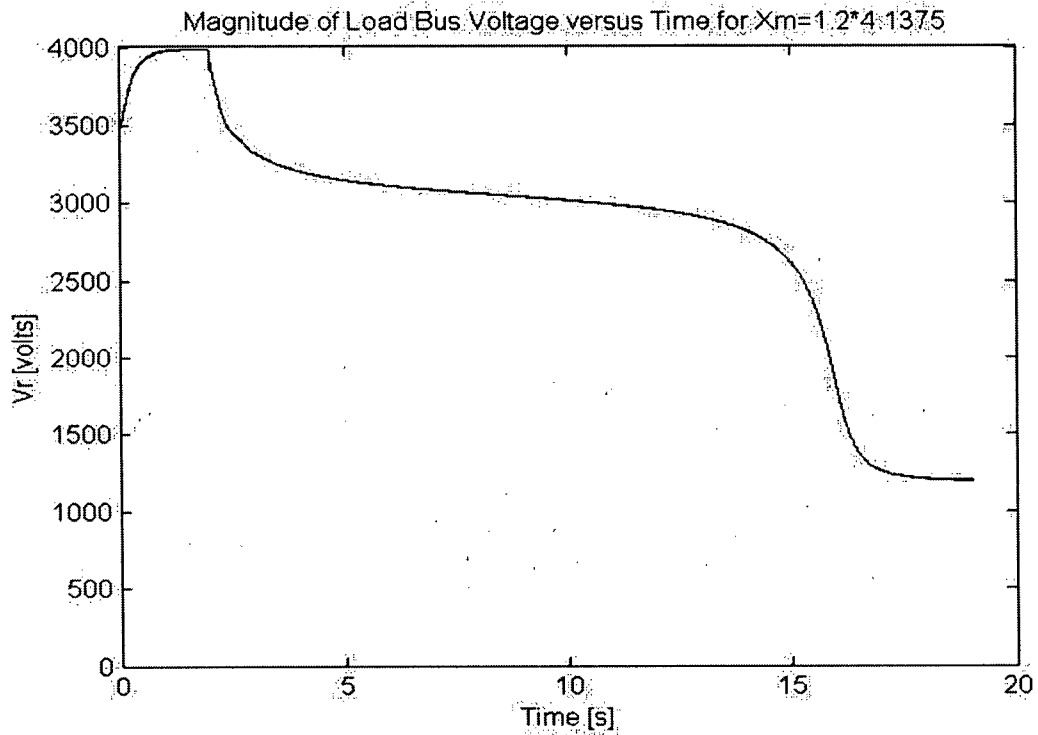Figure 22: Magnitude of the load bus voltage versus time with Xm=4.1375 p.u. for case 1A.

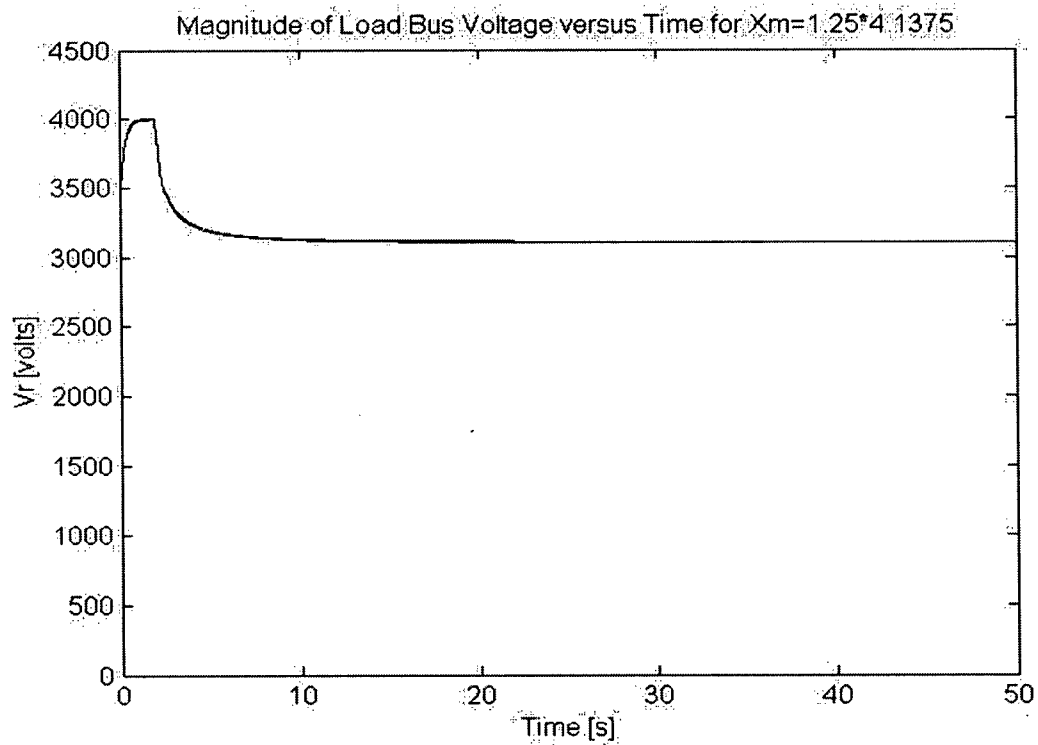**Figure 23: Magnitude of the load bus voltage versus time with Xm= 1.2*4.1375 p.u. for case 1A.**



**Figure 24: Magnitude of the load bus voltage versus time with Xm=1.25*4.1375 p.u. for case 1A.**

For completeness, graphs of pertinent quantities have been included below for H = 3 seconds and $X_M$ = 4.1375 p.u.
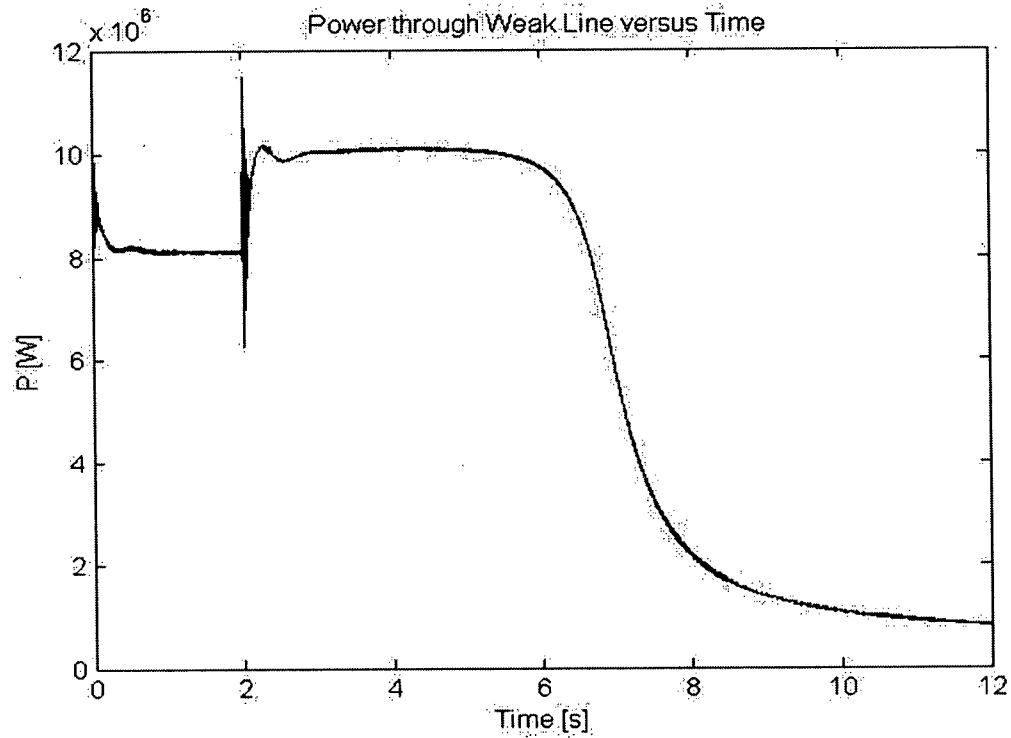


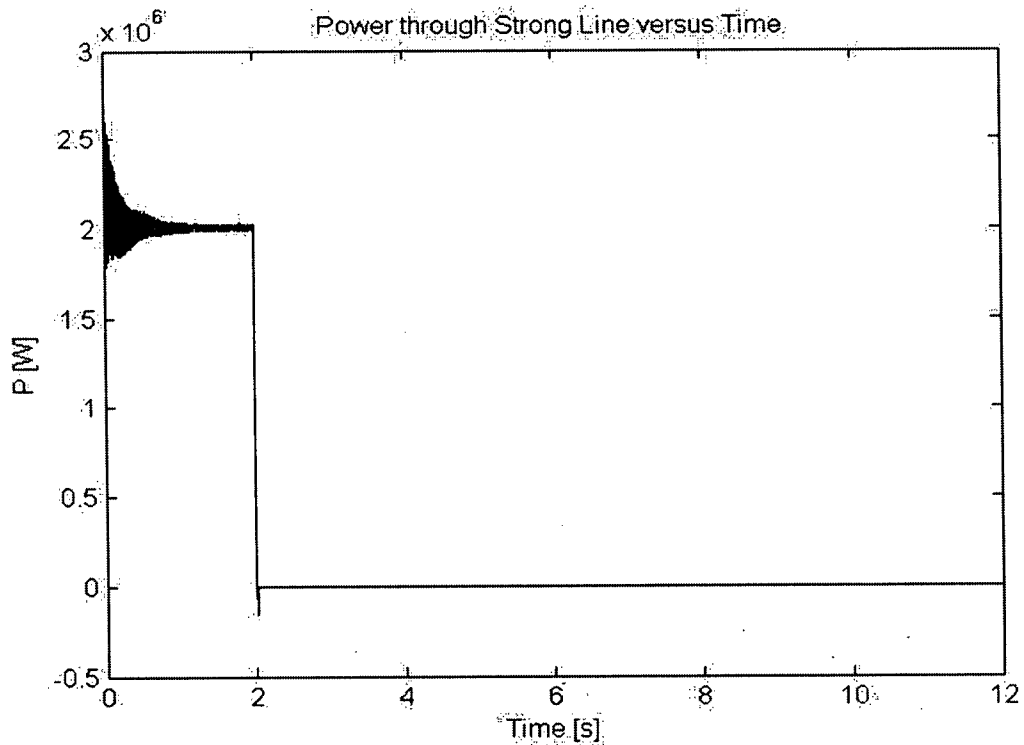Figure 25: Power through weak line versus time for case 1A.



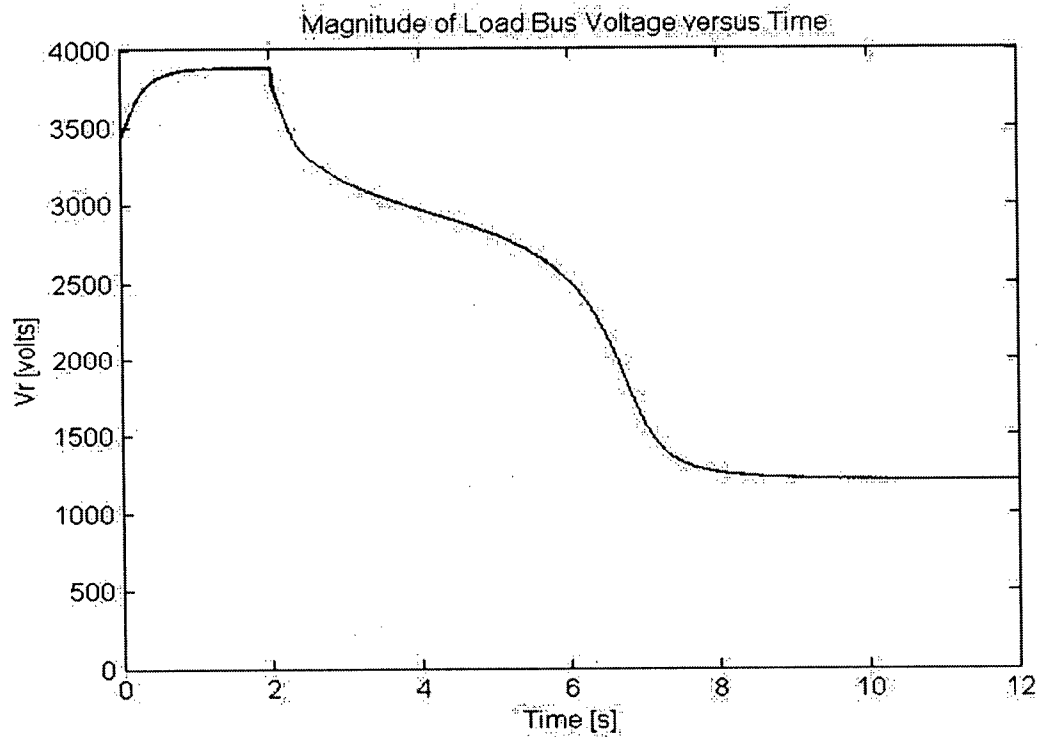Figure 26: Power through strong line versus time for case 1A.

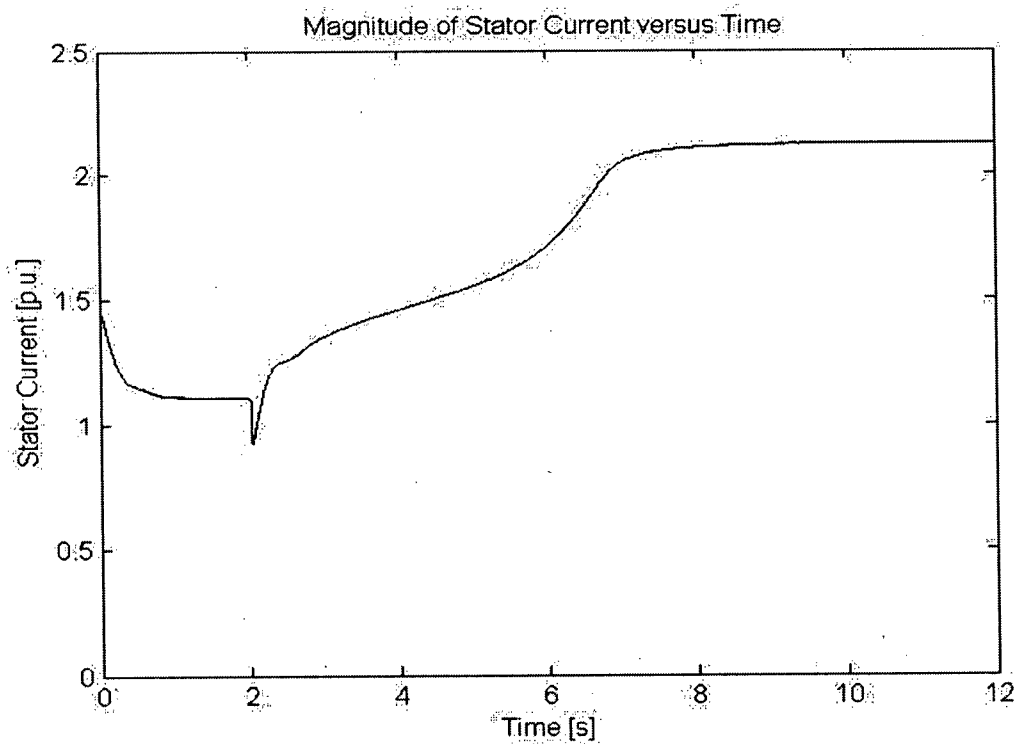**Figure 27: Magnitude of load bus voltage versus time for case 1A.**



**Figure 28: Magnitude of stator current versus time for case 1A.**
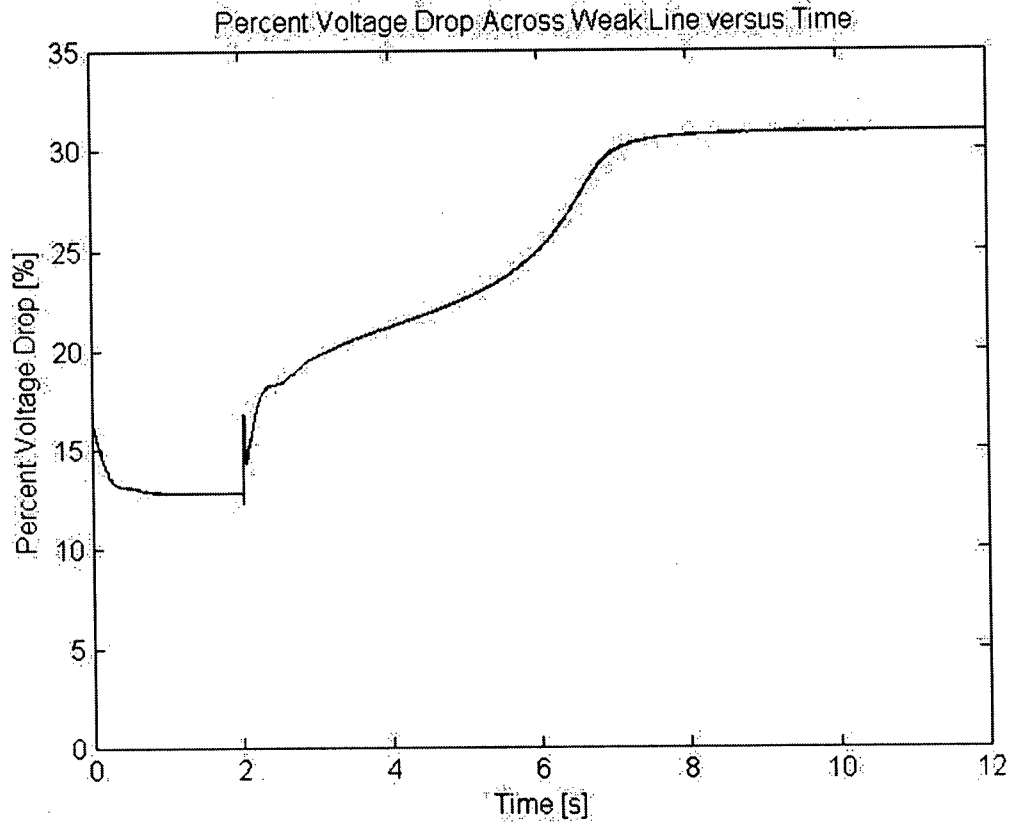
**Figure 29: Percent voltage drop across weak line versus time for case 1A.**

### 3.1.b Case 1B

In practice, three phase faults rarely remain for extended periods of time. They are cleared within several cycles, depending on the rated voltage. The breakers re-close and the line is operational. In this case, we assume that the fault is cleared after 10 cycles and the breakers re-close. We investigate the voltage stability of the system Figure 11.

It is apparent from Figure 30 that the system does not collapse. Looking at Figure 31 through Figure 35, one notices that the system stabilizes after a momentary transient. This case supports the claim that the simulations are representative of actual systems.
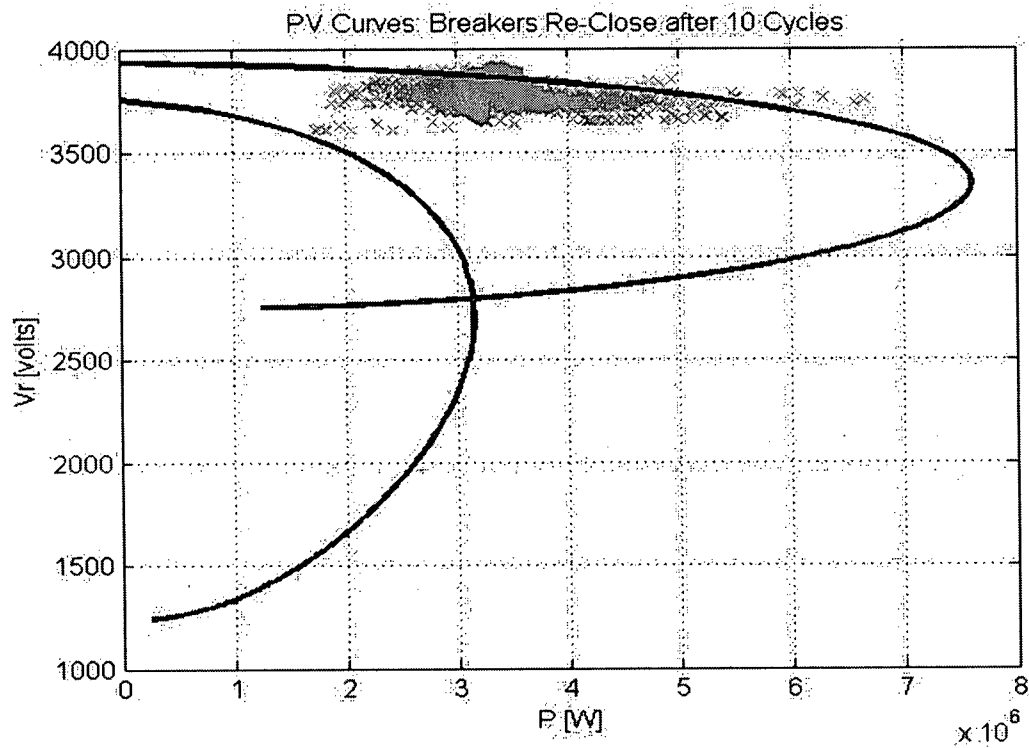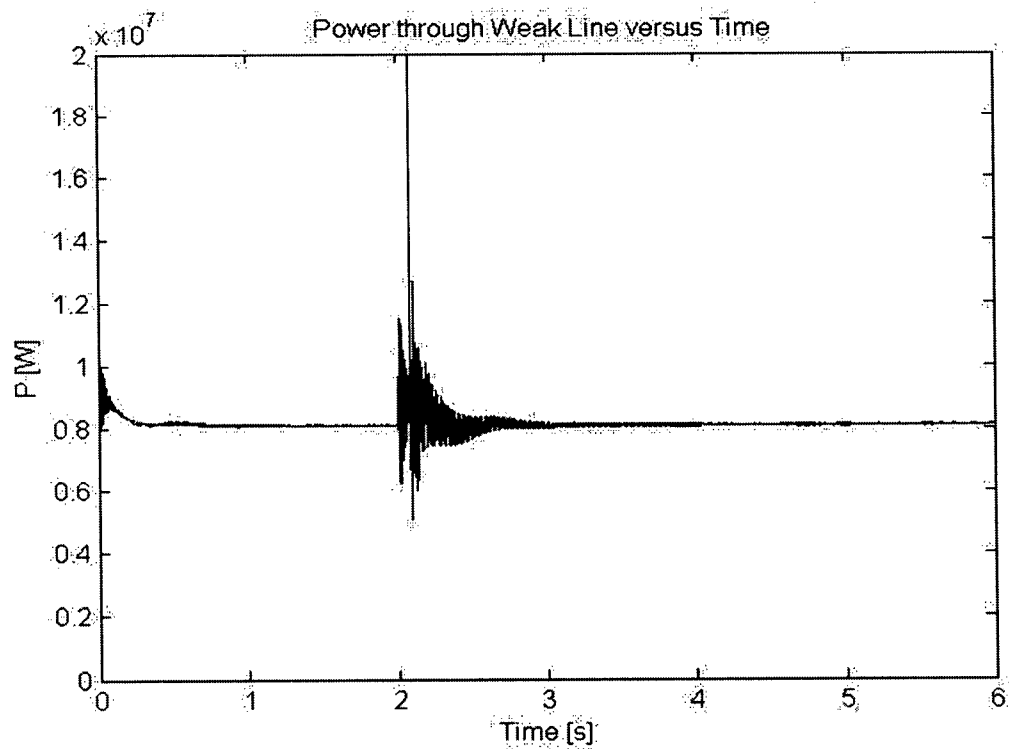
**Figure 30: PV curves for case 1B.**



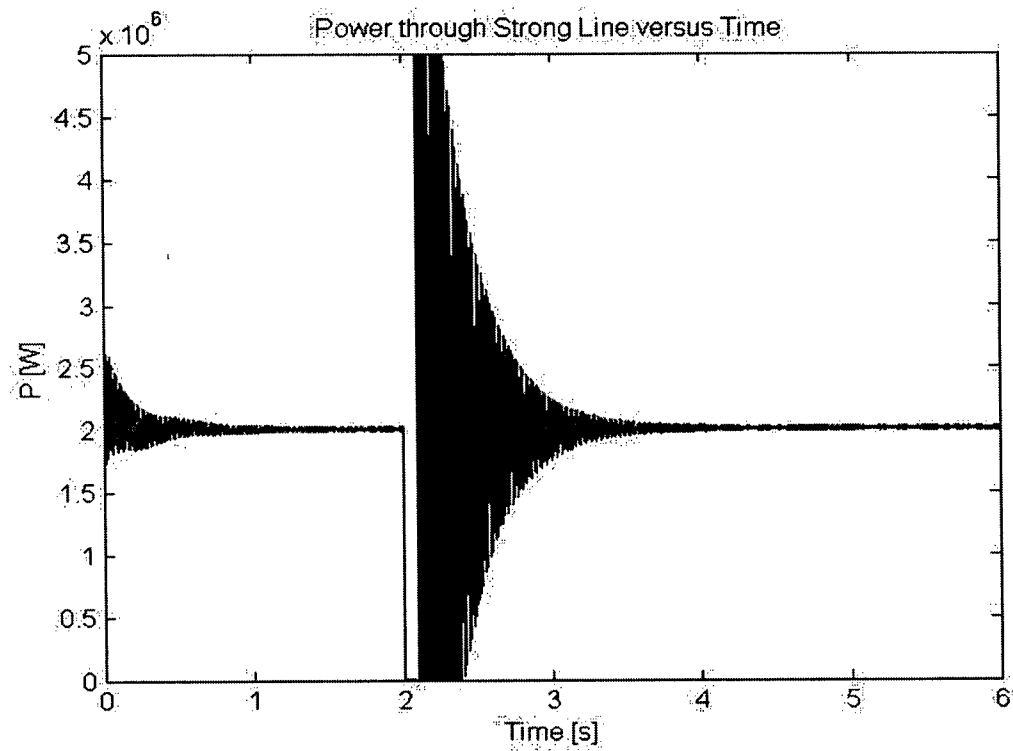**Figure 31: Power through the weak line versus time for case 1B.**

33

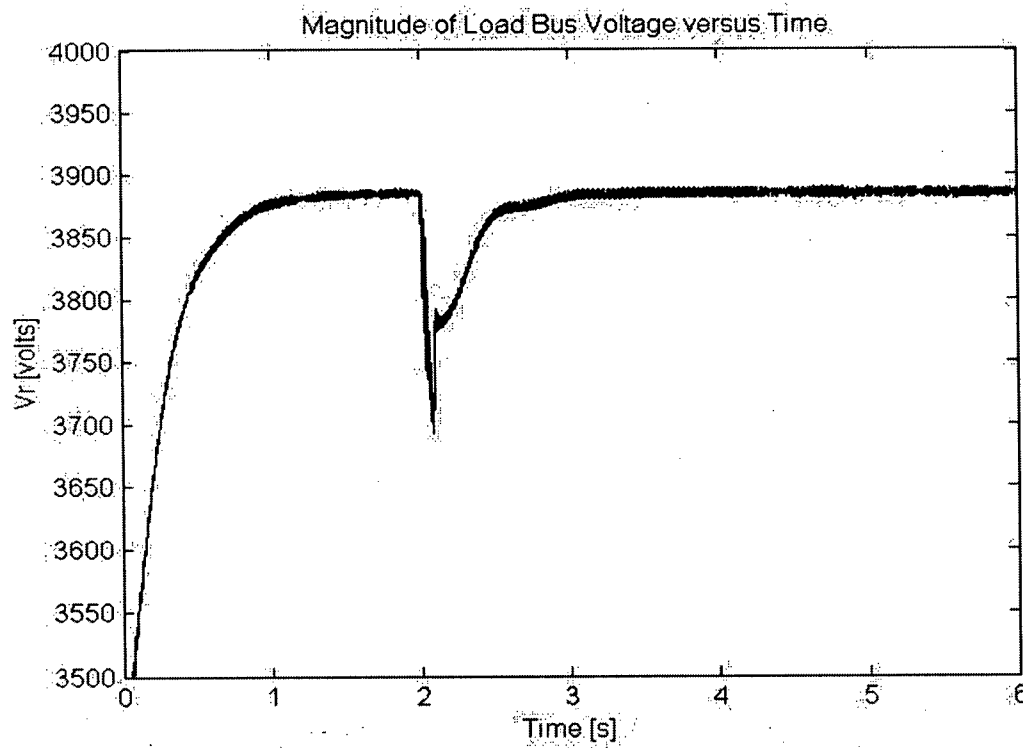**Figure 32: Power through the strong line versus time for case 1B.**



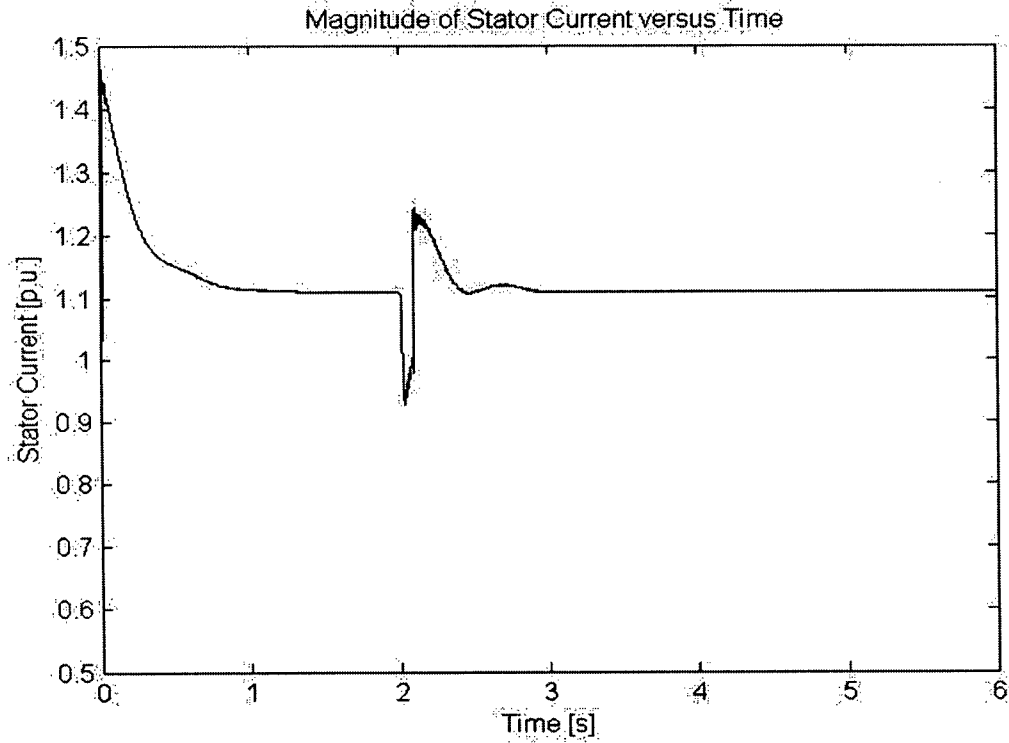**Figure 33: Magnitude of the load bus voltage versus time for case 1B.**

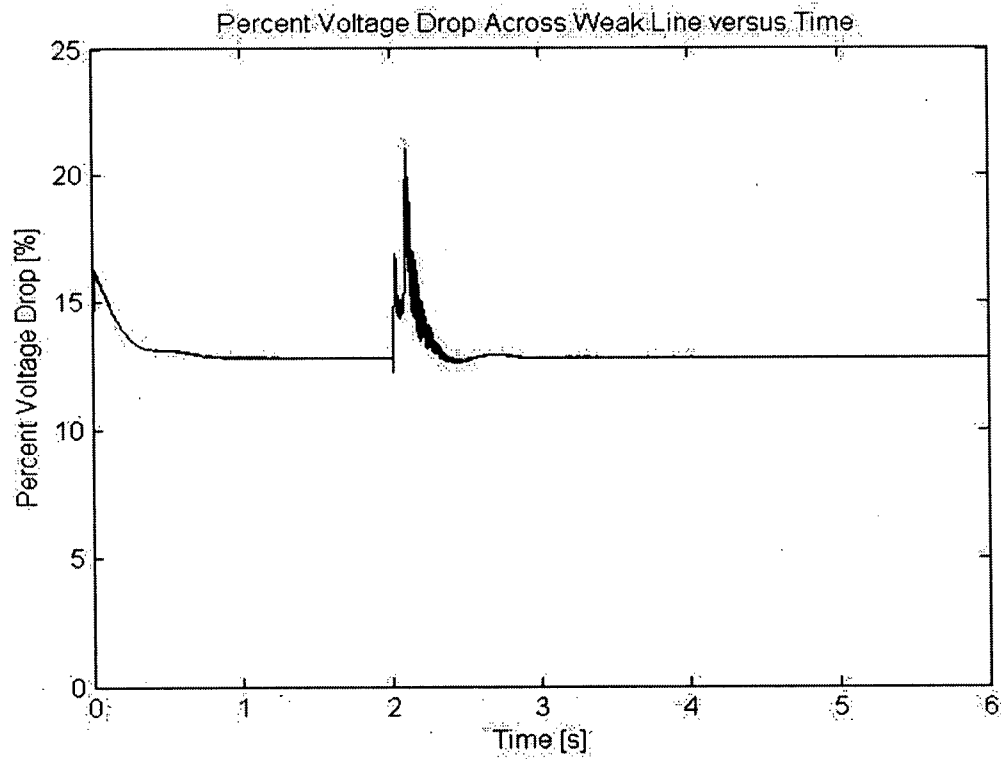**Figure 34: Magnitude of the stator current versus time for case 1B.**



**Figure 35: Percent voltage drop across the weak line versus time for case 1B.**

## 3.1.c Case 1C

In case 1C, we examine the effects of increasing the percentage of resistive load. This will be done by maintaining the total load at 10MVA. This case is meant to represent a more realistic scenario where 50% of the load is resistive and 50% of the load is an induction machine. The induction machine is modeled with a squirrel cage rotor, rated at 5MVA and 6.9kV. The power supplied by the idealized wind turbine, modeled as a constant voltage source, remains at 20% of the total load requirement. After 2 seconds, a three phase fault will disturb the strong line. The voltage stability of the system is analysed using PV curves.

The load in case 1C has a larger power factor. This means that the load draws less reactive power which therefore, results in a larger voltage at the load. The increased voltage is not of concern because it is within the accepted range of ±10% (see Figure 39).
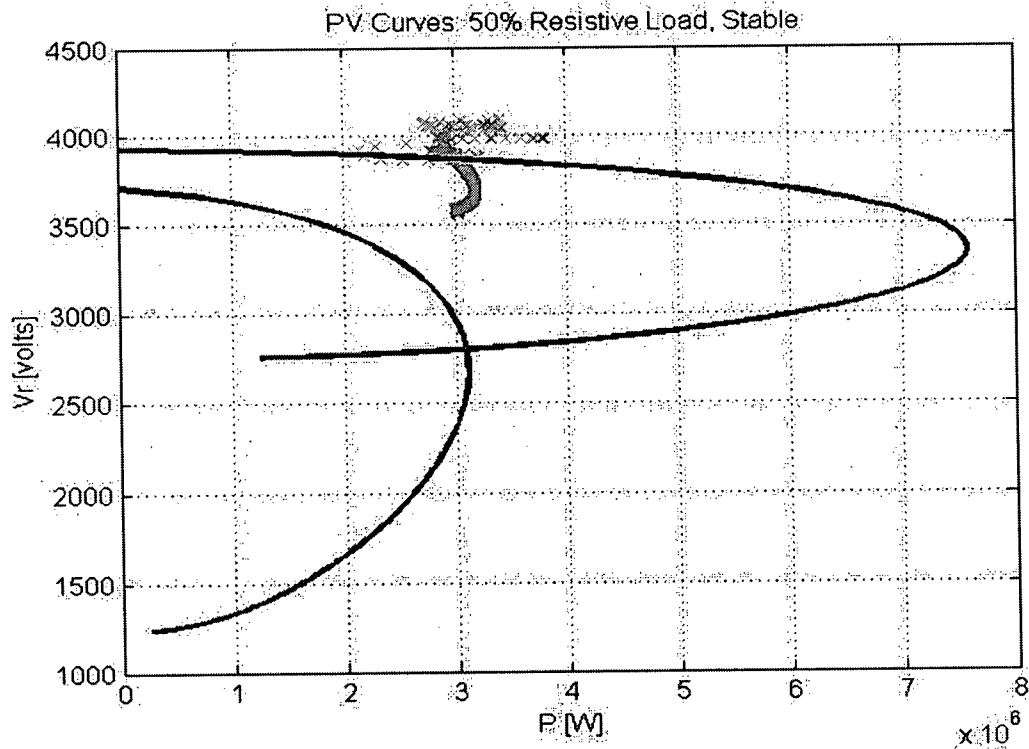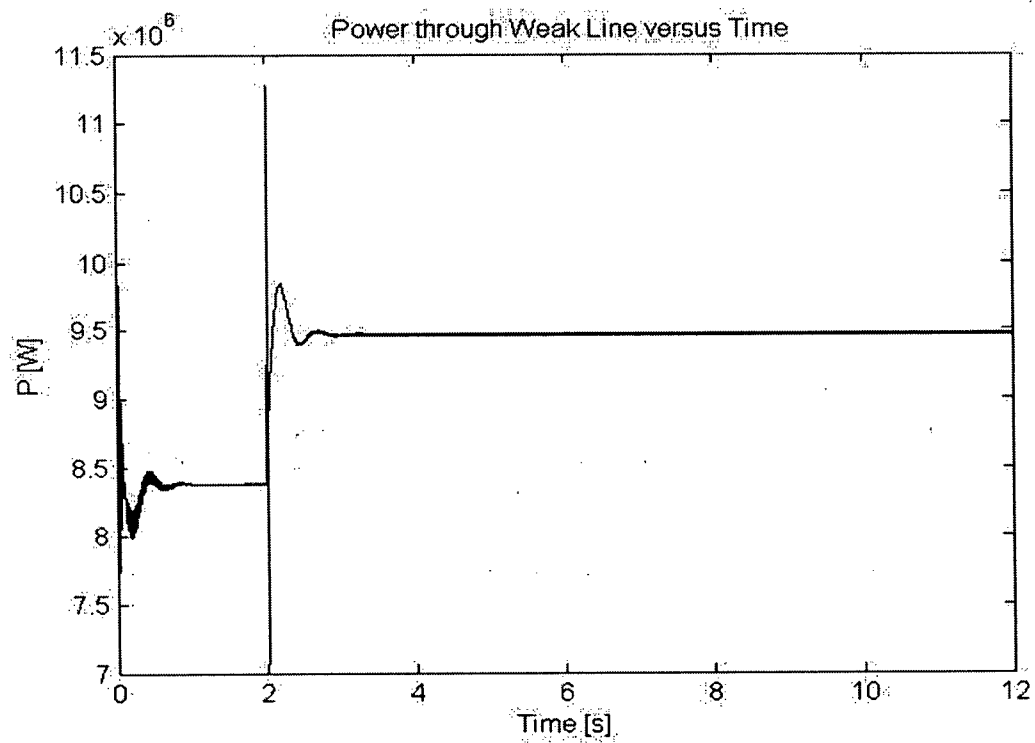


Figure 36: PV curves for case 1C.

**Figure 37: Power through the weak line versus time for case 1C.**
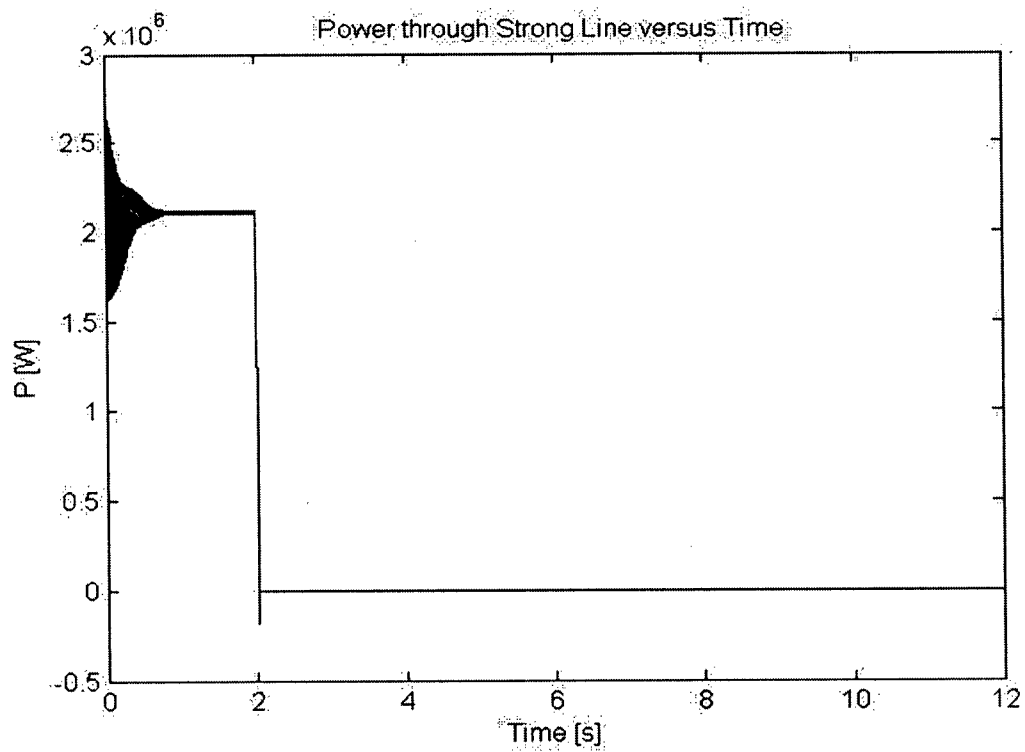


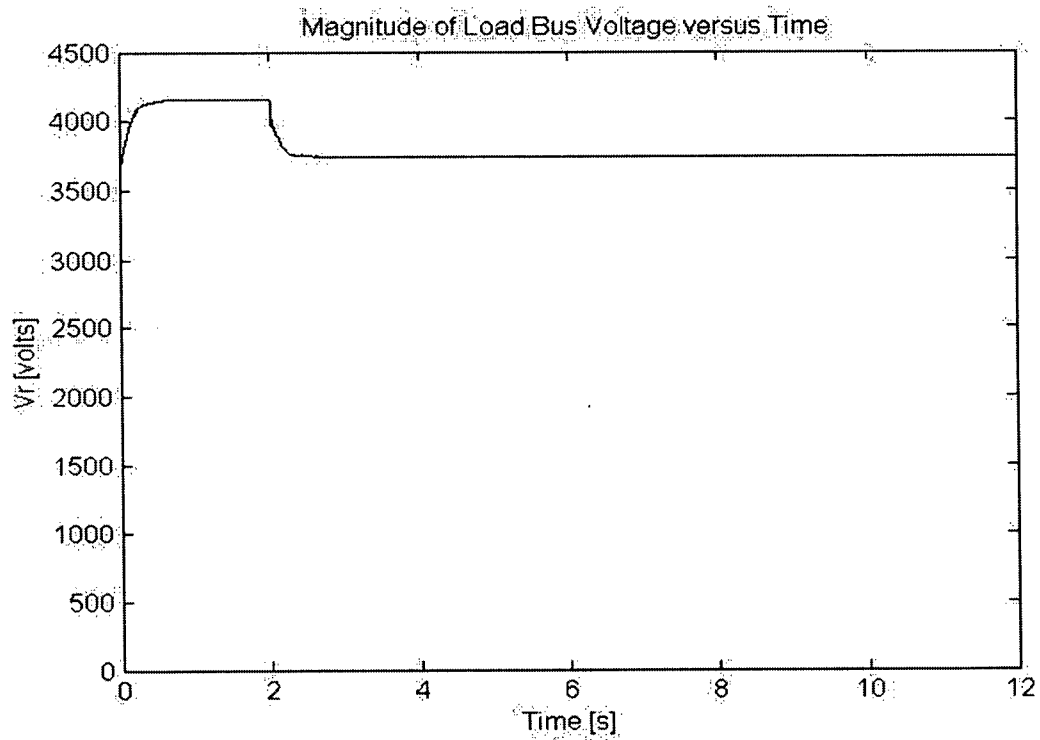**Figure 38: Power through the strong line versus time for case 1C.**

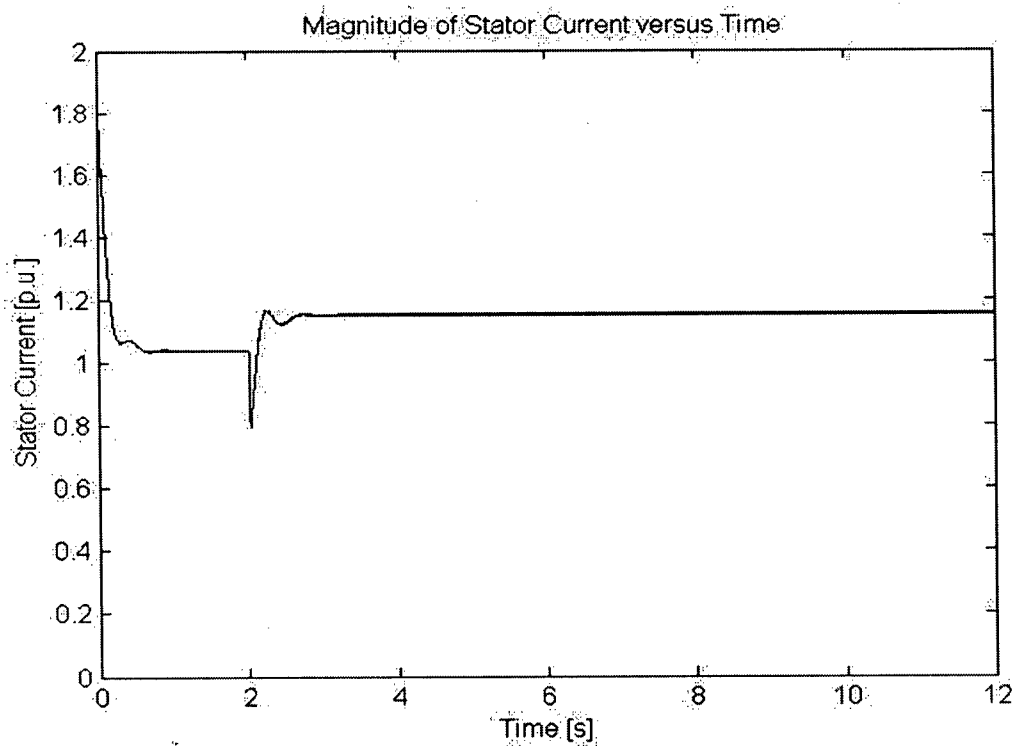**Figure 39: Magnitude of the load bus voltage versus time for case 1C.**



**Figure 40: Magnitude of the stator current versus time for case 1C.**
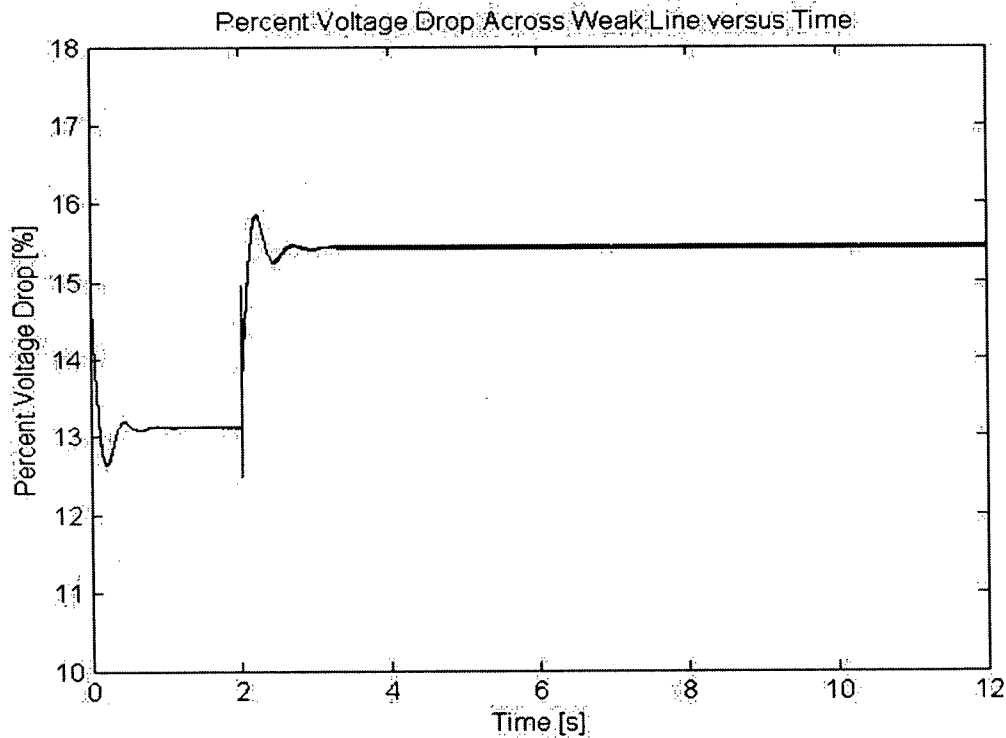
38

Figure 41: Percent voltage drop across the weak line versus time for case 1C.

The preceding figures demonstrate that the system is stable after the three phase fault. No re-closing was necessary to achieve the stability. This result is expected. As the load becomes more passive (i.e. more resistive), then less reactive power is required. Therefore, one expects greater stability. It provides further evidence that the simulations are realistic and accurate. It also emphasizes the necessity of analysing a system to ensure reliable power delivery.

Case 1 demonstrates that, in most situations, the constant power factor PV curves and the exponential load model are sufficient to predict the voltage stability of the system. Specifically, these two models accurately describe the system when post fault re-closing is successful (Case 1B) and when the load contains a significant resistive component (Case 1C). However, in cases where re-closing is unsuccessful and the load is mostly (or entirely) inductive, then a more detailed description of the system is necessary. This is especially relevant when the operation point of the system is near the nose of the PV curve. In such cases, an equivalent circuit of induction machine PV curves and a dynamic load model are necessary to predict the voltage stability of the system.

## 3.2 Case 2

In case 1, the grid was connected to the load by a WL. In case 2, the same situations are performed as in case 1 but with the grid connected to the load by a medium strength distribution line (ML). The results from case 2 will be compared to case 1. This will demonstrate the effects of a WL versus a ML for the simplest model of a wind turbine. The load is an induction machine, with a squirrel cage rotor, rated at 10MVA and 6.9kV. It is equipped with current protection device which disconnects the motor if the current surpasses 1.2 p.u. Case 2A will examine the effects of a three phase fault on the SL after two seconds. In practise, three phase faults do not remain for extended periods of time. In case 2B, the breakers will re-close after 10 cycles. The voltage stability of the system will be monitored. In addition, varying the percent resistive load will be demonstrated in case 2C. Case 2 will depict a different type of system collapse. The loss of distribution capacity will result in the tripping of the current protection of the induction machine. Below is a diagram of the system,
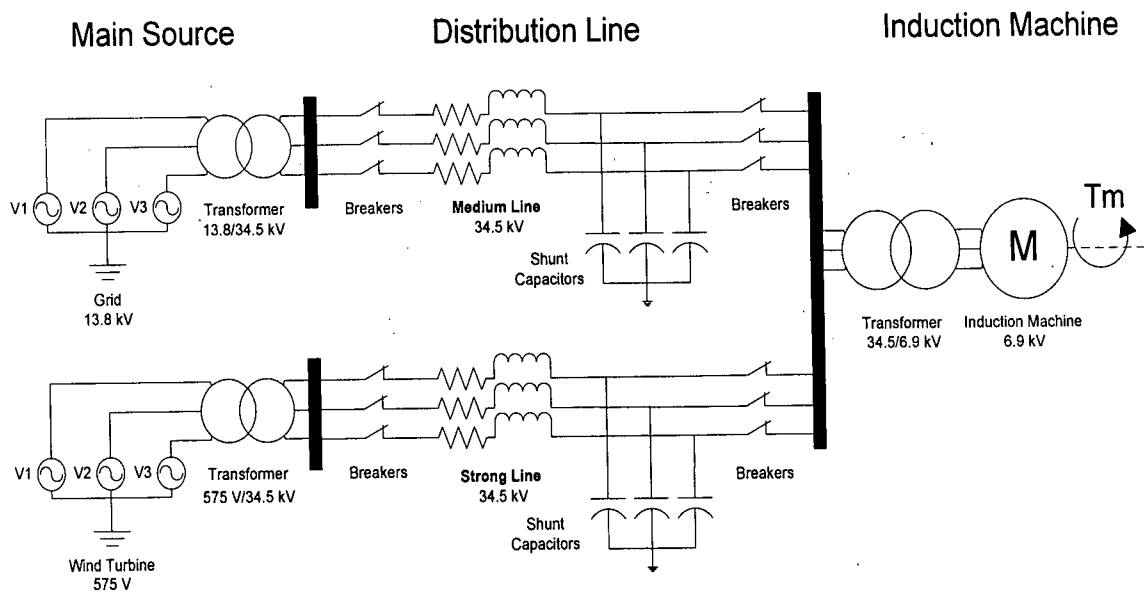


**Figure 42: Diagram for case 2.**

| | Medium Line | Strong Line | Transformer 13.8/34.5kV | Transformer 575V/34.5kV | Transformer 34.5/6.9kV |
|---|---|---|---|---|---|
| Line Length L | 50 km | 25 km | N/A | N/A | N/A |
| Reactance X | 25 Ω | 12.50 Ω | 1.73 Ω | 8.11 Ω | 1.54 Ω |
| Resistance R | 2.50 Ω | 1.25 Ω | 0.10 Ω | 0.45 Ω | 0.09 Ω |
| Shunt Capacitor Q | 3.8 MVAR | 2.0 MVAR | N/A | N/A | N/A |
| Power Base S | N/A | N/A | 12 MVA | 2.2 MVA | 12 MVA |

Table 4: System parameters for case 2. X/R ratio obtained from [1] and [16].

### 3.2.a Case 2A

After two seconds, the SL is interrupted by the opening of the breakers in response to a three phase fault. To assess the voltage stability of the system, we produce PV curves. Figure 43 depicts the movement of the operation point in the PV plane. The more stable curve represents the system before the fault: the SL and the ML in parallel. The less stable curve represents the system after the fault: the ML only. It appears that the system is stable; however, it is important to investigate further. Figure 46 shows that the voltage is slightly elevated, due to the large shunt capacitors, but within the acceptable range of ±10%. Figure 44 displays the power through the ML. Figure 45 shows the power through the strong line. Figure 46 and Figure 47 demonstrate the magnitude of the load bus voltage and the stator current respectively. Finally, in Figure 48, the percent voltage drop across the ML is displayed. Based on Figure 43, the system seems stable. The final position of the operation point is within 10% of the voltage for the PV curve with the ML only. However, upon closer investigation, one notices that the system is unstable. Figure 47 depicts the magnitude of the stator current versus time. In this figure, the magnitude of the stator current clearly reaches 1.2 p.u. which would trip the motor's protective breaker. This means that the load would have to be shut down and re-started. This is an enormous concern for industrial and residential users who depend on a reliable power supply. As expected, the ML has increased the stability of the system. In case 1, the grid was connected to the load via a WL. After two seconds, a three phase fault disturbed the SL. Subsequently, the system experienced a total voltage collapse. In comparison, when the grid was connected to the load by a medium strength line, as in case 2, the voltage did not
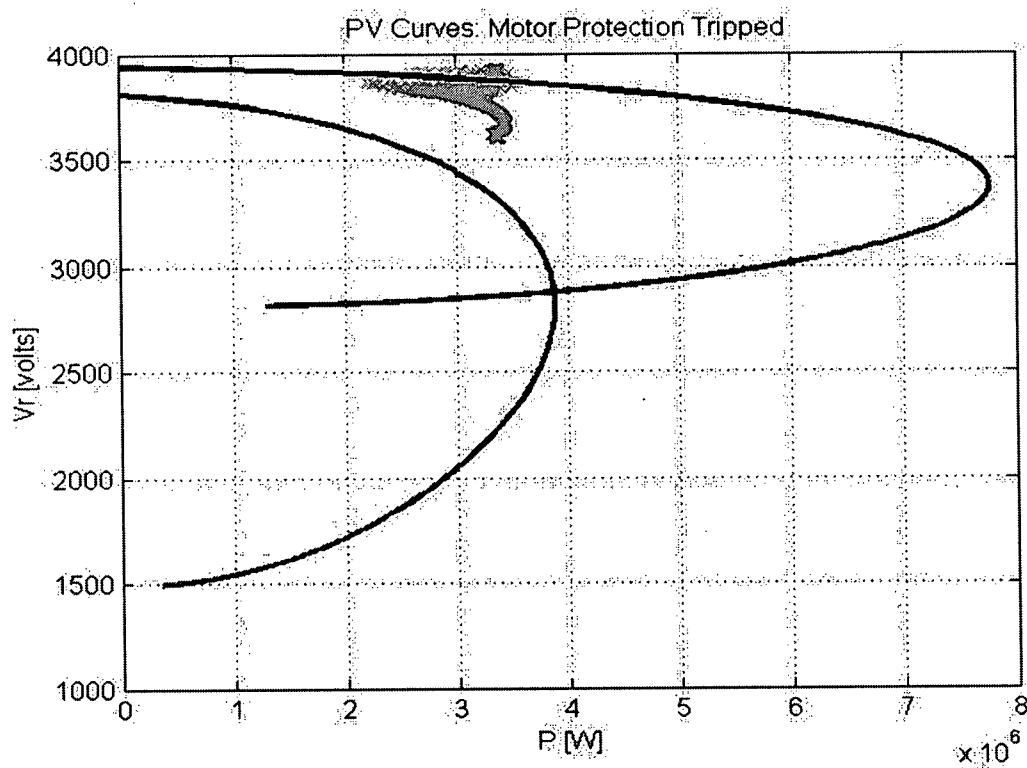
41

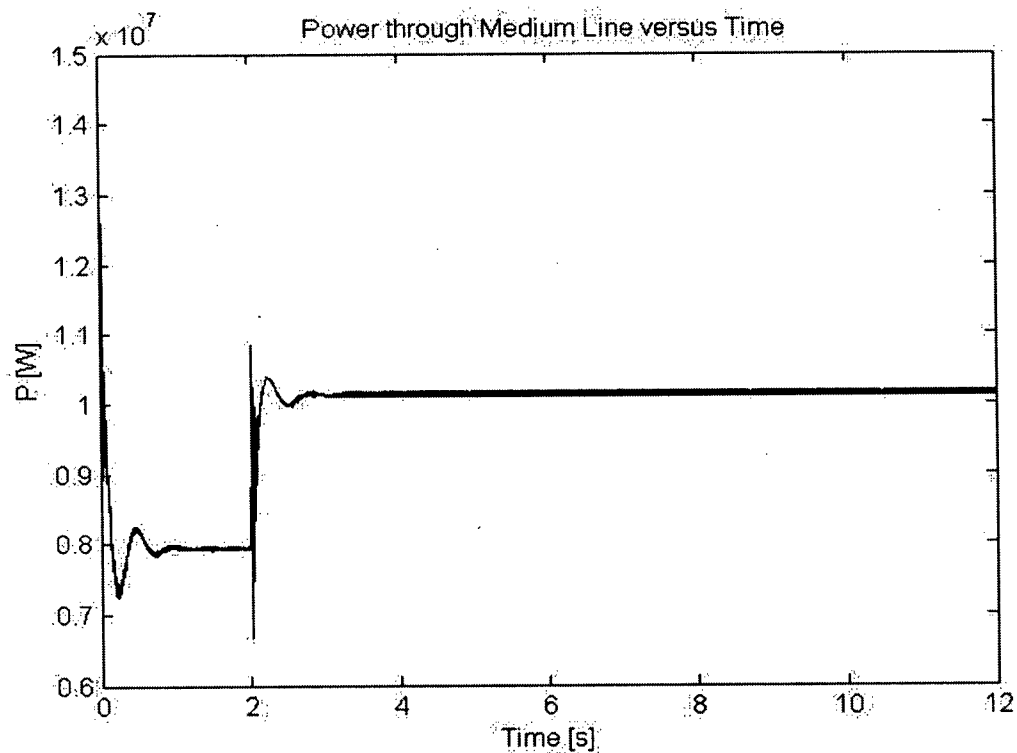**Figure 43: PV curves for case 2A.**



**Figure 44: Power through the medium line versus time for case 2A.**

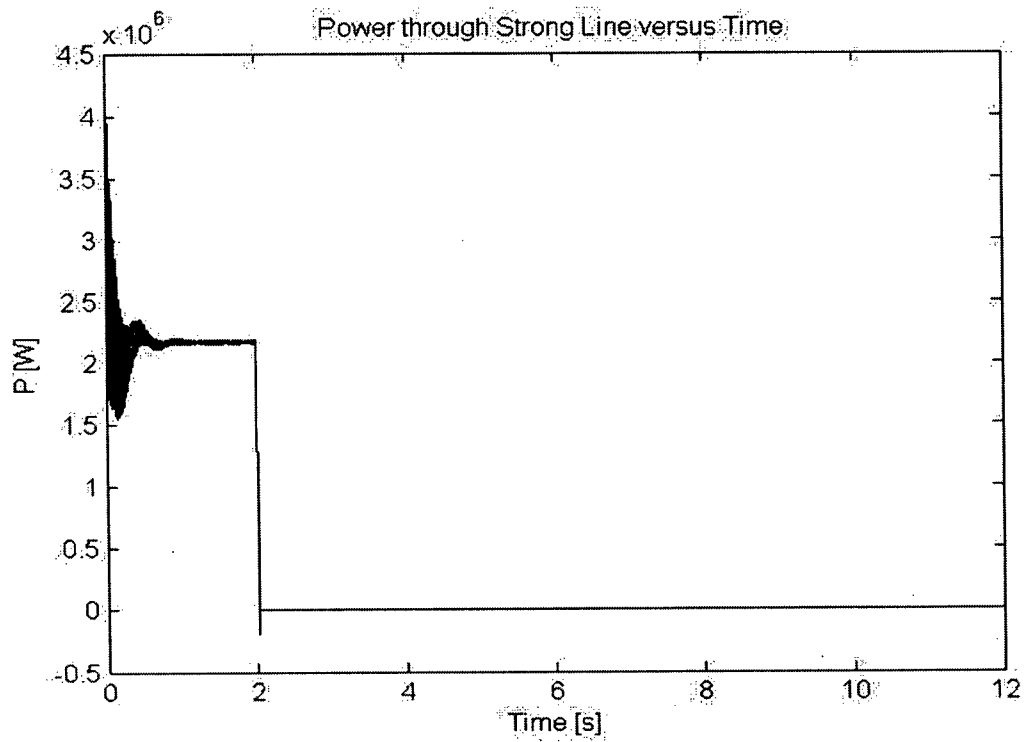**Figure 45: Power through the strong line versus time for case 2A.**
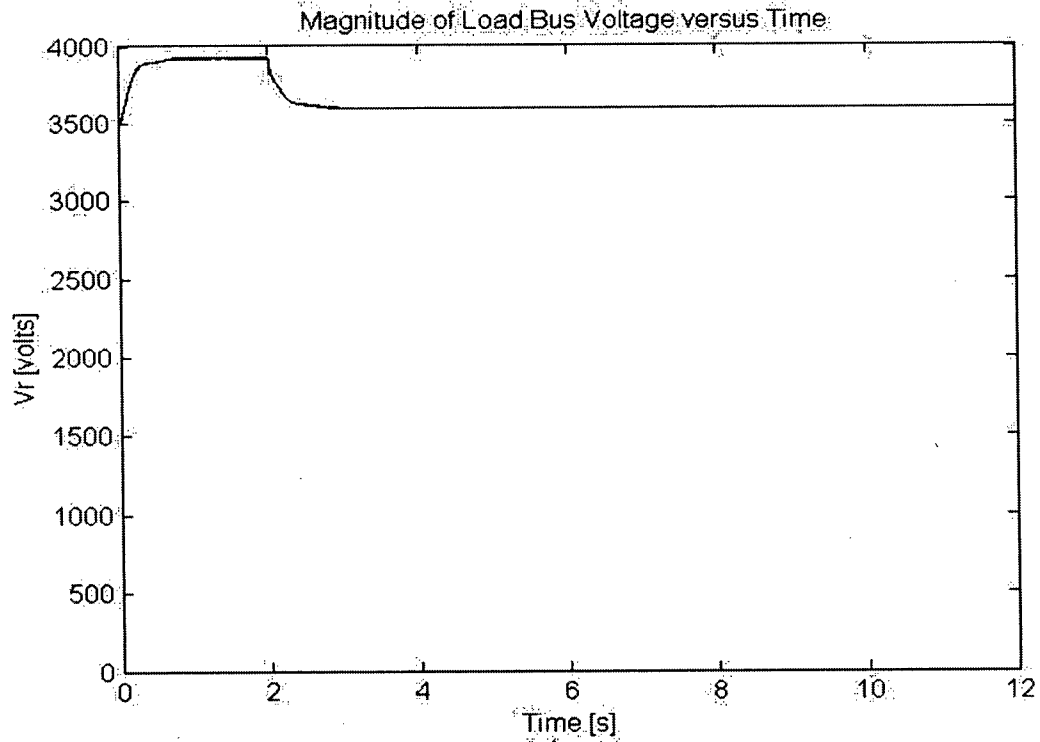


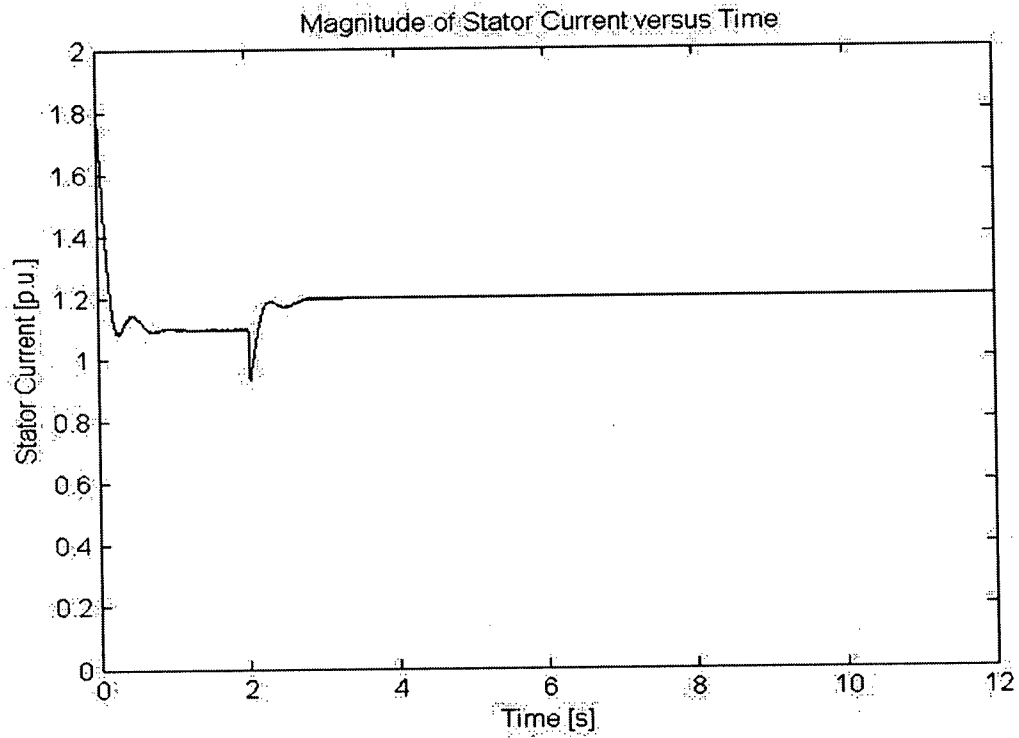**Figure 46: Magnitude of the load bus voltage versus time for case 2A.**

43

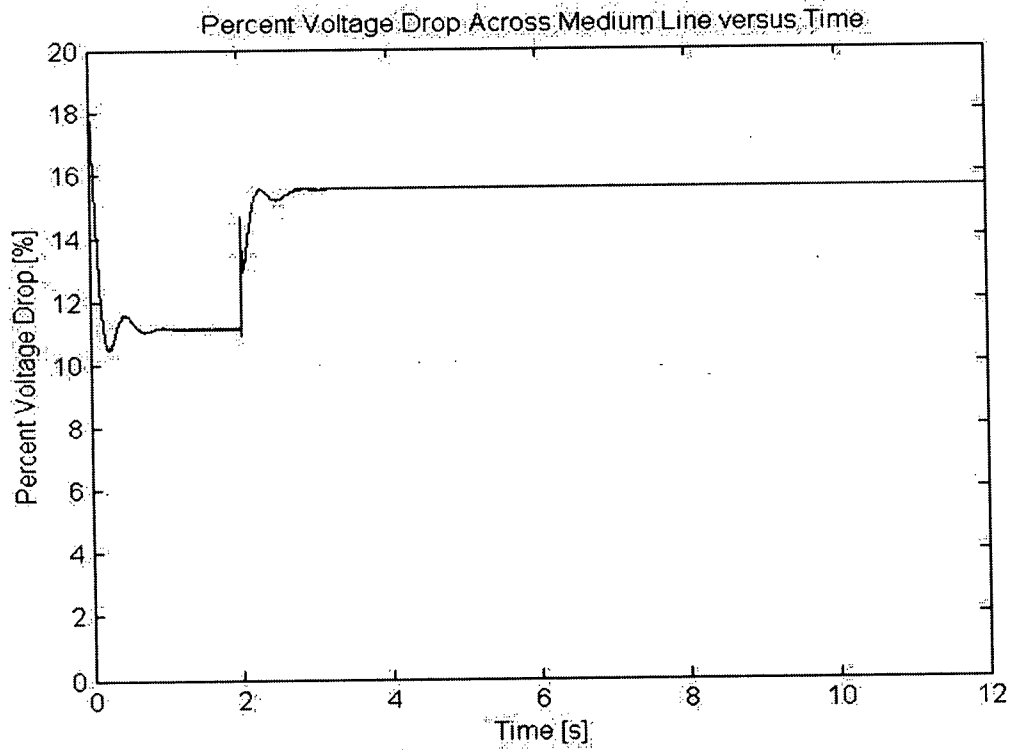**Figure 47: Magnitude of the stator current versus time for case 2A.**



**Figure 48: Percent voltage drop across medium line versus time for case 2A.**

collapse. Nevertheless, the load was disconnected due to a large stator current. This describes a second type of voltage instability which is less severe than a complete voltage collapse. However, the system is still considered to be unstable because it is not capable of supplying the load with an appropriate stator current magnitude.

### 3.2.b Case 2B

In practice, three phase faults rarely remain for extended periods of time. They are cleared within several cycles, depending on the rated voltage. The breakers re-close and the line is operational. In this case, we assume that the fault is cleared after 10 cycles and the breakers re-close. The voltage stability of the system is investigates in Figure 49. It is apparent from Figure 49 that the system does not collapse. Looking at Figure 50 through Figure 54, one notices that the system stabilizes after a momentary transient. This case demonstrates the robust nature of the system.
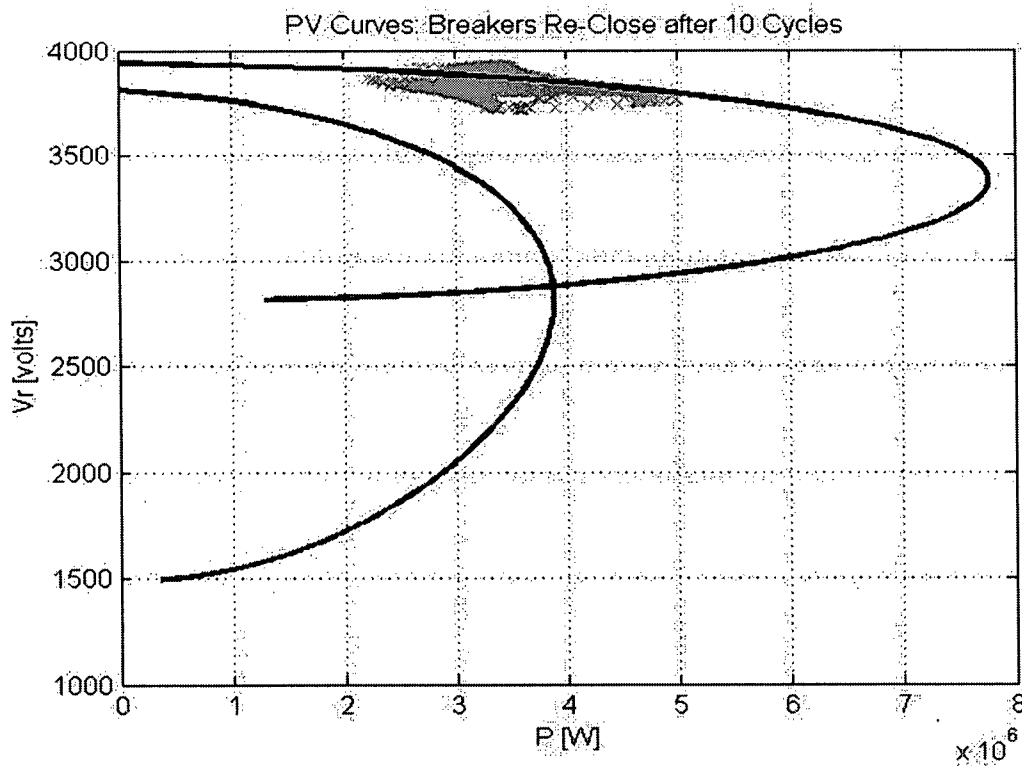
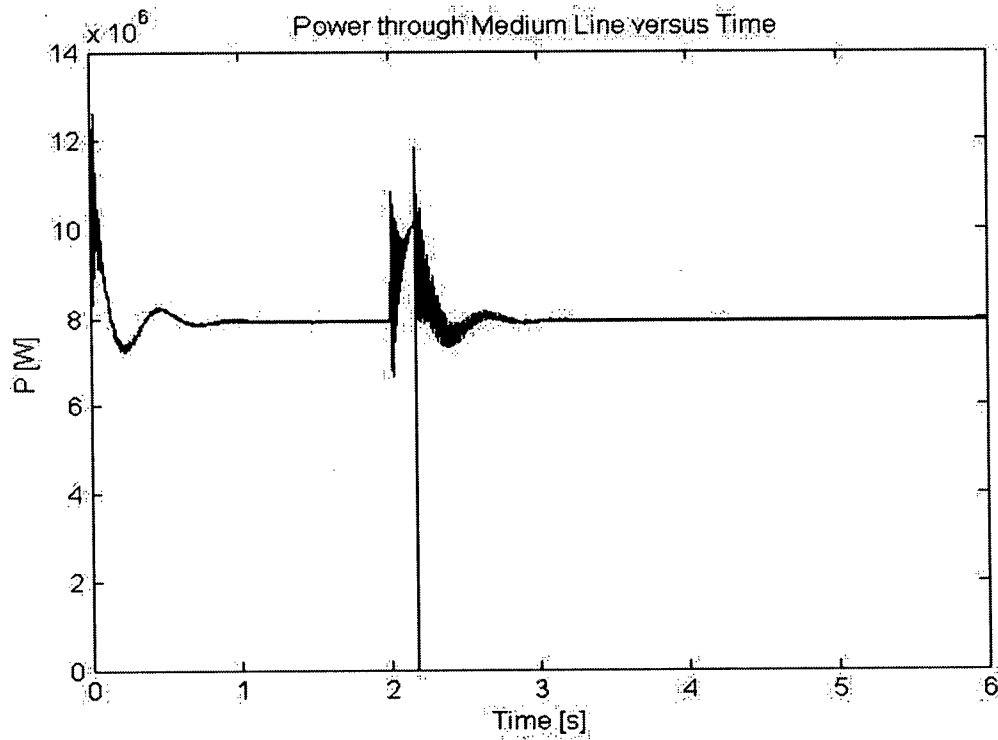

Figure 49: PV curves for case 2B.

45

**Figure 50: Power through the medium line versus time for case 2B.**
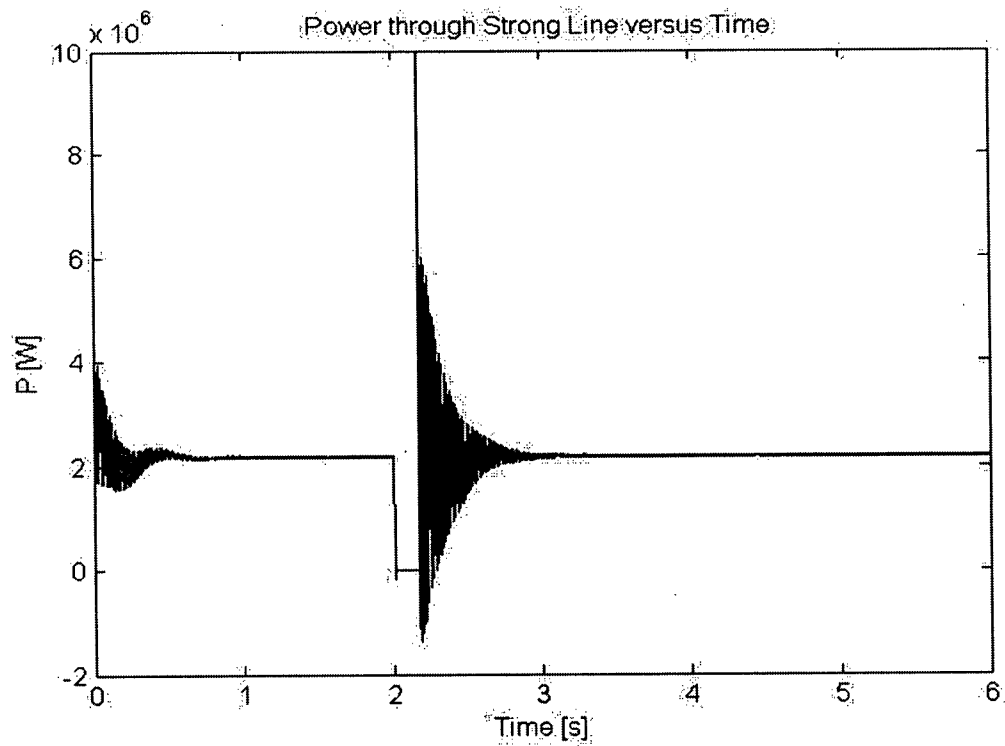


**Figure 51: Power through the strong line versus time for case 2B.**

46

**Figure 52: Magnitude of the load bus voltage versus time for case 2B.**



**Figure 53: Magnitude of the stator current versus time for case 2B.**
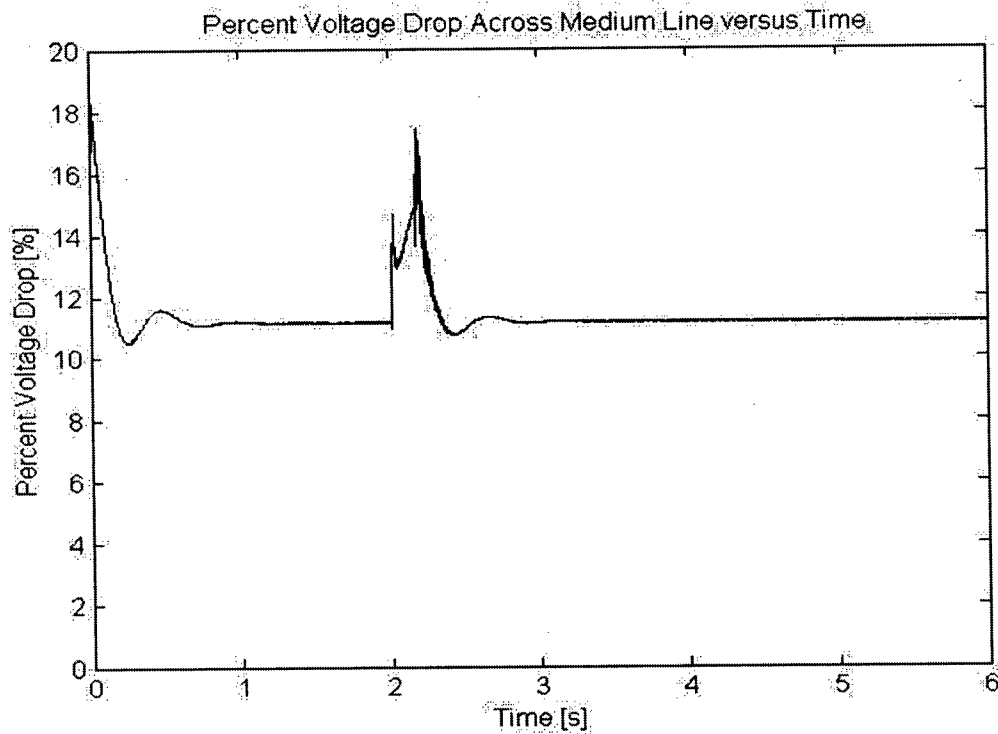
**Figure 54: Percent voltage drop across the medium line versus time for case 2B.**

### 3.2.c Case 2C

In case 2C, we examine the effects of increasing the percentage of resistive load. This will be done by maintaining the total load at 10MVA. This case is meant to represent a scenario where 50% of the load is resistive and 50% of the load is an induction machine. The induction machine is modeled with a squirrel cage rotor, rated at 5MVA and 6.9kV. The power supplied by the idealized wind turbine, modeled as a constant voltage source, remains at 20% of the total load requirement. After 2 seconds, a three phase fault will disturb the strong line. The voltage stability of the system is analysed using PV curves. It is worth noting that the voltage for this case is slightly increased                                                                                          (see
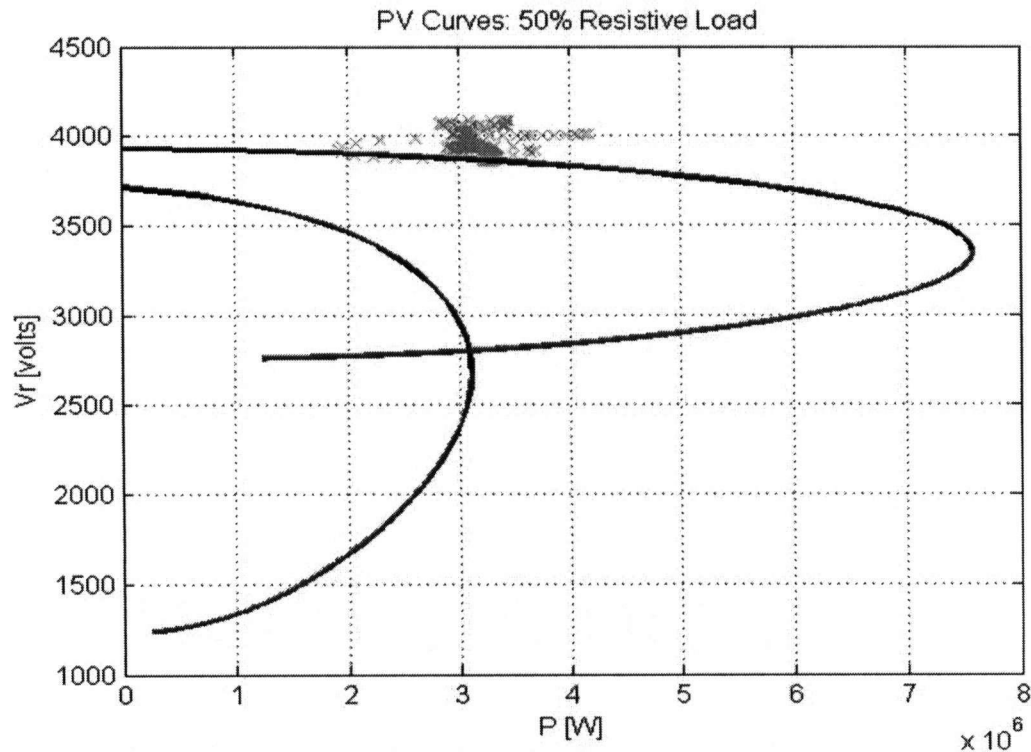
Figure 55). The reason is that the load in case 2C has a larger power factor. This means that the load draws less reactive power, which therefore, results in a larger voltage at the load. The increased voltage is not of concern because it is within the accepted range of ±10% (see Figure 58).
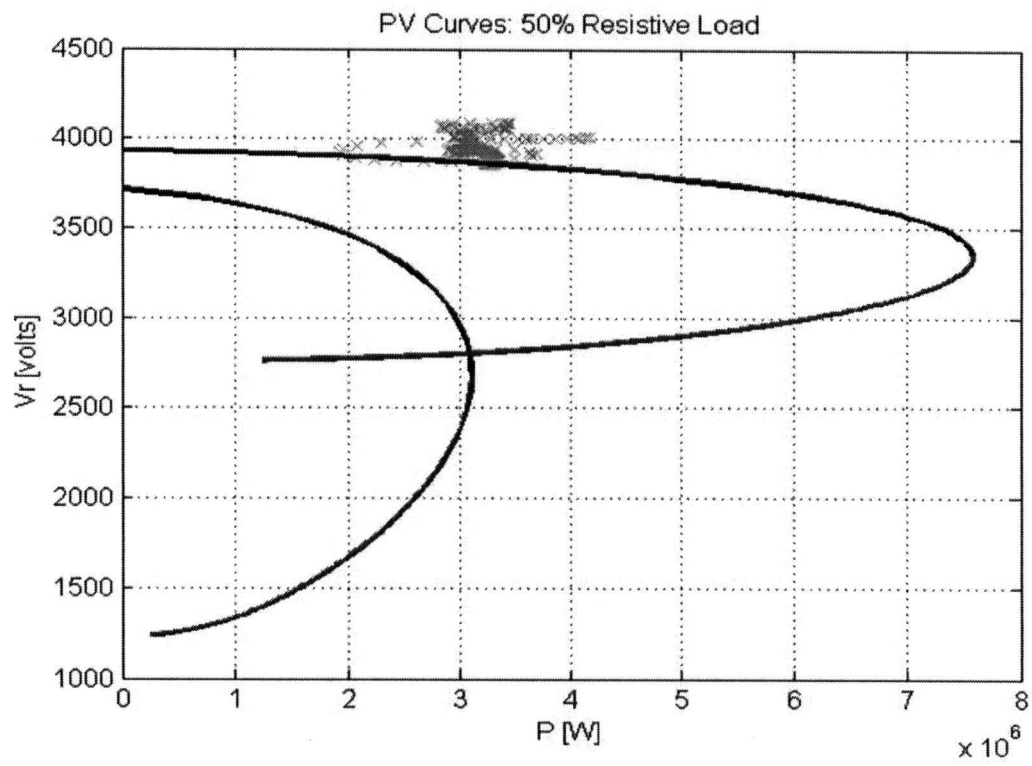
**Figure 55: PV curves for case 2C.**
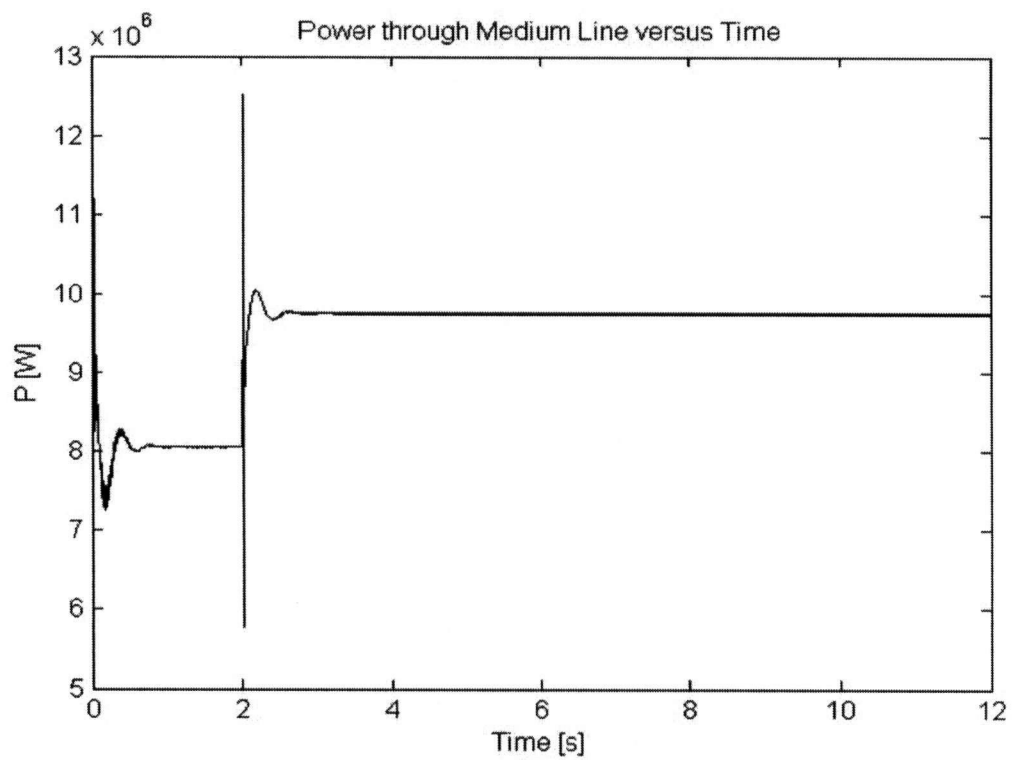


**Figure 56: Power through the medium line versus time for case 2C.**
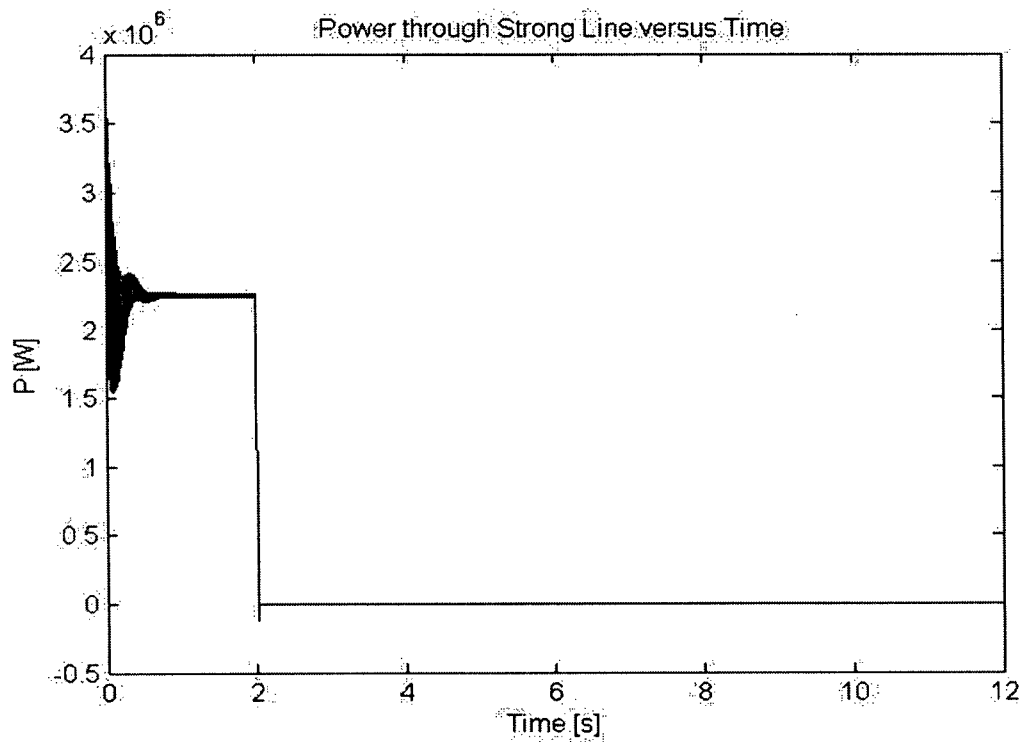
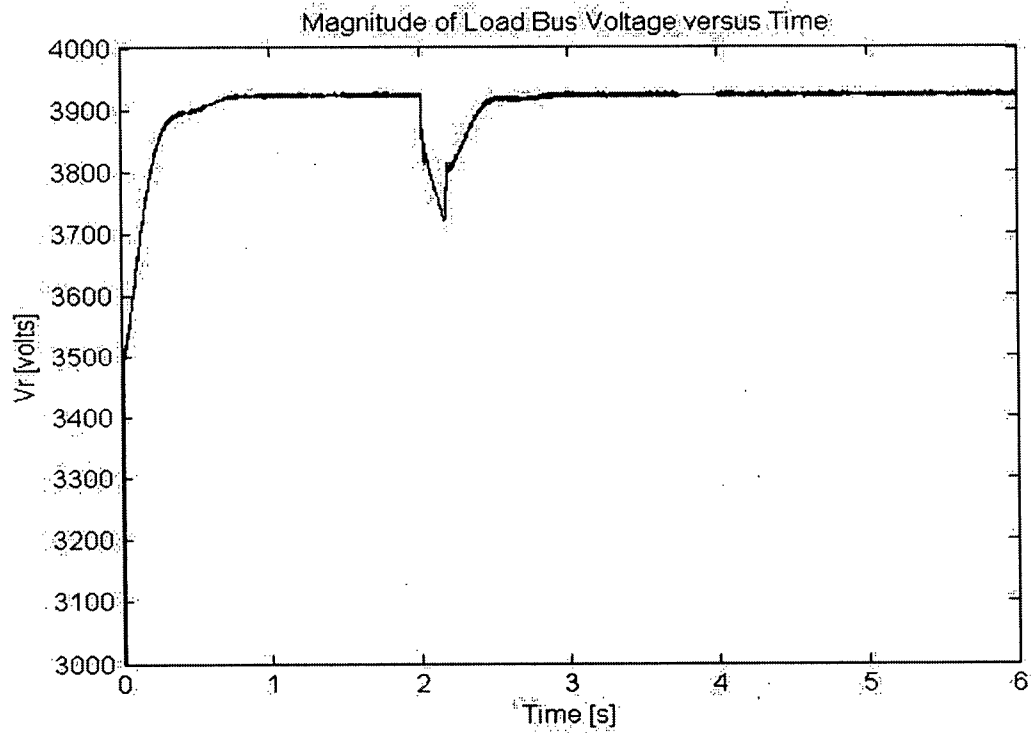**Figure 57: Power through the strong line versus time for case 2C.**
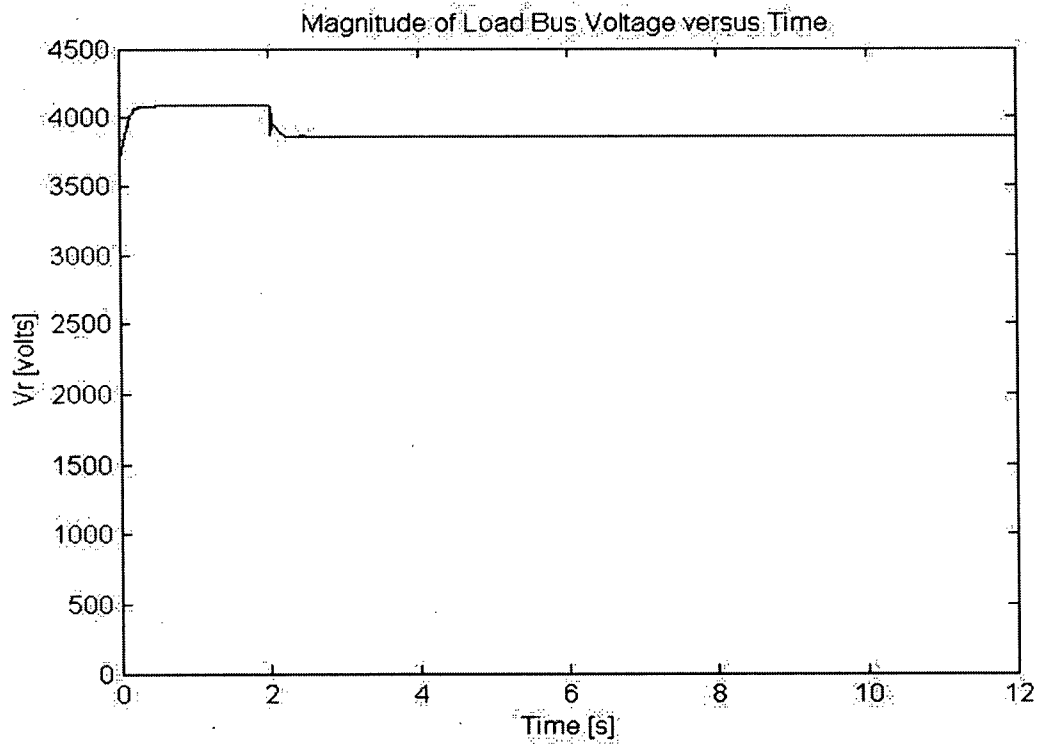


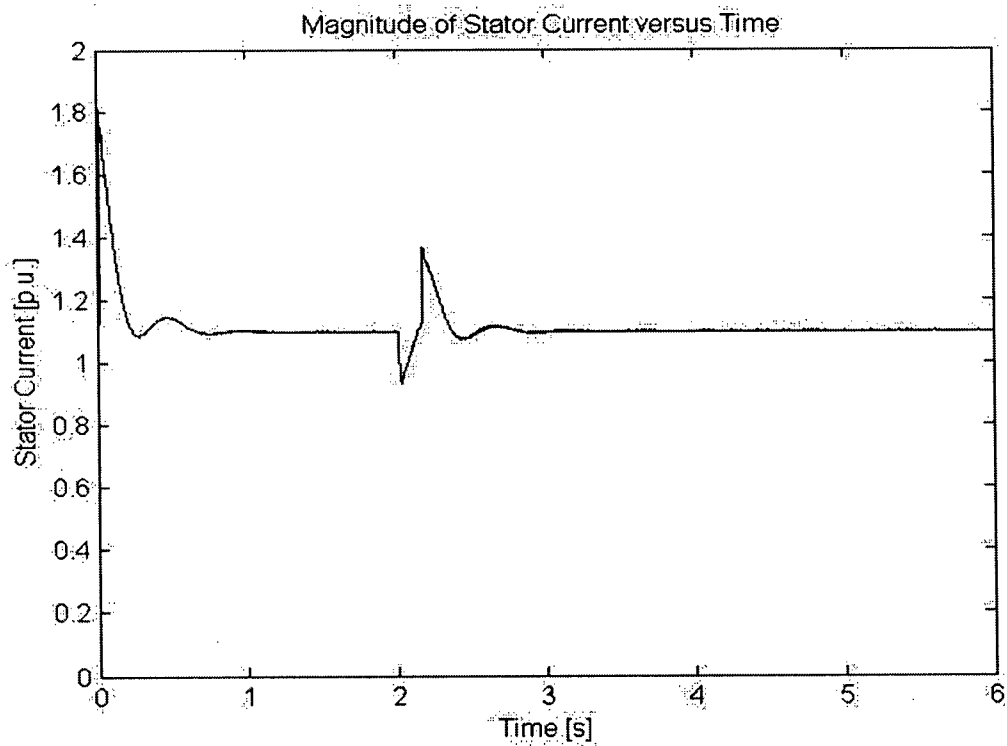**Figure 58: Magnitude of the load bus voltage versus time for case 2C.**

51

**Figure 59: Magnitude of the stator current versus time for case 2C.**



**Figure 60: Percent voltage drop across the medium line versus time for case 2C.**

52

The preceding figures demonstrate that the system is stable after the three phase fault. No re-closing was necessary to achieve the stability. This result is expected. As the load becomes more passive (i.e. more resistive), one expects greater stability. It provides further evidence that the simulations are realistic and accurate. It also emphasizes the necessity of analysing a system to ensure reliable power delivery.

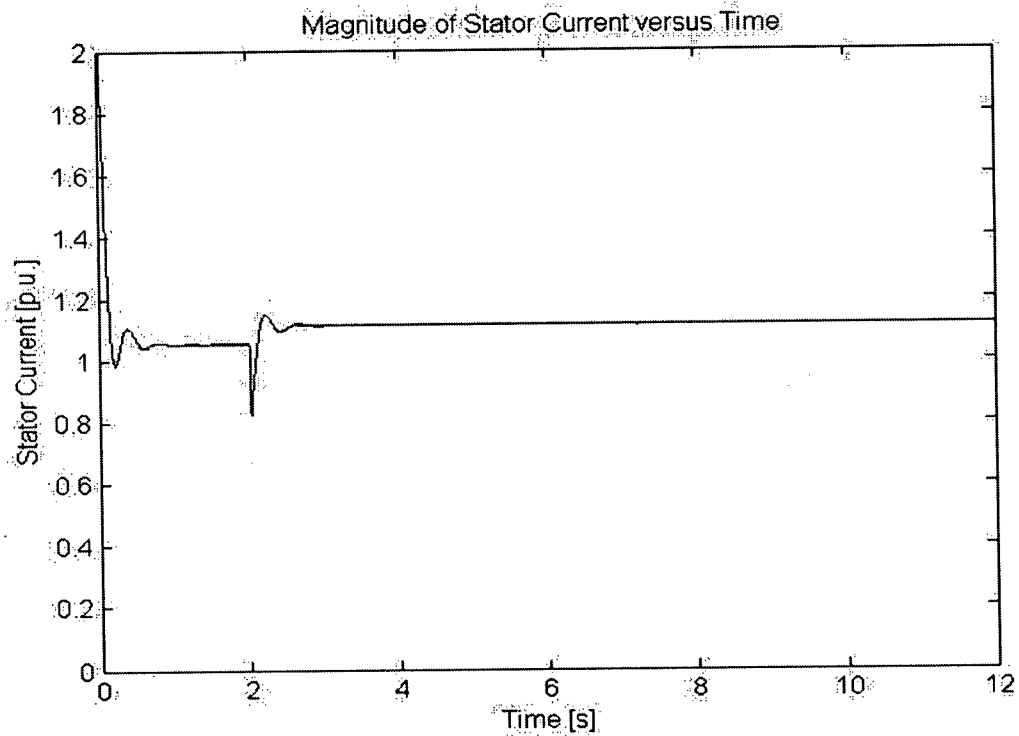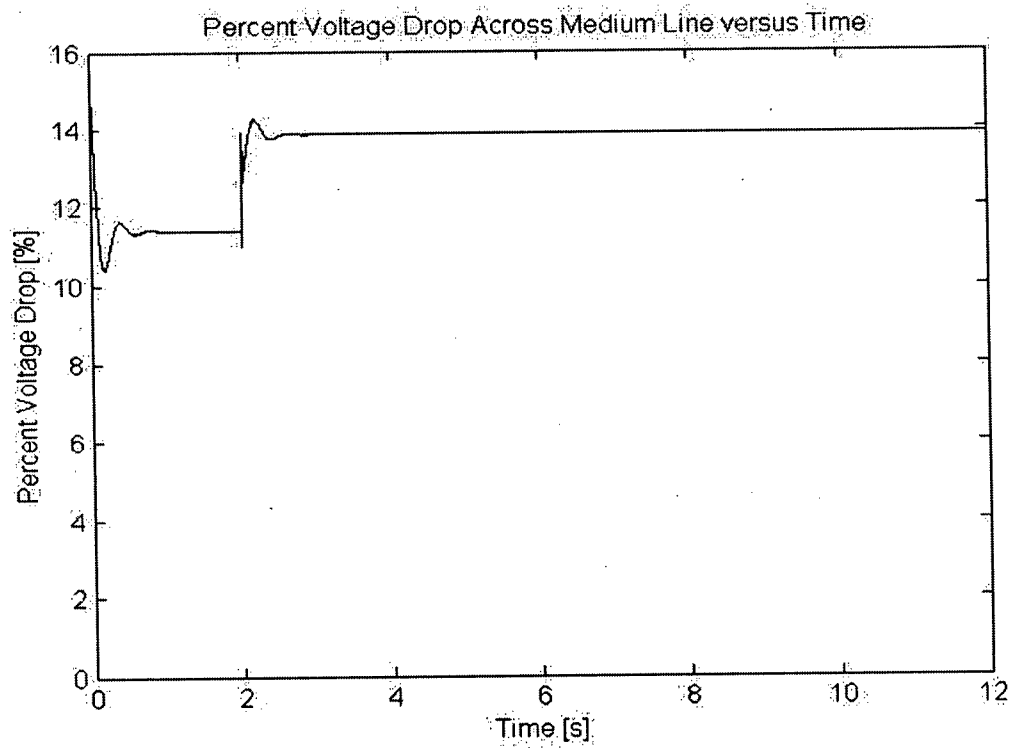In Case 1, the voltage collapse of the system was apparent. The WL did not provide enough distribution capacity to meet the load requirements after the fault. In Case 2, a ML is used to compare results with Case 1. Case 2 demonstrates a subtle type of system collapse. The voltage remains at acceptable levels; however, it is the stator current which is elevated. The stator current trips the protective breakers of the induction machine. This causes a shut down of the load. Again, when re-closing is successful, then the system is stable. As well, when the load contains a significant resistive component, then the system is stable. Therefore, it is important to properly analyse the system to determine whether protective breakers will be tripped during external fault conditions. This will provide more reliable power delivery.

## 3.3 Case 3

Case 3 examines the voltage stability of the system with a basic wind turbine model. The fixed speed wind turbine (FSWT) model replaces the infinite source from cases 1 and 2. The FSWT model is described by an induction machine, with a squirrel cage rotor, rated at 2MVA and 575V. Shunt capacitors (1 MVAR) have been installed for reactive power compensation. The varying wind speed is converted to a varying torque. This acts as the driving torque for the motor. The system is monitored during steady state operation and the effects of having a variable source will be observed. The advantage of using a FSWT is that the generator is synchronized to the grid frequency. The variable power output from the FSTW is a direct result from the fluctuations in the wind speed. As the wind speed decreases, the current output increases and the power output of the FSWT decreases (Figure 67 and Figure 68). The stator current of the load is recorded to determine if typical wind fluctuations are sufficiently large to cause the current protection breaker of the motor to trip. The FSWT is connected to the load by a SL. The grid is represented by a constant voltage source but it is connected to the load by a WL. The load

is the same load from case 2, an induction machine rated at 10MVA and 6.9kV. It is equipped with current protection device which disconnects the motor if the current exceeds 1.2 p.u. The steady state response of the system is examined. The power through each line, the load bus voltage and the stator current are recorded. Below is a diagram of the system.
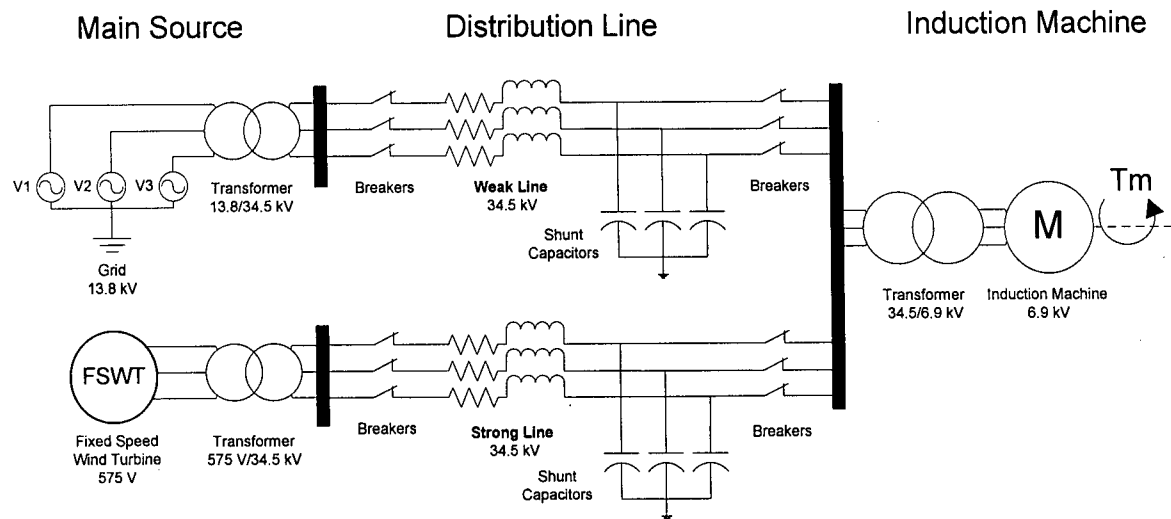


**Figure 61: Diagram of case 3.**

| | Weak Line | Strong Line | Transformer 13.8/34.5kV | Transformer 575V/34.5kV | Transformer 34.5/6.9kV |
|---|---|---|---|---|---|
| Line Length L | 66 km | 25 km | N/A | N/A | N/A |
| Reactance X | 32.75 Ω | 12.50 Ω | 1.73 Ω | 8.11 Ω | 1.54 Ω |
| Resistance R | 3.28 Ω | 1.25 Ω | 0.10 Ω | 0.45 Ω | 0.09 Ω |
| Shunt Capacitor Q | 3.8 MVAR | 2.0 MVAR | N/A | N/A | N/A |
| Power Base S | N/A | N/A | 12 MVA | 2.2 MVA | 12 MVA |

**Table 5: System parameters for case 3. X/R ratio obtained from [1] and [16].**
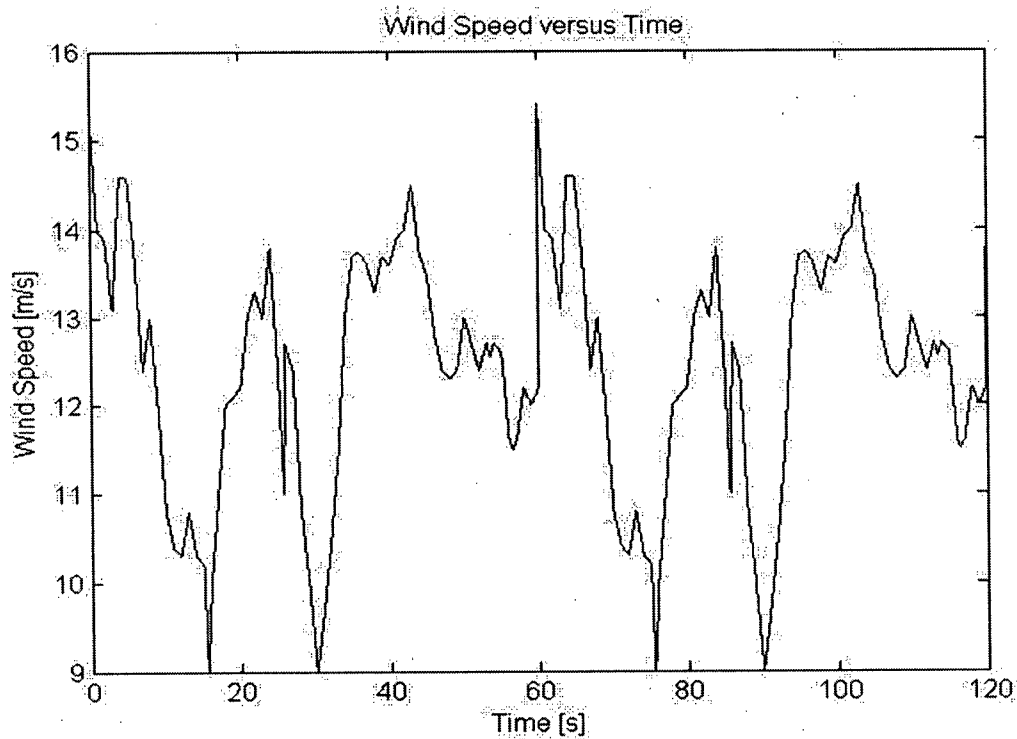
**Figure 62: Wind speed versus time for case 3 [12].**
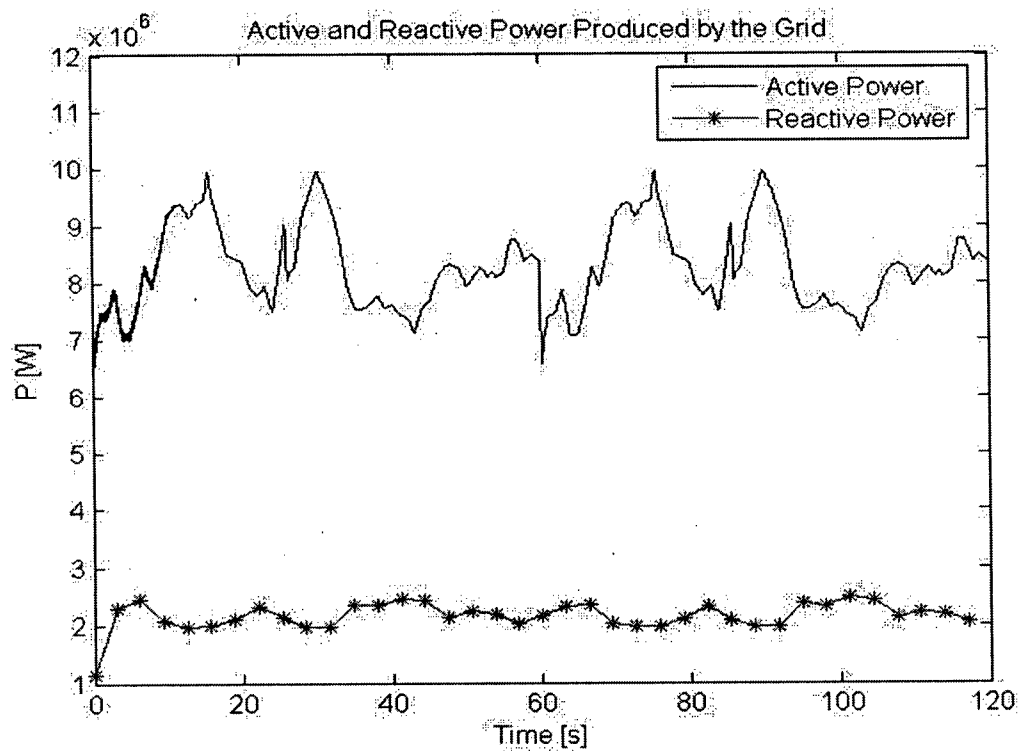


**Figure 63: Power through the weak line versus time for case 3.**
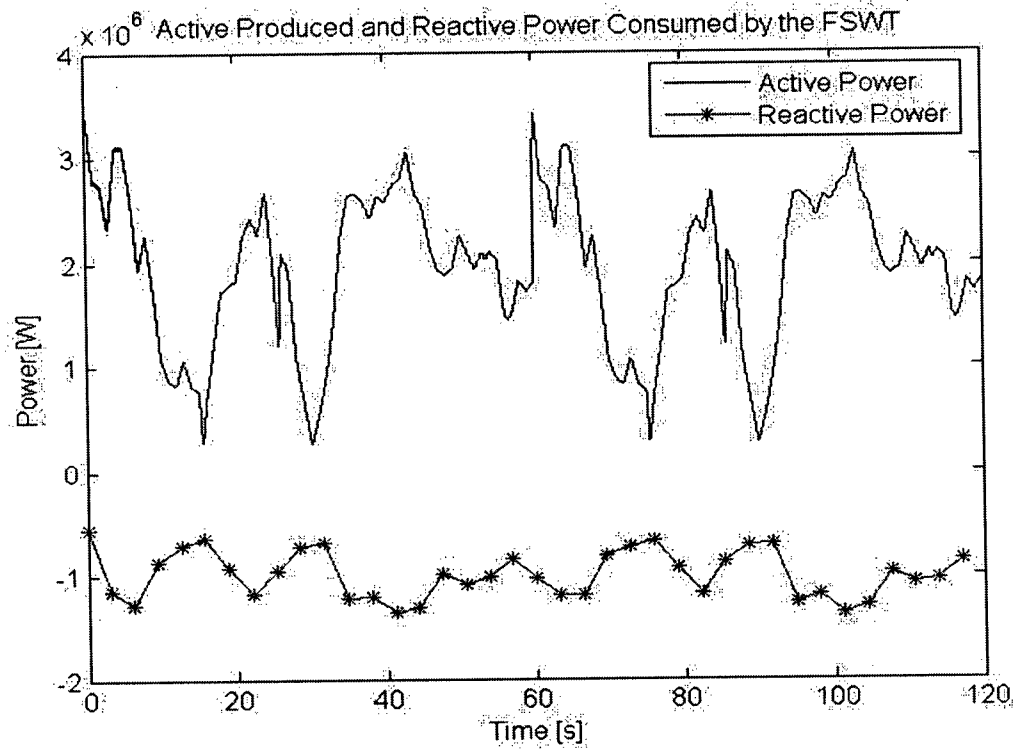
**Figure 64: Power through the strong line versus time for case 3.**
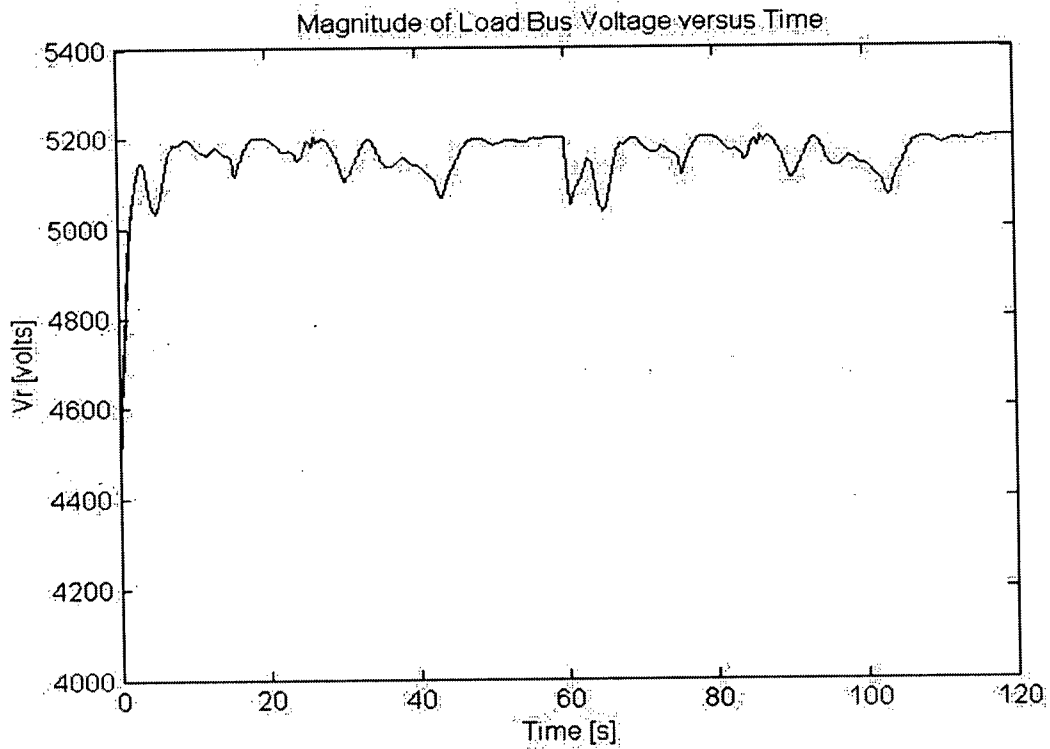


**Figure 65: Magnitude of the load bus voltage versus time for case 3.**
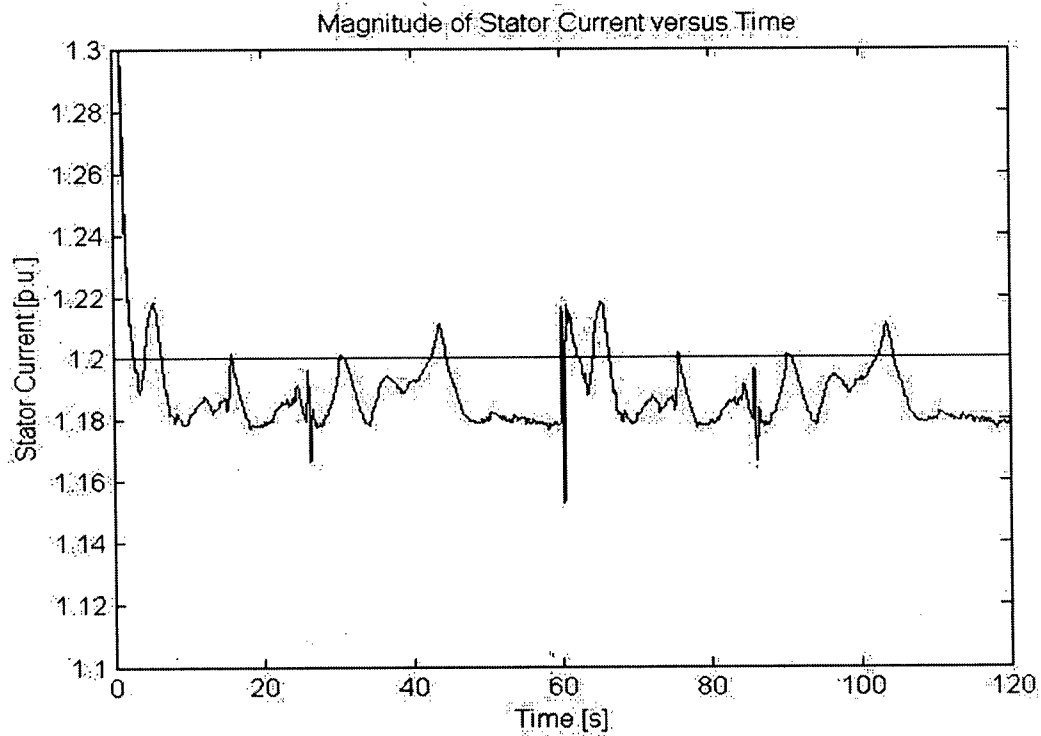
**Figure 66: Magnitude of the stator current versus time for case 3.**
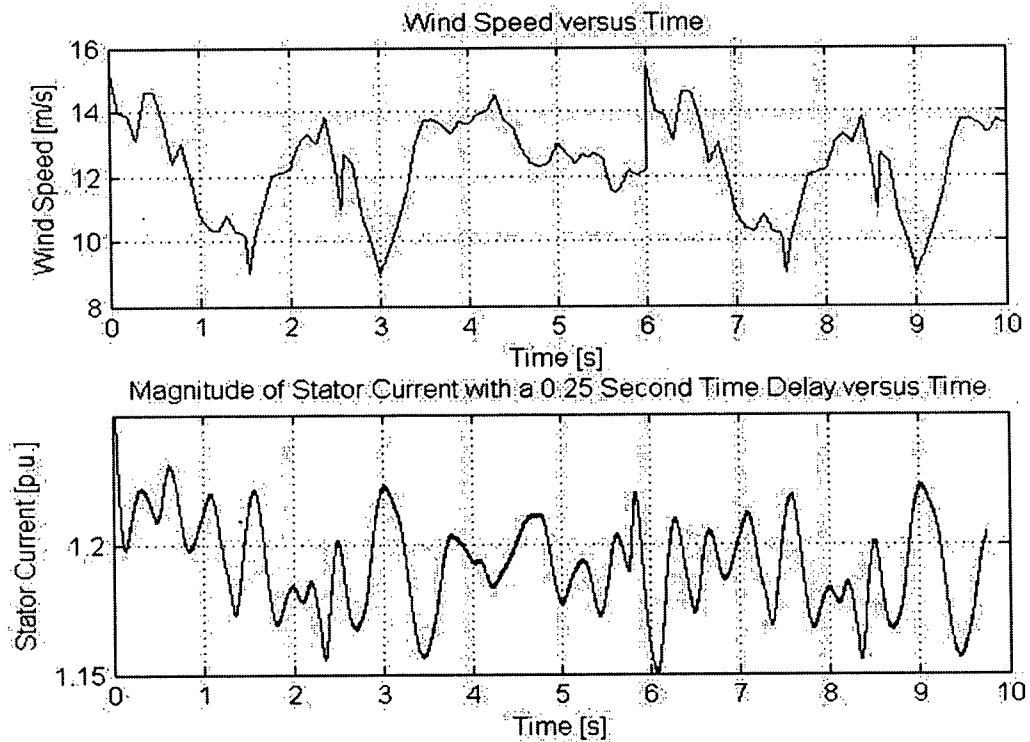


**Figure 67: Wind speed versus time and the magnitude of the stator current versus time for case 3.**
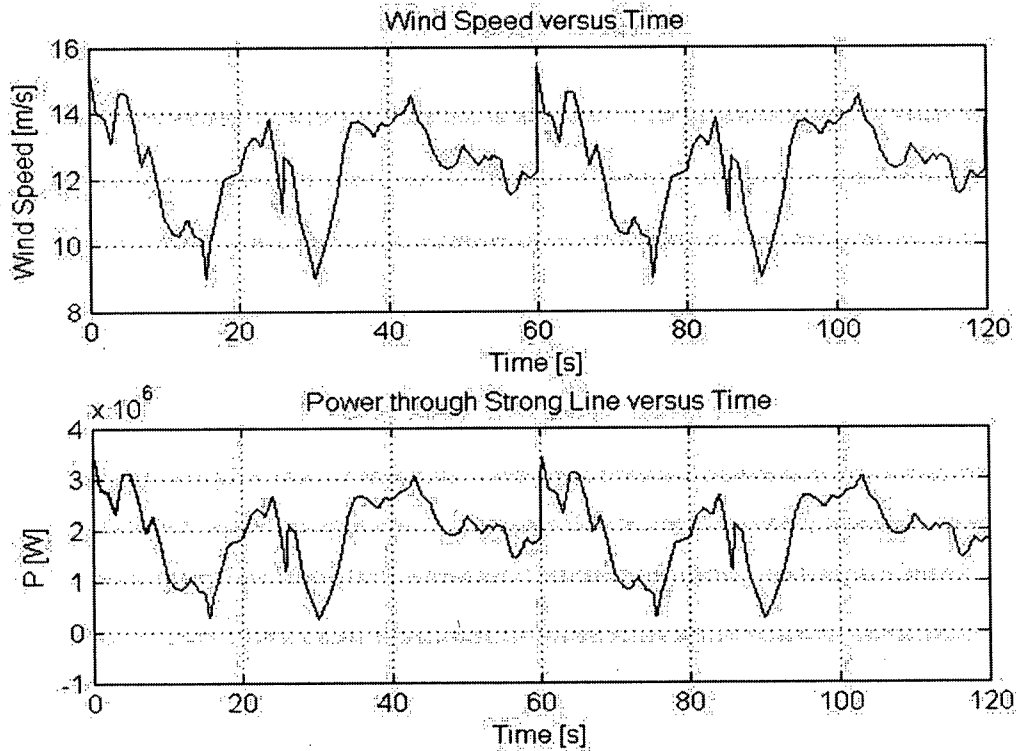
**Figure 68: Wind speed versus time and the power through the strong line versus time for case 3.**

There are several pertinent points in the above figures. It is clear from Figure 65 that the voltage of the system is lower than rated voltage; however, it is within the accepted range of ±10% of the rated voltage. In Figure 63 and Figure 64, the varying power output from the grid and FSWT are displayed respectively. These figures demonstrate that the fluctuating wind speed causes variations in the power output of the FSWT. The grid, modeled as a constant voltage source, counteracts the FSWT power output.

Figure 66 is of particular interest. Figure 66 displays the varying stator current as a result of the wind fluctuations. The significance of this result is that the stator current frequently surpasses the current protection threshold of the induction machine load. In addition, the current remains at these elevated levels for several seconds. This would trip the motor protection and result in a shut down of the load. Notice that the wind speed in Figure 62 fluctuates between 9m/s and 15m/s. This range for the wind speed is typical of areas where wind turbines are installed. In other words, this is a realistic example of how integration of wind turbines to the power grid could cause unwanted results. In this case,

it is the over-dependence on wind energy (approximately 20% of the power is supplied by wind energy) and the limited distribution capabilities of the grid that caused the current protection to trip. This is the reason that analysis of the system is critical. After the system has been analysed, then renewable energy sources can be installed with confidence. It is through the examination of the power system that potential problems will be avoided. If any measures are necessary, they can be taken to ensure reliable power delivery to meet the load demands. In this following case, the addition of power electronics to the FSWT will be explored as a means of reducing the fluctuations in the stator current.

## 3.4 Case 4

Case 4 examines the voltage stability of the system with a sophisticated wind turbine model. The doubly fed induction generator model (DFIG) replaces the constant voltage source from cases 1 and 2, and replaces the FSWT from case 3. The DFIG model is described by an induction machine, with a squirrel cage rotor, rated at 2MVA and 575V. It also includes a rectifier, DC link and a converter connected between the grid and the rotor of the machine. The varying wind speed is converted to a varying torque. This acts as the driving torque for the motor. The system is monitored during steady state operation and the effects of having a variable source with power electronics will be observed. The variable power output from the DFIG is a direct result from the fluctuations in the wind speed. As the wind speed decreases, the current output increases and the power output of the DFIG decreases. The stator current of the load is recorded to determine if typical wind fluctuations are sufficiently large to cause the current protection breaker of the motor to trip. Furthermore, the stator current of the load is recorded to determine if the power electronics of the DFIG are sufficient to prevent the tripping of the current protection breaker of the load that occurred in Case 3. The DFIG is connected to the load by a strong distribution line. The grid is represented by a constant voltage source but it is connected to the load by a weak distribution line. The load is the same load from case 3, an induction machine rated at 10MVA and 6.9kV. It is equipped with current protection device which disconnects the motor if the current surpasses 1.2 p.u.

The steady state response of the system is examined. The power through each line, the load bus voltage and the stator current are recorded. Below is a diagram of the system.
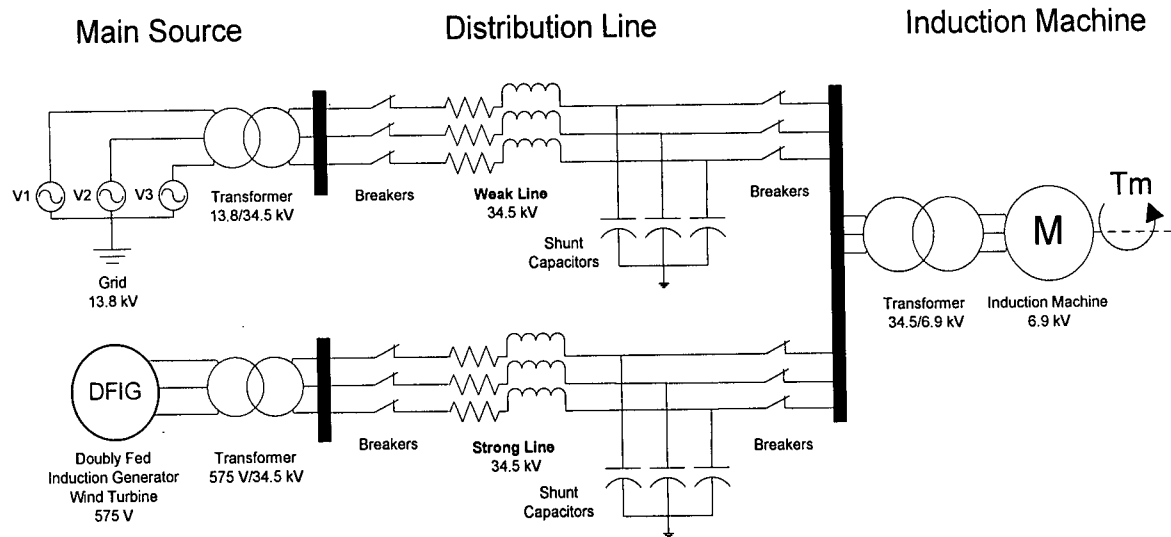


Figure 69: Diagram of case 4.

| | Weak Line | Strong Line | Transformer 13.8/34.5kV | Transformer 575V/34.5kV | Transformer 34.5/6.9kV |
|---|---|---|---|---|---|
| Line Length L | 66 km | 25 km | N/A | N/A | N/A |
| Reactance X | 32.75 Ω | 12.50 Ω | 1.73 Ω | 8.11 Ω | 1.54 Ω |
| Resistance R | 3.28 Ω | 1.25 Ω | 0.10 Ω | 0.45 Ω | 0.09 Ω |
| Shunt Capacitor Q | 3.8 MVAR | 2.0 MVAR | N/A | N/A | N/A |
| Power Base S | N/A | N/A | 12 MVA | 2.2 MVA | 12 MVA |

Table 6: System parameters for case 4. X/R ratio obtained from [1] and [16]..

### 3.4.a Case 4A

Case 4A examines the DFIG's performance when delivering 20% of the load requirement. There are several notable points in the figures below. From Figure 73, the voltage at the load bus is nearly at rated voltage. This is a significantly better voltage

**Figure 70: Wind speed versus time for case 4A [12].**



**Figure 71: Power through the weak line versus time for case 4A.**

61

**Figure 72: Power through the strong line versus time for case 4A.**



**Figure 73: Magnitude of the load bus voltage versus time for case 4A.**
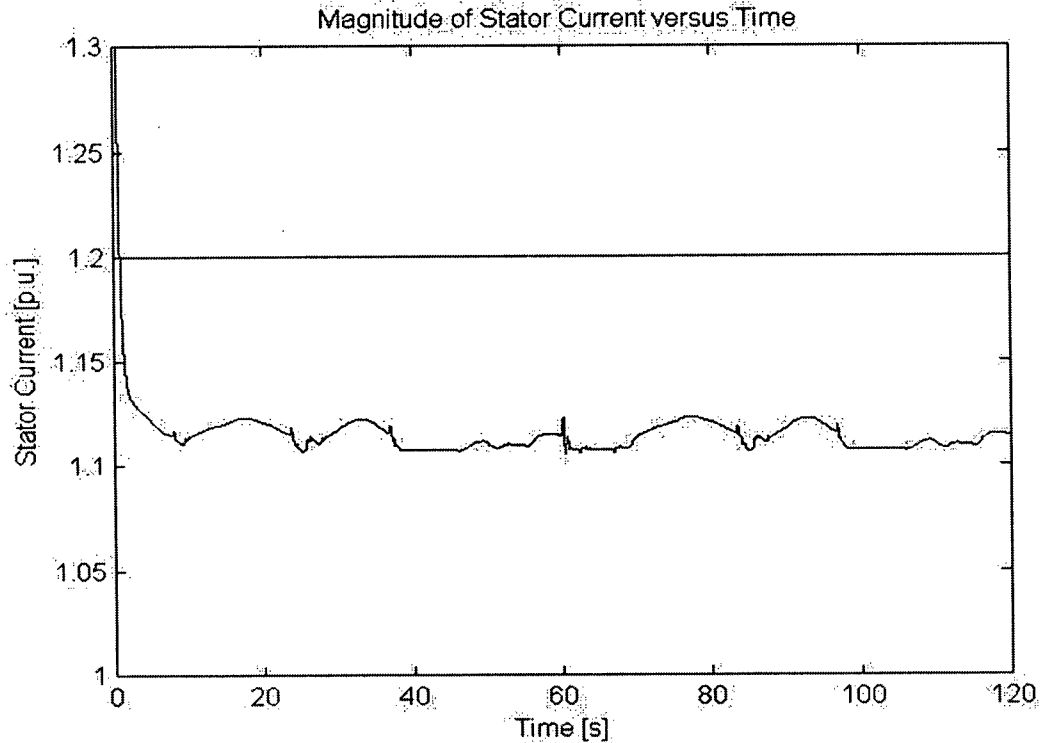
**Figure 74: Magnitude of the stator current versus time for case 4A.**

level than the FSWT (Figure 66). In Figure 71 and Figure 72, the varying power output from the grid and DFIG are displayed respectively. These figures demonstrate that the fluctuating wind speed causes variations in the po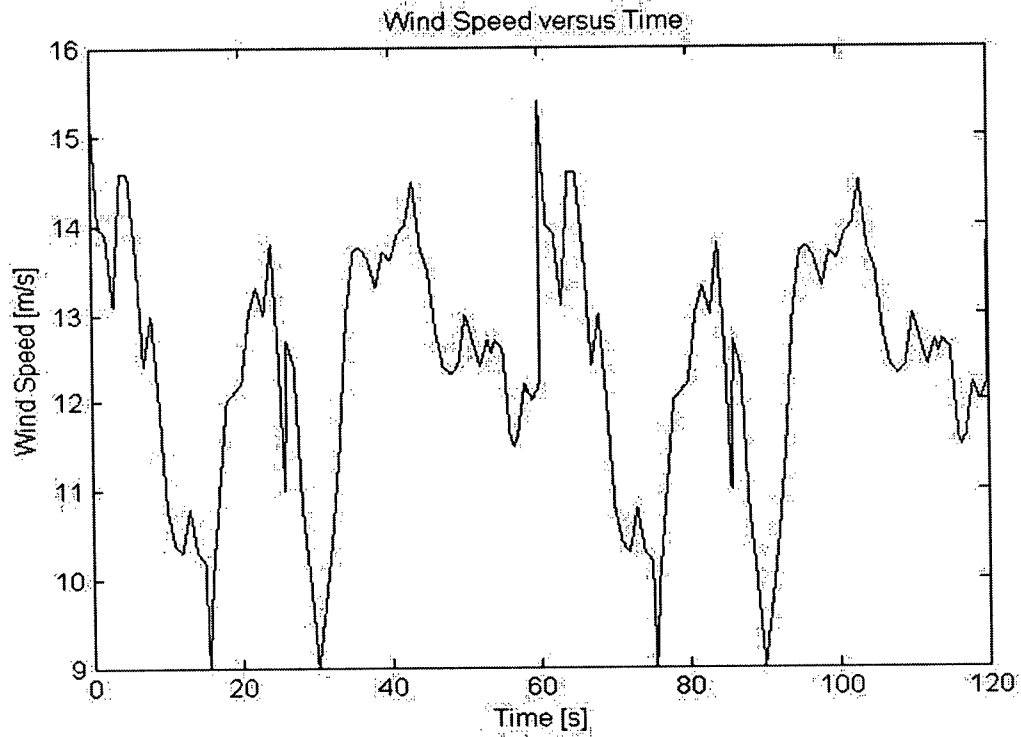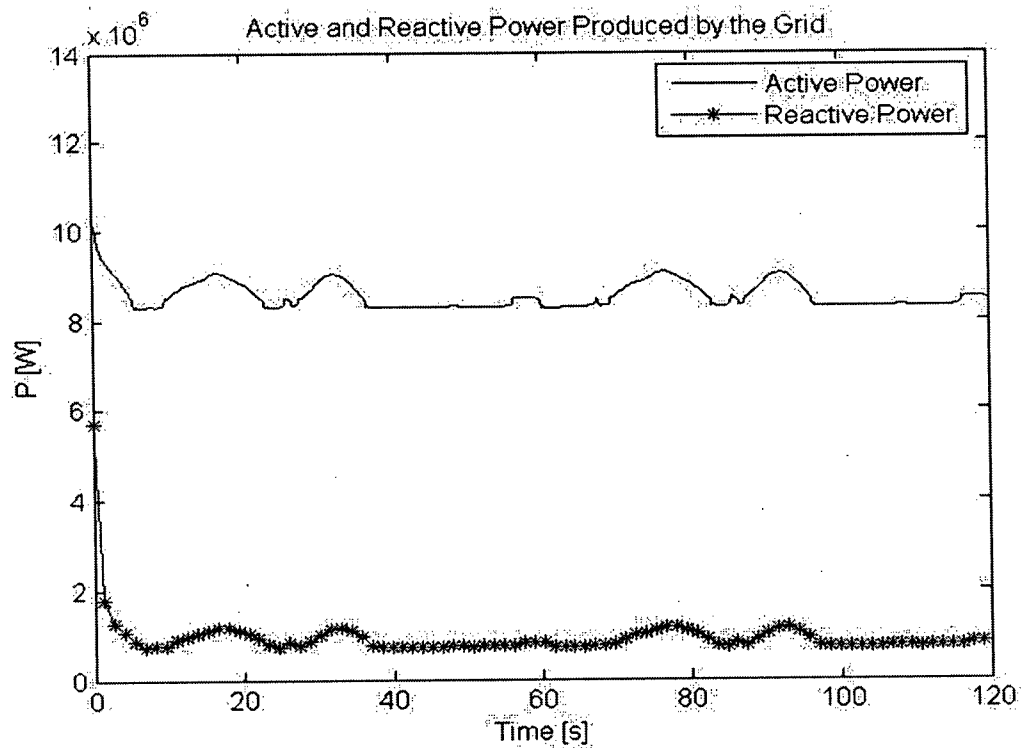wer output of the DFIG. The grid, modeled as a constant voltage source, counteracts the DFIG power output. Comparing the power variation of the DFIG (Figure 72) to the power variation of the FSWT (Figure 64), one can observe that the power output from the DFIG is controlled. This means that the power electronics in the DFIG are effectively regulating the variations in the power output due to the fluctuations in the wind speed.

Figure 74 is of particular interest. Figure 74 displays the varying stator current as a result of the wind fluctuations. The significance of this result is that the stator current never surpasses the current protection threshold of the induction machine load. Comparing to the FSWT (Figure 66), where the stator current frequently surpasses the current protection threshold and remains at these elevated levels for several seconds, we can conclude that the DFIG wind turbine produces a stable system. Notice that the wind speed (Figure 70), which is the same as in Case 3 (Figure 62), fluctuates between 9m/s

and 15m/s. This wind speed range is typical of areas where wind turbines are installed. In other words, upon analysis of the system this example of integration of wind turbines to the power grid could be successful. In this case, the dependence on wind energy is approximately 20% of the total power is supplied to the load. This is the reason that analysis of the system is critical. After the system has been analysed, then renewable energy sources can be installed with confidence. It is through the examination of the power system that potential problems will be avoided. If any measures are necessary, they can be taken to ensure reliable power delivery to meet the load demands.

### 3.4.b Case 4B

In Case 4B, one change is made. The amount of power produced by the DFIG is increased to approximately 80% of the load requirement. This is meant to represent a
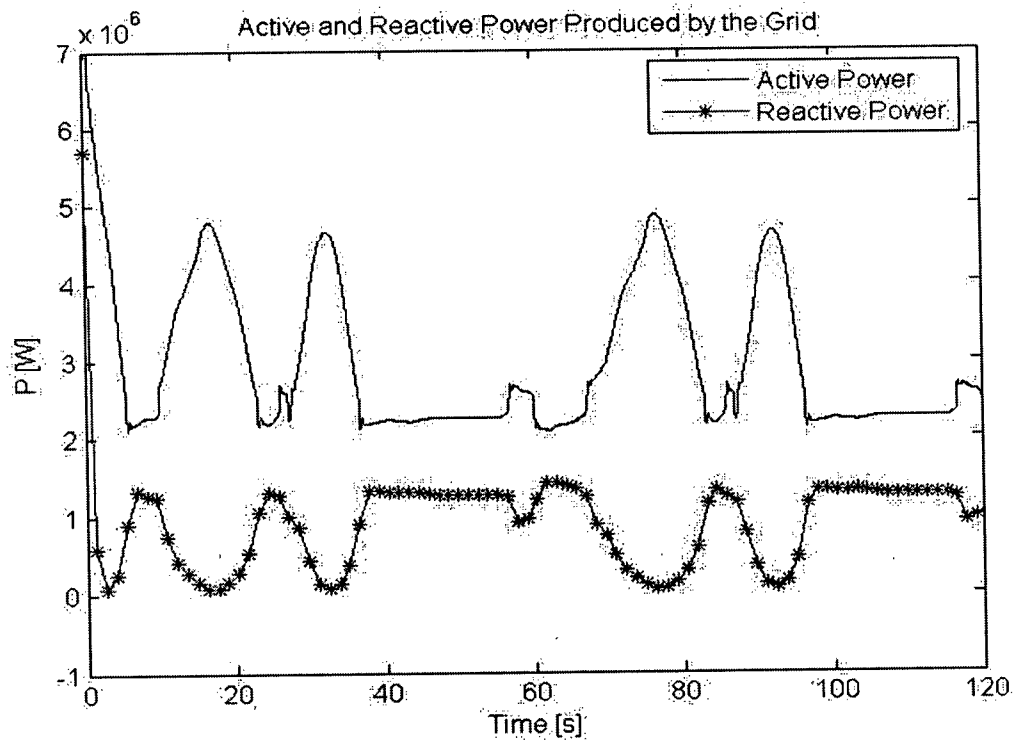


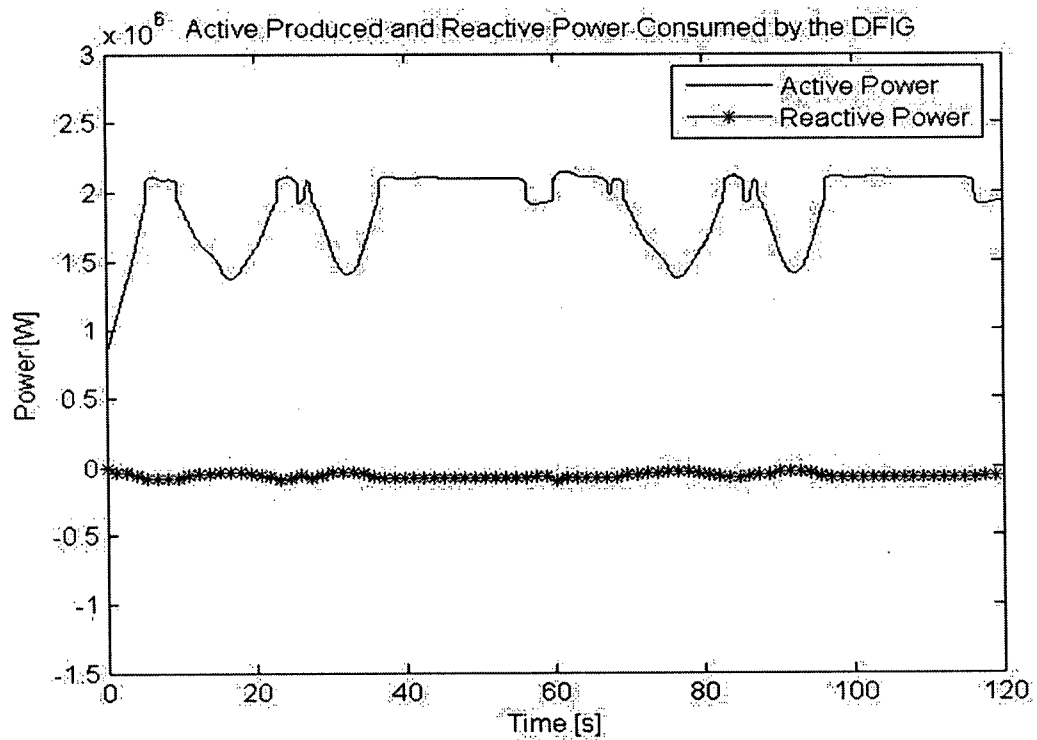**Figure 75: Power through the weak line versus time for case 4B.**
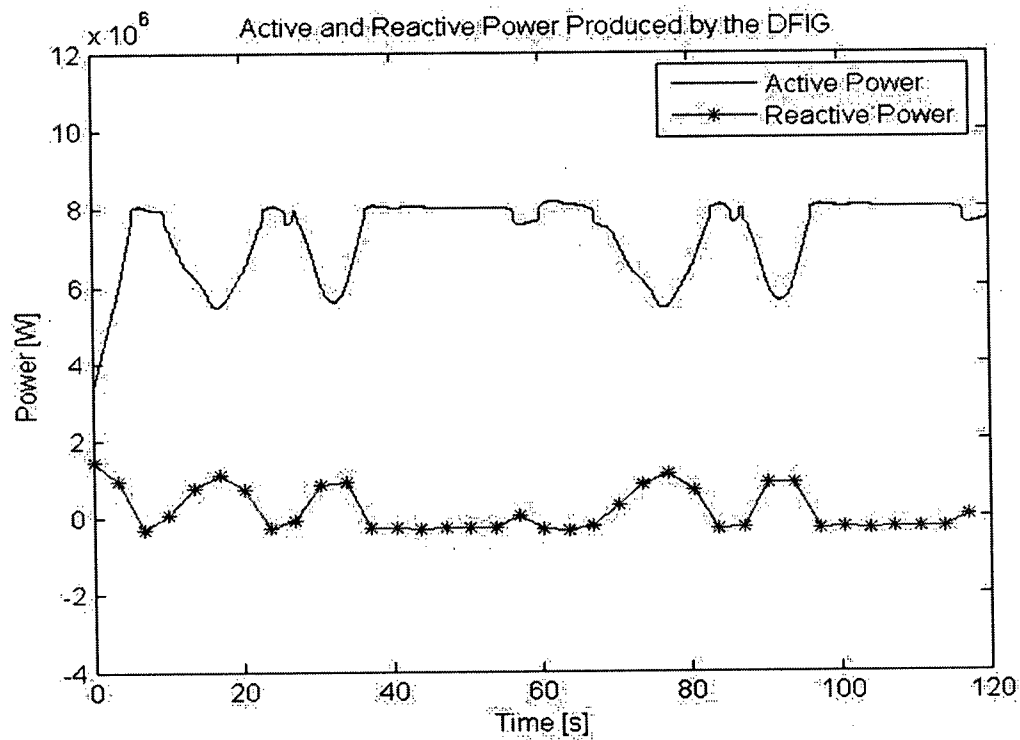
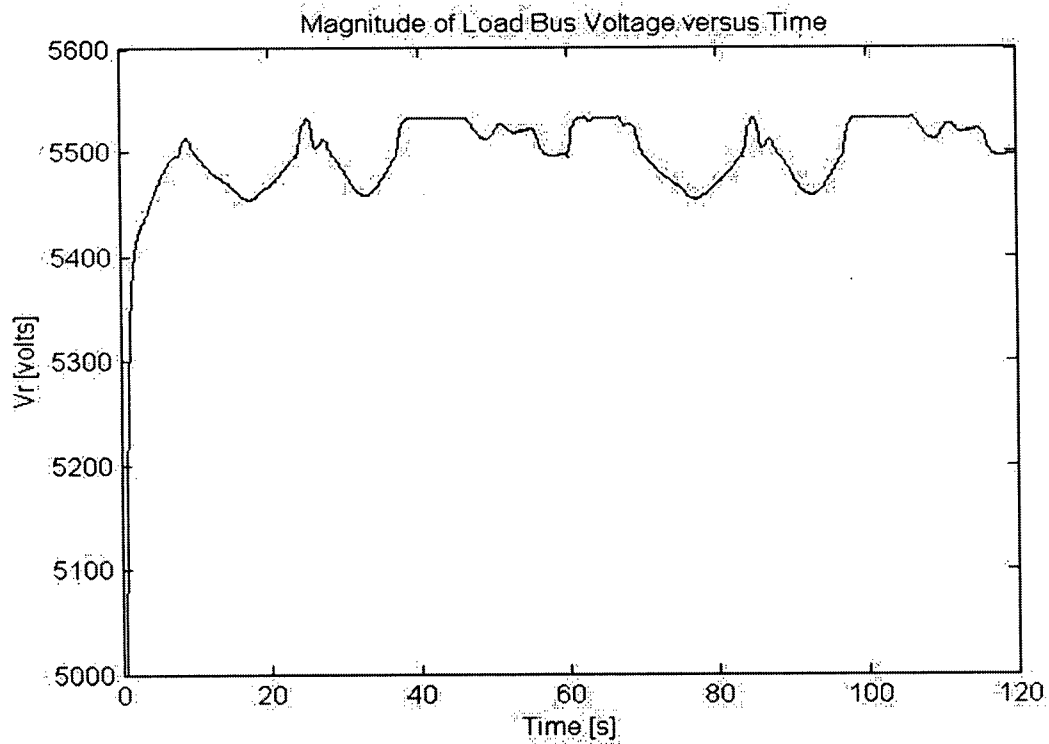Figure 76: Power through the strong line versus time for case 4B.
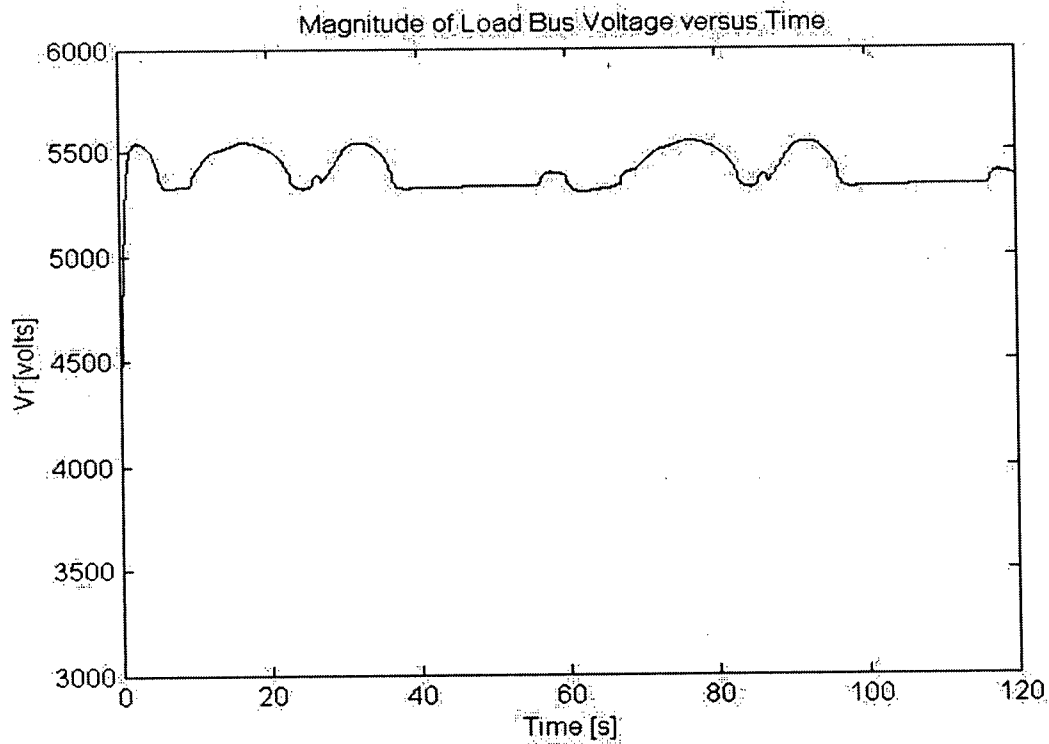


Figure 77: Magnitude of the load bus voltage versus time for case 4B.
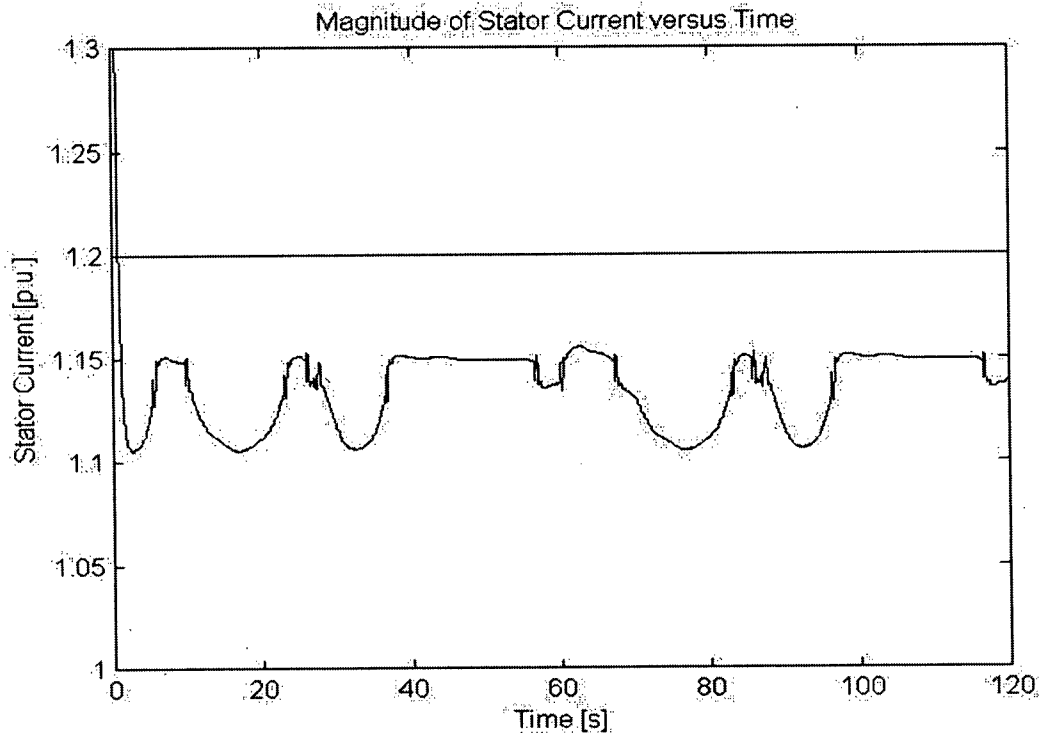
**Figure 78: Magnitude of the stator current versus time for case 4B.**

remote load which is primarily supplied by local wind energy. The grid is connected to the load by a WL. Again, the stator current of the load is monitored to determine if the power electronics of the DFIG can prevent the loss of the load due to over currents. By increasing the percentage of the power supplied by the DFIG, this increases the possibility that the stator current of the load may surpass 1.2 p.u. It is demonstrated in Figure 78 that the DFIG controls the stator current so that it does not exceed 1.2 p.u. This meets the criteria for stable steady state operation. Based on these results, the use of DFIG is recommended.

# 4. Conclusion

Case studies were presented to demonstrate the potential problems of installing wind turbines to the power grid. These problems are manifested when the dependence on wind energy is large and the grid capacity is near its limit. These potential pitfalls are avoidable if careful consideration of the system is pursued. Two types of cases were performed to demonstrate that proper analysis of the system could correctly predict its behaviour and thus, prevent system instability. The first type of cases examined was a three phase fault. Using static models (constant power factor PV curves and exponential load model) the system was determined to be steady state stable when both the lines were operational and when only the WL was operational. Thus, it was predicted that the system was also transient stable between those two operating conditions. To verify this prediction, the system was simulated using a dynamic load model. A voltage collapse was observed. After analysing the system, it was determined that the dynamic load model and the equivalent circuit of induction machine PV curves correctly predict the transient voltage instability of the system. The commonly accepted static models were invalid under transient conditions and near the maximum power delivery of the system.

The second type of cases assessed the steady state stability of the system. Two wind turbine models were compared: FSWT and DFIG. The FSWT caused the current protection of the load to trip when providing only 20% on the total power. This resulted in the loss of the load. On the other hand, the DFIG wind turbine compensated for the wind fluctuations. This prevented the loss of the load. In addition, the DFIG was capable of delivering significantly more power, up to 80% of the load demand, without tripping the current protection system of the load. This demonstrates that studies into the power system provide solutions to determine the wind turbine model which is most appropriate. As the world's energy demands are increasing, there is a transition to cleaner energy generation. With the advancement in wind power technology, a renewable and clean energy source has become a viable alternative to traditional power generation. Wind power does, however, have potential problems. These pitfalls are manifested when dependence on wind energy is large and grid capabilities are near their limit. By

performing analysis, the power industry will ensure reliable and affordable power delivery for future generations.

There is a significant amount of future work which stems from this research. The system can be expanded to represent a more complex network. Instead of using one large aggregate load, many smaller loads can be modelled. Cascading voltage collapses may be modelled. Methods to prevent this situation could be explored. This will provide a more detailed understanding of the system. The development of more detailed PV curves and their applications to specific system would be another logical extension of this thesis. Another topic of research would be the testing of load models and their ability to predict the trajectory of the transient in the PV plane. In addition, one could examine the control of the operation point in the PV plane. An analysis of the best method to restore the system to a stable region of the PV plane may be of great interest. Other wind turbine models may be investigated. Another direction of research would be to refine the simulation technique. Presently, continuous time simulations take between 5 and 20 minutes to complete a 20 second simulation with full accuracy. Phasor simulations run at real time; however, they only solve for the 60 Hz frequency component. The implementation of dynamical phasors to solve the system would provide a solid balance between simulation speed and accuracy.

# References

[1] Glover, J. D. and Sarma, M. S., "Power System Analysis and Design", 3$^{rd}$ edition, Thomson Learning, 2002.

[2] Masters, G. M., "Renewable and Efficient Power Systems", Wiley, 2004.

[3] Press Release, World Wind Energy Association, March 5, 2004.

[4] Hau, E. "Wind Turbines Fundamentals, Technologies, Application, Economics", Springer, 2000.

[5] Wilkie, J.; Leithead, W. E. and Anderson, C. "Modeling of wind turbines by simple models," *Wind Engineering*, vol. 14, no. 4, 1990.

[6] Bao, N. Sh.; Chen, Q. X. and Jiang, T., "Modeling and identification of a wind turbine system," *Wind Eng.*, vol. 20, no. 4, pp. 203–218, 1990.

[7] Jenkins, N. and Saad-Saoud, Z., "A simplified model for large wind turbines," in *Eur. Union Wind Energy Conf.*, Göteborg, Sweden, 1996, pp. 443–446.

[8] Usaola, J.; Vilar, C.; Amaris, P.; Ledesma, P. and Rodriguez, J. L., "Characterization of WECS through power spectra for power quality studies," in *Proc. Eur. Wind Energy Conf.*, Nice, France, Mar. 1999, pp. 766–769.

[9] Kazachkov, Y.A.; Feltes, J.W. and Zavadil, R., "Modeling wind farms for power system stability studies", in Power Engineering Society General meeting, 2003 IEEE, Vol. 3, 13-17 July 2003.

[10] Petru, T.; Thiringer, T., "Modeling of wind turbines for power system studies", IEEE Transactions on Power Systems, Vol. 17, Issue: 4, Nov. 2002 pp.1132 – 1139.

[11] Thiringer, T; "Measurement and modelling of low-frequency disturbances in induction machines" ISBN 91-7197-384-2.

[12] Slootweg, J.G.; Polinder, H.; Kling, W.L.; "Dynamic modelling of a wind turbine with doubly fed induction generator", Power Engineering Society Summer Meeting, IEEE, Vol. 1, 15-19 July 2001 pp. 644 – 649.

[13] Lundberg, S.; Thiringer, T. and Petru, T., "Electrical limiting factors for wind energy installations in weak grids," *Int. J. Renewable Energy Eng.*,vol. 3, no. 2, 2001.

[14] Larson, Å.; Sorensen, P. and Santjer, F., "Grid impact of variable-speed wind turbines," in *Proc. Eur. Wind Energy Conf. Exh.*, Nice, France, Mar. 1–5, 1999.

[15] Sun, T. S. and Blaabjerg, F., "Transient analysis of grid-connected wind turbines with DFIG after an external short-circuit fault", Nordic Wind Power Conference, 1-2 March, 2004, Chalmers University of Technology.

[16] Kundur, P. "Power system stability and control", McGraw Hill, 1994.

[17] Fairley, P., "The unruly power grid" Spectrum, IEEE Volume 41, Issue 8, Aug. 2004 pp. 22 – 27.

[18] Sato, H., "Computation of bifurcation and maximum loading limit in electrical power systems" Electric Utility Deregulation, Restructuring and Power Technologies, 2004. (DRPT 2004). Proceedings of the 2004 IEEE International Conference onVol. 1, 5-8 April 2004 pp. 84 – 89.

[19] Feng, Z.; Xu, W., "Fast computation of post-contingency system margins for voltage stability assessments of large-scale power systems", Generation, Transmission and Distribution, IEE Proceedings-, Volume 147, Issue 2, March 2000 pp. 76 – 80.

[20] Semlyen, A.; Gao, B. and Janischewskyj, W., "Calculation of extreme loading condition of a power system for the assessment of voltage stability", IEEE *Trans. on Power Systems,* vol. 6, no. 1, February 1991, pp. 307-315.

[21] Chang, H. D.; Wang, C. S. and Flueck, A. J., "Look-ahead voltage and load margin contingency selection functions for large scale powersystems", IEEE Trans. Power Syst. 1997, Vol. 12, pp. 173-180.

[22] Overbye, T. J. and Hump, R. P., "Effective calculation of power systems low-voltage solutions", *IEEE Trans. on Power Systems,* vol. 11, no. 1. February 1996, pp. 75-82.

[23] Slootweg, J.G.; de Haan, S.W.H.; Polinder, H.; Kling, W.L., "Modeling wind turbines in power system dynamics simulations", Power Engineering Society Summer Meeting, 2001. IEEE, Vol. 1, 15-19 July 2001 pp. 22 – 26.

[24] Help manual of Matlab/Simulink toolbox SimPowerSystem.

[25] Xu, W; Mansour, Y., "Voltage stability analysis using generic dynamic load models" *IEEE Trans. On Power Systems,* vol. 9, no. 1, February 1994 pp. 479-493

# Appendix 1: Machine Parameters

## Induction machine load:

Rating: $S_{base}$=10 MVA, $V_{Line-Line, RMS}$ = 6.9 kV, f = 60 Hz, squirrel cage rotor.

| Stator Resistance | Stator Inductance | Rotor Resistance | Rotor Inductance | Mutual Inductance | Inertia constant Constant | Pole Pairs |
|---|---|---|---|---|---|---|
| 9.2e-3 p.u. | 7.2e-2 p.u. | 6.9e-3 p.u. | 7.2e-2 p.u. | 4.138 p.u. | 3 seconds | 2 |

## FSWT:

Rating: $S_{base}$=2 MVA, $V_{Line-Line, RMS}$ = 575 V, f = 60 Hz, squirrel cage rotor.

| Stator Resistance | Stator Inductance | Rotor Resistance | Rotor Inductance | Mutual Inductance | Inertia constant Constant | Pole Pairs |
|---|---|---|---|---|---|---|
| 1.6e-2 p.u. | 6.0e-2 p.u. | 1.5e-2 p.u. | 6.0e-2 p.u. | 2.9 p.u. | 2 seconds | 2 |

## DFIG:

Rating: $S_{base}$=2 MVA, $V_{Line-Line, RMS}$ = 575 V, f = 60 Hz, wound rotor.

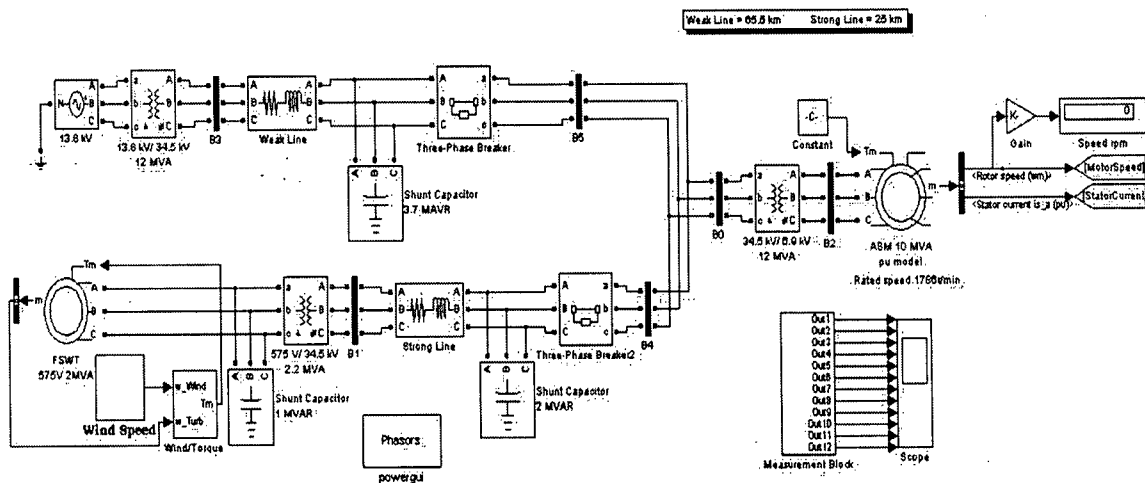| Stator Resistance | Stator Inductance | Rotor Resistance | Rotor Inductance | Mutual Inductance | Inertia constant Constant | Pole Pairs |
|---|---|---|---|---|---|---|
| 7.1e-3 p.u. | 1.7e-1 p.u. | 5.0e-3 p.u. | 1.6e-1 p.u. | 2.9 p.u. | 5 seconds | 3 |

| Grid Side Coupling Inductor | Grid Side Coupling Resistor | DC Bus Voltage | DC Bus Capacitor | Max. Pitch Angle | Max. Rate of Change of Pitch Angle | $Q_{ref}$ |
|---|---|---|---|---|---|---|
| 1.5e-1 p.u. | 1.5e-3 p.u. | 1200 V | 2.0e-2 p.u. | 45 degrees | 2 deg/sec | 0 p.u. |

# Appendix 2: Block Diagrams

## Matlab Block Diagrams for Cases 1 and 2:
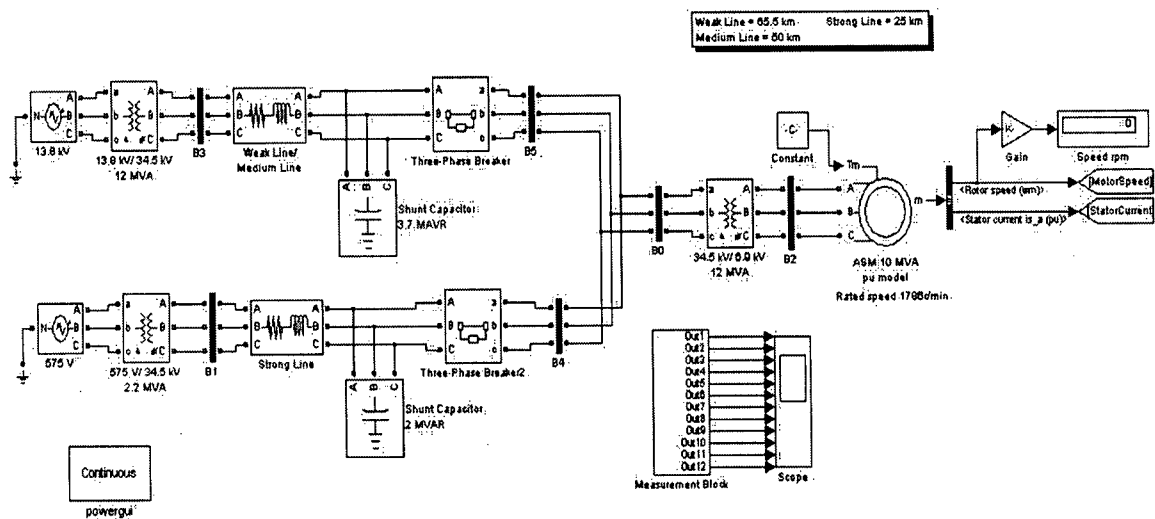


## Matlab Block Diagram for Case 3:

# Matlab Block Diagram for Case 4: